

**EXPERIMENTAL AND COMPUTATIONAL STUDIES ON
LIQUID POISON INJECTION IN THE CALANDRIA OF
PRESSURE TUBE TYPE REACTOR**

By
Anuj Kumar Kansal
ENGG01201004014

Bhabha Atomic Research Centre, Mumbai

A thesis submitted to the
Board of Studies in Engineering Sciences
In partial fulfillment of requirements
for the Degree of
DOCTOR OF PHILOSOPHY
of
HOMI BHABHA NATIONAL INSTITUTE

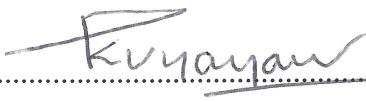
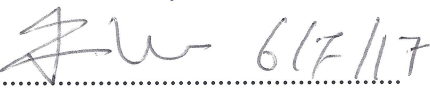


July, 2017

Homi Bhabha National Institute

Recommendation of Vice Voce Committee

As members of the Vice Voce Committee, we certify that we have read the dissertation prepared by Anuj Kumar Kansal entitled “*Experimental and computational studies on liquid poison injection in the calandria of pressure tube type reactor*” and recommend that it may be accepted as fulfilling the thesis requirement for the award of Degree of Doctor of Philosophy.

- 1) Chairman Prof. P.K. Vijayan.....  6/7/17
- 2) Guide Prof. N.K. Maheshwari.....  6/7/17
- 3) Co-Guide Prof. J.B. Joshi.....  6/7/17
- 4) Examiner Prof. R.P. Vedula.....  6/7/17
- 5) Member 1 Prof. A.K. Nayak.....  6/7/17
- 6) Member 2 Prof. Atul Sharma.....  6/7/17
- 7) Member 3 Prof. K. Velusamy.....  6/7/2017

Final approval and acceptance of this dissertation is contingent upon the candidate's submission of the final copies of the dissertation to HBNI.

We hereby certify that we have read this dissertation prepared under our directions and recommend that it may be accepted as fulfilling the dissertation requirement.

Date: 06/07/17

Place: Mumbai



(Prof. J.B. Joshi)

Co-guide



(Prof. N.K. Maheshwari)

Guide

Statement by author

This dissertation has been submitted in partial fulfilment of requirements for an advanced degree at Homi Bhabha National Institute (HBNI) and is deposited in the Library to be made available to borrowers under the rules of the HBNI.

Brief quotations from this dissertation are allowable without special permission, provided that accurate acknowledgement of the source is made. Requests for permission for extended quotation from or reproduction of this manuscript in whole or in part may be granted by the Competent Authority of HBNI when in his or her judgment the proposed use of the material is in the interests of scholarship. In all other instances, however, permission must be obtained from the author.

Anuj Kumar Kansal

Declaration

I, hereby declare that the investigation presented in the thesis has been carried out by me. The work is original and has not been submitted earlier as a whole or part for a degree/ diploma at this or any other institution/ university.

Anuj Kumar Kansal

List of publications arising from the thesis

Journal

1. Kansal, A.K., Maheshwari, N.K. and Vijayan, P.K., 2014. Analytical model for performance verification of liquid poison injection system of a nuclear reactor, Nuclear Engineering and Design, 275, 329–335.
2. Kansal, A.K., Joshi, J.B., Maheshwari, N.K. and Vijayan, P.K., 2015. CFD analysis of moderator flow and temperature fields inside a vertical calandria vessel of nuclear reactor, Nuclear Engineering and Design, 287, 95-107.
3. Kansal, A.K., Maheshwari, N.K. and Vijayan, P.K., 2016. Effect of Inlet and Outlet Nozzle Locations on Moderator Temperature Distribution, International Journal of Mechanical Engineering and Automation, 3 (9), 384-390.
4. Kansal, A.K., Kumawat, G.L., Kamble, M.T., Maheshwari, N.K. and Joshi, J.B., 2017. Poison injection in AHWR calandria: Flow pattern and mixing characteristics, International Journal of Heat and Mass Transfer, 105, 359-375.

Conferences

International Conference

1. Kansal, A.K., Maheshwari, N.K. and Vijayan, P.K., 2011. Development of poison injection code-COPJET for high pressure liquid poison injection in pressure tube type heavy water reactor, 19th International Conference on Nuclear Engineering (ICONE-19), Chiba, Japan.
2. Kansal, A.K., Suryanarayana, P., Maheshwari, N.K. and Vijayan, P.K., 2014. CFD analysis of moderator flow and temperature fields inside calandria vessel of AHWR

using OpenFOAM, 5th International conference on Fluid Mechanics and Fluid Power (FMFP-2014), IIT Kanpur (UP), India.

3. Kansal, A.K., Kamble, M.T., Maheshwari, N.K. and Vijayan, P.K., 2014. CFD Analysis of Poison Injection in AHWR Calandria, Int. Workshop on New Horizons in Nuclear Reactor Thermal Hydraulics and Safety, Mumbai, India.
4. Kansal, A.K., Suryanarayana, P., Maheshwari, N.K. and Vijayan, P.K., 2015. Effect of distribution of volumetric heat generation on moderator temperature distribution, International Thorium Energy Conference 2015 (ThEC15), Mumbai, India.

National Conference

1. Kansal, A.K., Kamble, M.T., Maheshwari, N.K. and Vijayan, P.K., 2013. CFD analysis of liquid poison injection for high pressure liquid poison injection of AHWR, Proceedings of the Fortieth National Conference on Fluid Mechanics and Fluid Power (FMFP-40), NIT Hamirpur, Himachal Pradesh, India.
2. Kansal, A.K., Maheshwari, N.K. and Vijayan, P.K., 2015. Validation of CFD code and effect of inlet and outlet nozzles locations on moderator temperature distribution, Proceedings of the Forty Second National Conference on Fluid Mechanics and Fluid Power (FMFP-2015), NITK Surathkal, Karnataka, India

(Anuj Kumar Kansal)

**Dedicated to GOD
and
my little son**

Acknowledgement

I would like to express my deep and sincere gratitude to my Guide Prof. N.K. Maheshwari and co-guide Prof. J.B. Joshi for their constant guidance, encouragement and all round support that led to the successful completion of this work. This work would not have been possible without their encouragement and support in every aspect of it. I would like to express my sincere gratitude to my co-guide Prof. J.B. Joshi for introducing me to CFD code OpenFOAM. I would like to thank Prof. P.K. Vijayan, ex-Director, RDDG for giving me the opportunity to carry out my Ph.D.

I would also like to thank all the members of the monitoring committee for their valuable suggestions and support throughout the duration of work. I would like to thank Mayur Ghandi and Mayur Sathe from ICT, Mumbai for helping me in my initial phase of CFD and experimental work. I would like to thank my fellow members of my section Shri S.K. Bhatia, Shri P. Suryanarayana, Shri Anil Antony, Shri M.T. Kamble, Shri G.L. Kumawat and Shri Rakesh Chouhan for their kind advice and suggestions to improve the quality of this work. I would like to thank Shri M.T. Kamble with whom I had done many discussions regarding basic understanding of results. I would like to thank my office roommates Alok, Vinay and Subrata for listening patiently to my good, bad and super intelligent theories during this research work. I would like to thank my senior Shri S.V. Prasad for giving valuable advice during preparation of final presentation. Without my friends, this work would have been impossible. I would like to thank my friends Vaibhav, Vinod and Sandeep for their constant encouragement and support.

Finally, big thanks to my family for always being there for me. My father, Shri Desh Raj has always emphasised on the importance of fundamentals and mathematics in the

technical field. My mother, Uma Gupta who always had faith in me. My brother Ankur, sister-in-law Anjali and niece Pogo who always remind me that there is world outside research. My sister-in-law Nidhi for given valuable editorial input for thesis. Finally, I would like to thank my Dear wife Geetika Kansal and my cute little son Darsh for their precious time that I have given to this work. I could not have been able to complete my thesis without their love and support.

Contents

Statement by author.....	iii
Declaration.....	v
List of publications arising from the thesis	vii
Acknowledgement	xiii
Synopsis	xix
List of Figures	xxv
List of Tables	xxix
Nomenclature	xxxii
1 INTRODUCTION	1
1.1 Background.....	1
1.2 Indian Nuclear Power Program	2
1.3 Brief description of AHWR.....	3
1.4 Reactor Protection System.....	5
1.4.1 Types of shut down systems.....	6
1.4.2 Shut down system in various reactors.....	9
1.5 Shut Down System-2 of AHWR.....	10
1.6 Challenges and Motivation for Present Work.....	12
1.7 Objectives.....	15
1.8 Outline of Thesis.....	16
2 LITERATURE REVIEW	19
2.1 Introduction.....	19
2.2 Literature Review	19
2.2.1 Flow distribution from lateral holes in an injection tube.....	19
2.2.2 Transient submerged jet injection in water	20
2.2.3 Moderator flow and temperature distribution in calandria.....	23

2.2.3.1	Analogy between calandria having tubes and flow through tube bundles....	26
2.2.4	Liquid poison injection in calandria	29
2.3	Gap Areas	30
2.3.1	Transient flow distribution from lateral holes in injection tube	30
2.3.2	Transient submerged jet injection in water	30
2.3.3	Moderator flow in calandria	31
2.3.4	Liquid poison injection in calandria	31
2.4	Conclusions	32

3 ANALYTICAL MODEL FOR LIQUID POISON INJECTION SYSTEM 33

3.1	Introduction	33
3.2	Development of Analytical Model.....	35
3.2.1	Flow geometry	35
3.2.2	Assumptions in analytical model	37
3.2.3	Governing equations	37
3.2.3.1	Gas expansion module.....	38
3.2.3.2	System piping module	38
3.2.3.3	Injection tube module	39
3.2.3.4	Poison jet progression module	43
3.2.4	Initial and boundary condition.....	47
3.2.5	Method of solution	48
3.2.6	Model validation.....	48
3.2.6.1	Lateral flow distribution.....	48
3.2.6.2	Poison jet progression.....	49
3.3	Results and discussions.....	50
3.3.1	Time delay in poison injection	51
3.3.2	Mass flow rate and gas tank pressure.....	54
3.3.3	Poison jet progression	54
3.3.4	Input for reactor physics analysis	56
3.4	Conclusions.....	56

4 EXPERIMENTAL STUDIES ON POISON INJECTION..... 57

4.1	Introduction	57
4.2	Experiments	58
4.2.1	Scaling philosophy.....	58
4.2.2	Experimental facility	66
4.2.2.1	Model with scaled dimensions	66
4.2.2.2	Model with full scale dimensions	70
4.2.3	Experimental techniques.....	71

4.2.3.1	Dye injection	71
4.2.3.2	Camera	71
4.2.4	Data Processing	71
4.3	Results and Discussions	72
4.3.1	Free jet.....	72
4.3.2	Jet with tube bundle	74
4.3.2.1	Axial tube bundle in scaled model.....	74
4.3.2.2	Cross tube bundle in scaled model.....	76
4.3.2.3	Full scale experimental setup.....	78
4.4	Conclusions.....	79
5	SOURCE TERM MODULE FOR POISON JET IN CFD	81
5.1	Introduction	81
5.2	Computational Fluid Dynamics	82
5.2.1	Flow geometry	82
5.2.2	Governing equations.....	82
5.2.3	Model assumptions	82
5.2.4	Method of solution.....	83
5.2.5	Boundary conditions.....	84
5.3	Results and Discussions	85
5.3.1	Steady state jet without tube bundle.....	85
5.3.2	Impulsively started jet without tube bundle.....	87
5.3.2.1	Validation with experimental data of scaled facility.....	87
5.3.2.2	Validation with experimental data from literature	90
5.3.3	Impulsively started jet with tube bundle.....	91
5.3.3.1	Axial tube bundle in scaled facility	91
5.3.3.2	Cross tube bundle in scaled facility	93
5.3.3.3	Full scale experimental setup.....	96
5.4	Conclusions.....	98
6	CFD ANALYSIS OF MODERATOR FLOW AND TEMPERATURE DISTRIBUTION	101
6.1	Introduction	101
6.2	Computational Fluid Dynamics	103
6.2.1	Flow geometry	103
6.2.2	Governing equations.....	105
6.2.3	Model assumptions	106
6.2.4	Boundary condition and volumetric heat generation	106
6.2.5	Method of solution.....	108
6.2.6	Grid independence.....	108

6.3	Results and discussions.....	109
6.3.1	Validation of CFD model.....	110
6.3.2	Moderator flow and temperature fields inside calandria vessel.....	119
6.3.2.1	Normal operating condition having spatial variation of heat generation ..	119
6.3.2.2	Effect of volumetric heat distribution.....	122
6.3.2.3	Effect of Archimedes number.....	126
6.3.2.4	CFD Analysis of full calandria.....	127
6.4	Conclusions.....	130
7	POISON INJECTION IN AHWR CALANDRIA: FLOW PATTERN AND MIXING CHARACTERISTICS.....	131
7.1	Introduction.....	131
7.2	Computational Fluid Dynamics.....	132
7.2.1	Flow geometry.....	132
7.2.2	Governing equations.....	135
7.2.3	Model assumptions.....	135
7.2.4	Method of solution.....	135
7.2.5	Boundary conditions.....	136
7.2.6	Grid independence studies.....	136
7.3	Results and Discussions.....	137
7.3.1	Effect of calandria tubes on poison jet progression.....	138
7.3.2	Effect of neighbouring group of injection nozzles on poison jet progression.....	143
7.3.3	Poison distribution in calandria.....	145
7.3.3.1	In stagnant moderator condition.....	146
7.3.3.2	Effect of moderator flow distribution without heat generation.....	152
7.3.3.3	Effect of moderator flow distribution with heat generation.....	152
7.4	Conclusions.....	154
8	CONCLUSIONS AND RECOMMENDATIONS FOR FUTURE WORK.....	155
	REFERENCES.....	159

Synopsis

Major augmentation of power production capacity is essential for sustainable growth of India. Nuclear power is considered as a "Clean and Green" energy source, which can cope with large demand of energy in near future. Safety of nuclear reactors is critical for such a large scale development of nuclear energy. The design and operation of nuclear reactors ensure that the likelihood of malfunction leading to unsafe conditions is extremely small. However, primary initiating events leading to unsafe states are postulated and safety systems are provided to minimise the impact of such failures. The reactor protection system has the capability to detect unsafe plant conditions and to initiate safety actions automatically to actuate the safety systems necessary for achieving and maintaining safe plant conditions. Shut Down System (SDS) is one of the safety systems which brings the reactor to safe shutdown state that is subcritical state from any operational state including design basis accidents and can hold the reactor in subcritical state even for the most reactive conditions of the reactor core. This function is usually achieved by adding a neutron absorbing material in reactor core.

Considering the importance of shut down system, as per guidelines by International Atomic Energy Agency on Safety of Nuclear Power Plants: Design (2016), at least two diverse and independent shut down systems are required for nuclear reactors. At least one of the two different shut down systems shall be capable, on its own, of maintaining the reactor subcritical with an adequate margin and with high reliability, even for the most reactive conditions of the reactor core. In most reactors, the two types of shut down systems used are shut off rods and liquid poison injection.

India is developing Advanced Heavy Water Reactor (AHWR) which will demonstrate enhanced safety. AHWR is a 300 MWe vertical, pressure tube type, boiling light water cooled, and heavy water moderated reactor. In AHWR, the reactor core is housed in calandria, a cylindrical stainless steel vessel containing heavy water, which acts as moderator and reflector. In AHWR two active, independent, functionally diverse, fast acting shut down systems are provided. Shut Down System-1 (SDS-1) consists of mechanical shut off rods and Shut Down System-2 (SDS-2) is based on liquid poison injection into the moderator. In SDS-2, gadolinium nitrate solution acts as neutronic poison, which is injected in heavy water moderator through a set of nozzles located inside calandria vessel. This poison injection into moderator inside calandria is expected to take place in a very short time to shut down the reactor. The effectiveness of the system depends on the dispersion of liquid poison in the moderator throughout the calandria in a short time. Based on the dispersion of poison, absorption of neutrons will take place and the reactor will shut down. As SDS-2 is critical for the safety of the plant, detailed knowledge of poison distribution in calandria under given operating condition is required.

SDS-2 consists of helium storage tank, an array of quick opening valves, poison tanks, connecting piping and injection tubes. High pressure helium is stored in a tank known as helium storage tank, which is connected to the eight poison tanks through an array of quick opening valves. These valves are opened following a reactor trip signal and consequently the high pressure helium forces the poison in poison tanks into the calandria through the injection tubes. There are eight injection tubes located inside calandria, connected to eight poison tanks through connecting pipe lines separately. These injection tubes contain injection nozzles of diameter 6 mm each. There are four injection nozzles located centrally between calandria tubes forming a group of injection nozzles. Each injection tube has 20 such groups of injection nozzles and hence there are total 640

injection nozzles in eight injection tubes for poison injection in calandria. When there is no injection of poison, each tank is kept at the moderator cover gas pressure by connecting line between poison tanks and calandria. In these conditions, there is a natural boundary between the moderator and the liquid poison solution. This boundary is usually outside the core and is known as Poison Moderator Interface (PMI).

Injection nozzles permit the liquid poison to flow into the calandria as submerged jets which get merged to form continuous poison curtain in the moderator. AHWR calandria is a vertical cylindrical tank having a total height of 5 m, filled with heavy water. The calandria vessel comprises a main shell with a diameter of 6.9 m and a height 3.5 m. At each end of the main shell there is a smaller diameter sub-shell with a diameter of 6.3 m and height of 0.75 m and these regions are known as top and bottom reflectors. Inside the calandria, a total of 513 calandria tubes having diameter of 0.168 m are arranged vertically in a square pitch (p) having p/d of 1.34 to form a lattice array. Thus, starting from finding injection nozzles velocity distribution and injection poison starting time along the length of injection tube, estimating the poison distribution from 640 injection jets of diameter 6 mm having velocity around 45 m/s in 5 m high calandria having 513 calandria tubes is complex modelling problem. Along with this, the effect of moderator flow distribution with spatial distribution of heat generation on poison distribution should also be accounted. Based on the literature review, it can be concluded that number of issues needed to be addressed to estimate the liquid poison distribution in AHWR calandria like (i) formulation for transient flow distribution from lateral holes in a injection tube, (ii) development of semi-empirical equation for predicting the progression of poison jet considering the effect of dead time, (iii) generation of moderator flow and temperature fields by considering spatial distribution of volumetric heat generation and (iv) transient study of liquid poison distribution in AHWR calandria with calandria tube and moderator flow. Under these conditions, an

attempt has been made to understand the flow and mixing characteristics inside calandria vessel. The study performed consists of five steps.

In the first step, a transient 1-D computer code (COPJET) is developed to predict injection velocity and poison initiation time from each injection nozzle. This output is used as input parameters for CFD analysis. Computer code COPJET does the simulation of gas expansion, system piping, injection tubes and progress of the poison jet with time. A semi-empirical equation is formulated for progression of poison jet. As PMI is maintained at some distance from the calandria, injection of the poison takes place after exhaustion of moderator present between PMI and injection tube. Due to this, poison front moves faster compared to impulsively started jet but slower than steady state jet due to inertia effect of partially developed jet flow. All these effects are included in semi-empirical equation developed from the experimental studies available in the literature. The computer code developed has been validated with the experimental data available in the literature.

In the second step, experimental studies are performed on transient poison injection in presence of calandria tubes. Based on the survey of published literature it was found that the experimental studies on jet injection in presence of tube bundle are not addressed sufficiently. The location and number of poison jets are design parameters, which can greatly affect dispersion, and penetration of poison jets in calandria. The experiments are performed in the presence of tube bundles with respect to poison jet. Two different orientations of the bundles have been used to study poison jet progression. Results show that lateral spread of jet is more in cross bundle compared to axial bundle case. In axial bundle injection, the bundle has a tendency to maintain jet core in injection path whereas; cross bundle offers flow resistance and dissipate the jet energy faster.

In the third step, a module is developed in open source CFD code OpenFOAM to simulate transient poison jet injection at nozzle inlets using source term. There are 513 calandria tubes and 640 poison injection nozzles in calandria. In such complex geometry, in order to facilitate the grid generation source term approach is used for modelling inlet conditions. The inlet conditions have been taken care by defining the source terms in mass, momentum, energy and species equations. Modified model is validated with the experimental results obtained in second step. In addition to this, velocity distribution in steady state jet is also used for validation. This developed and validated source term module will be used for defining the poison jet injection through the nozzles in calandria.

In the fourth step, estimation of moderator flow and temperature distribution in vertical calandria vessel of the AHWR using OpenFOAM is performed. A large amount of heat (50MW) is generated within the moderator mainly due to neutron slowing down and attenuation of gamma radiation. To remove this energy, moderator is kept under continuous circulation through a heat removal system. Hence, to estimate the liquid poison distribution in AHWR calandria, moderator flow and its temperature field should be known. Analysis is performed with spatial variation of heat generation in calandria. Effect of Archimedes number on temperature distribution has been also studied. The flow and temperature distribution of moderator has been used as input for further analysis of poison distribution in calandria.

In the fifth step, CFD analysis of liquid poison injection and its dispersion into the moderator in calandria is performed. For modelling of poison distribution in calandria, inputs from previous steps are taken. Three cases are considered in poison distribution analysis. In the first case, poison distribution is simulated in stagnant moderator condition. In the second case, effect of moderator flow without moderator heat generation on poison distribution is studied. In the last case, effect of moderator flow with moderator heat

generation on poison distribution is studied. In addition to this, effects of calandria tubes and neighbouring injection nozzles on poison jet progression are studied. Results of CFD simulations are compared with the results obtained from the analysis performed with computer code COPJET. Based on the above studies it is found that shut down system-2 of AHWR works effectively with the configuration considered in the studies.

List of Figures

Figure 1.1: Vertical cross-sectional view of the AHWR reactor block.....	4
Figure 1.2: Simplified schematic diagram of the AHWR	4
Figure 1.3: AHWR fuel cluster	5
Figure 1.4: Schematic of Shut Down System -2 (SDS-2)	11
Figure 1.5: Details of AHWR calandria and calandria tubes.....	13
Figure 3.1: Schematic of SDS-2 injection tubes (Elevation view without internals)	36
Figure 3.2: Schematic of a group of jet nozzles at a typical lattice location.....	36
Figure 3.3: Schematic of injection tube	41
Figure 3.4: Progression of impulsively started poison jet with time	45
Figure 3.5: Effect of dead time of poison jet progression.....	46
Figure 3.6: Comparison of predicted lateral flow distribution with experimental data.....	49
Figure 3.7: Comparison of COPJET predicted progression of poison jet with experiment data and CFD simulation	51
Figure 3.8: Schematic of injection tube with injection nozzle group number.....	53
Figure 3.9: Poison injection starting time for different nozzle location.....	53
Figure 3.10: Variation of mass flow rate and gas tank pressure with time.....	54
Figure 3.11: Progression of poison jet at different time	55
Figure 3.12: Injection velocity for 11 th group of injection nozzle	55
Figure 4.1: Schematic layout of experimental setup	67
Figure 4.2: Schematic arrangement of acrylic tubes for (a) axial bundle and (b) cross bundle in scaled facility	68
Figure 4.3: Tube bundle arrangement in transparent water tank.....	69
Figure 4.4: Schematic of full scale experimental setup for jet injection	70
Figure 4.5: Image captured by high speed camera (a) actual image (b) processed image	72
Figure 4.6: Jet spread angle of free jet for different Reynolds number	73
Figure 4.7: Progression of 2 mm diameter free jet with time (Re = 15000)	73
Figure 4.8: Progression of free jet with time	74
Figure 4.9: Progression of 2 mm diameter jet in axial bundle with time (Re = 15000)	75
Figure 4.10: Progression of poison jet through axial bundle	75
Figure 4.11: Non-dimensional progression of poison jet through axial bundle.....	76

Figure 4.12: Progression of 2 mm diameter jet in cross bundle with time ($Re = 15000$).....	77
Figure 4.13: Progression of poison jet through cross bundle	77
Figure 4.14: Non-dimensional progression of poison jet through cross bundle.....	78
Figure 4.15: Full scale poison jet facility-Jet cross first row of calandria tubes.....	79
Figure 4.16: Progression of poison jet in full scale experimental setup.....	79
Figure 5.1: Effect of grid size on CFD predicted axial velocity of steady state jet.....	86
Figure 5.2: Comparison of CFD predicted axial velocity with correlation given by Abramovich (1963) for steady state jet	86
Figure 5.3: Comparison of CFD predicted radial velocity with Trupel steady state jet experiments (1915).....	87
Figure 5.4: Effect of grid size on CFD predicted progression of poison jet for 2mm free jet	88
Figure 5.5: Effect of cut-off concentration on progression of poison jet for 2mm free jet... ..	89
Figure 5.6: Comparison of CFD predicted progression of poison jet with experiment for 2 mm free jet.....	89
Figure 5.7: Effect of grid size on CFD predicted progression of poison jet for 6.35 mm free jet	90
Figure 5.8: Comparison of CFD predicted progression of poison jet with experiment results of Johari et al. (1997) for 6.35 mm free jet.....	91
Figure 5.9: Comparison of CFD predicted progression of poison jet with experiment for axial bundle in scaled facility.....	92
Figure 5.10: Comparison of CFD predicted progression of poison jet with experiment for 2 mm axial jet at $t = 0.7$ s.....	93
Figure 5.11: Comparison of CFD predicted progression of poison jet with experiment for 2 mm axial jet at $t = 1$ s.....	93
Figure 5.12: Comparison of CFD predicted progression of poison jet with experiment for cross bundle in scaled facility.....	94
Figure 5.13: Comparison of CFD predicted progression of poison jet with experiment for 2 mm cross jet at $t = 0.7$ s	95
Figure 5.14: Comparison of CFD predicted progression of poison jet with experiment for 2 mm cross jet at $t = 1$ s.....	95
Figure 5.15: Mesh details of quarter symmetry model for poison injection in cross bundle in full scaled facility.....	96
Figure 5.16: CFD predicted velocity and poison concentration contours for full scale facility	97
Figure 5.17: Comparison of jet penetration length based on velocity and concentration from CFD simulation and full scale experimental data	98
Figure 6.1: Schematic of vertical calandria vessel without internals (elevation)	102
Figure 6.2: Schematic of moderator inlet header in vertical calandria vessel.....	102
Figure 6.3: Simplified diagram of moderator circuit.....	103

Figure 6.4: Quarter symmetry solid model of calandria.....	104
Figure 6.5: Distribution of non-uniform volumetric heat generation at various vertical locations.....	107
Figure 6.6: Distribution of non-uniform volumetric heat generation at various horizontal locations.....	107
Figure 6.7: Computational mesh of calandria.....	109
Figure 6.8: Effect of grid size on axial distribution of temperature in calandria vessel.....	109
Figure 6.9: Schematic of calandria model in SPEL experimental facility.....	110
Figure 6.10: Effect of grid size on CFD predicted temperature along prob 4 of SPEL experiment.....	114
Figure 6.11: Velocity and temperature distribution in axial mid-plane of SPEL experimental setup.....	115
Figure 6.12: Predicted vertical component of velocity along ports 4 and 5 of SPEL experimental setup.....	116
Figure 6.13: Comparison of predicted results with experimental data of SPEL experimental facility.....	118
Figure 6.14: Distribution of volumetric heat generation in calandria vessel.....	120
Figure 6.15: Velocity distribution at inlet and outlet nozzle plane of calandria vessel.....	120
Figure 6.16: Velocity distribution in calandria vessel along the axis of inlet nozzles.....	121
Figure 6.17: Velocity and temperature distribution in calandria vessel under normal operating condition at plane $x^*=0.5$	122
Figure 6.18: Effect of volumetric heat generation distribution on vertical component of velocity along axis of calandria vessel.....	123
Figure 6.19: Distribution of vertical component of velocity at plane $z = 2.5$ m.....	124
Figure 6.20: Effect of volumetric heat generation distribution on temperature distribution.....	125
Figure 6.21: Effect of volumetric heat generation distribution on temperature distribution in calandria vessel.....	125
Figure 6.22: Effect of Archimedes number on maximum and volumetric average moderator temperature in calandria vessel.....	126
Figure 6.23: Solid model of full calandria.....	128
Figure 6.24: Temperature distribution in three-fourth section view of calandria.....	128
Figure 6.25: Velocity distribution in three-fourth section view of calandria.....	129
Figure 6.26: Comparison of centre line temperature of full calandria model with one-fourth model.....	129
Figure 7.1: Schematic of SDS-2 injection tubes.....	134
Figure 7.2: Schematic arrangement of jet nozzles in typical lattice location.....	135
Figure 7.3: Effect of grid size on CFD predicted progression of poison jet.....	137
Figure 7.4: Model grid details for a lattice location.....	138

Figure 7.5: Poison jet progression with time at plane $x = 2.5 p$	139
Figure 7.6: Poison jet progression with time at plane $y = 3.5 p$	140
Figure 7.7: Poison jet progression at plane $z = 2 m$	141
Figure 7.8: Comparison of OpenFOAM and COPJET prediction for 11 th group of injection nozzle	142
Figure 7.9: Comparison of OpenFOAM and COPJET predicted progression of poison jet along the injection tube	142
Figure 7.10: Domain details for full injection tube without calandria tubes	143
Figure 7.11: Poison jet progression with time at plane $y = 0$	144
Figure 7.12: Comparison of OpenFOAM predicted progression of poison jet with and without neighbouring group	145
Figure 7.13: Time progression of poison at plane $x = 0.5p$	147
Figure 7.14: Flow pattern and concentration distribution at various vertical planes at 2 s ..	148
Figure 7.15: Concentration distribution at various horizontal planes at 2 s	149
Figure 7.16: Progression of poison jet for injection tube at $y = -3.5p$ with time	151
Figure 7.17: Poison mixing characteristics with time	151
Figure 7.18: Temperature distribution at various vertical planes at 2 s	153

List of Tables

Table 2.1: Summary of previous work.....	28
Table 3.1: Experimental conditions for impulsively started turbulent jets	44
Table 3.2: Limiting cases for progression of poison jet with delay injection.....	47
Table 3.3: Process parameters for analysis of SDS-2 poison injection.....	52
Table 5.1: Governing equations for CFD.....	84
Table 6.1: Governing equations for steady state incompressible buoyant flow.....	105
Table 6.2: Non dimensional governing equations of SPEL and AHWR.....	112
Table 6.3: Order of magnitude of non dimensional equations.....	113

Nomenclature

A	flow area of piping (m ²)
A_{IT}	flow area of injection tube (m ²)
A_n	flow area of injection nozzle per unit length (m)
Ar	Archimedes number (-)
C	concentration (-)
c_1, c_2 and c_3	constants (-)
C_o	initial concentration (-)
c_p	specific heat of fluid (J kg ⁻¹ K ⁻¹)
$C_\mu, C_{\varepsilon 1}$ and $C_{\varepsilon 2}$	standard k ε turbulence model constant (-)
d	diameter of calandria tube (m)
D	pipe diameter (m)
D_{AB}	diffusivity of species A in B (m ² s ⁻¹)
D_{jet}	diameter of jet (m)
d_n	injection nozzle diameter (m)
D_{Tank}	diameter of tank (m)
f	friction factor (-)
g	gravitational acceleration (m s ⁻²)
G_k	generation of turbulence kinetic energy due to the mean velocity gradients (kg m ⁻¹ s ⁻³)
g_x	gravitational acceleration in x-direction (m s ⁻²)
H	vertical dimension of vessel (m)
h	elevation (m)
i	axial location number of hole in injection tube
K	local loss coefficient (-)

k	turbulent kinetic energy ($\text{m}^2 \text{s}^{-2}$)
k'	momentum recovery factor (-)
kc	thermal conductivity ($\text{W m}^{-1}\text{K}^{-1}$)
kc_{eff}	effective thermal conductivity ($\text{W m}^{-1}\text{K}^{-1}$)
K_n	local loss coefficient of injection nozzle (-)
L	length of piping (m)
L_{inlet}	length of inlet nozzle (m)
L_{outlet}	length of outlet nozzle (m)
L_{Tank}	length of tank (m)
\dot{m}	mass flow rate (kg/s)
N	last axial location number of hole in injection tube (-)
N_{Tube}	number of tubes in tank (-)
OD_{Tube}	outer diameter of tube (m)
P	gas tank pressure (Pa)
pr	pressure (Pa)
p	lattice pitch (m)
Δp	pressure difference (Pa)
p_r	pressure recovery (Pa)
p_f	frictional pressure (Pa)
P_g	gas tank pressure (Pa)
P_i	initial gas tank pressure (Pa)
p_{IT}	pressure in injection tube (Pa)
p_o	pressure outside injection tube (Pa)
pr	pressure (Pa)
Pr	Prandtl number (-)
pr^*	non dimensional pressure (-)

P_{sp_it}	pressure at junction of system piping and injection tube (pa)
q^*	non dimensional volumetric heat generation (-)
\dot{q}	volumetric heat generation (W m^{-3})
r	radius (m)
$r_{1/2}$	radial distance at which velocity is half of the centre velocity (m)
Re	Reynolds number (-)
S_c and S_p	source term
Sc	Schmidt number (-)
Sc_t	turbulent Schmidt number (-)
$shgvol$	spatial distribution of volumetric heat generation (W m^{-3})
t	time (s)
T	temperature (K)
t^*	non-dimensional poison jet time (s)
T^*	non dimensional temperature (-)
T_{avg}^*	non dimensional volumetric average temperature (-)
T_{max}^*	non dimensional maximum temperature (-)
t_{dead}	dead time (s)
T_{inlet}	inlet temperature (K)
T_{outlet}	outlet temperature (K)
t_p	injection time of poison jet (s)
T_{ref}	reference temperature (K)
t_s	total injection time of jet (s)
u	velocity (m s^{-1})
u^*	non dimensional velocity (-)
U_c	jet centre line velocity (m s^{-1})
u_{IT}	velocity in injection tube (m/s)

U_o	average inlet nozzle velocity (m s^{-1})
V_g	gas tank volume (m^3)
V_i	initial gas tank volume (m^3)
Vol	volume (m^3)
$Volume_{dead}$	volume between poison moderator interface and first injection nozzle (m^3)
v_r	radial velocity (m s^{-1})
v_ϕ	circumferential velocity (m s^{-1})
v_z	z direction velocity (m s^{-1})
W_{inlet}	width of inlet nozzle (m)
W_{outlet}	width of outlet nozzle (m)
x	distance in x direction (m)
x^*	normalised x (-)
y	distance in y direction (m)
y^*	normalised y (-)
Y_A	concentration of species A (-)
z	distance in z direction (m)
z^*	normalised distance in z direction (-)

Greeks

ϕ	general variable (-)
Δ	difference in a quantity e.g. temperature
β	thermal expansion coefficient (K^{-1})
γ	adiabatic index
ε	turbulent kinetic energy dissipation rate ($\text{m}^2 \text{s}^{-3}$)
θ	half jet angle (degree)

μ	viscosity (N s m^{-2})
μ_t	turbulent viscosity (N s m^{-2})
ν	kinematic viscosity ($\text{m}^2 \text{s}^{-1}$)
ν_t	turbulent kinematic viscosity ($\text{m}^2 \text{s}^{-1}$)
ρ	density (kg m^{-3})
σ_k	turbulent Prandtl number for energy dissipation rate (-)
σ_ε	turbulent Prandtl number for turbulent kinetic energy (-)
τ	shear stress (N m^{-2})

Subscript

<i>avg</i>	average
<i>eff</i>	effective
<i>max</i>	maximum
<i>ref</i>	reference

Chapter 1

INTRODUCTION

1.1 Background

Worldwide experience indicates a strong correlation between the growth of a country and per capita energy consumption. Even with total installed capacity of 330 GWe (Central electricity authority - India, 2017), per capita energy consumption in India stands at 1075 kWh/annum, which is one-third of the world average. Therefore, major augmentation of power production capacity is essential for sustainable growth of India. Currently, fossil fuels are the mainstay of electricity generation in India with more than two-third of total installed capacity. Large scale use of fossil fuels poses serious threats to the environment due to the emission of Green House Gases (GHG) and concerns related to environmental pollution. Therefore, there is greater emphasis on green energy sources with low emission of GHG.

Nuclear power is considered as a "Clean and Green" energy source, which can cope with the large demand of energy in near future. Considering this, Government of India is continuously pursuing to increase the share of nuclear energy in India's energy generation. Safety of nuclear reactors is critical for large scale development of nuclear energy. Bhabha Atomic Research Centre (BARC) is developing Advanced Heavy Water Reactor (AHWR) which will demonstrate enhanced safety compared to current generation nuclear reactors.

AHWR incorporates many inherent safety characteristics and passive safety features along with improved performance reliability of active safety system. AHWR will provide long term energy security by utilising the large thorium reserves in India for generating commercial nuclear power. In the present work, a study related to the performance of the liquid poison injection system of AHWR which is the part of reactor protection system is taken up.

1.2 Indian Nuclear Power Program

Indian nuclear power program is a three-stage program, comprises Pressurised Heavy Water Reactors (PHWR) in the first stage, Fast Breeder Reactors (FBRs) in the second stage, and thorium-based systems in the third stage. It is a sequential program based on a closed fuel cycle where the spent fuel of one stage is reprocessed to produce fuel for the next stage, it multiplies manifold the energy potential of the fuel and greatly reduces the quantity of waste. Closed fuel cycle aims at the optimum utilisation of the country's nuclear resources of limited uranium and abundant thorium. It is thus a single-basket solution for meeting the country's energy needs in a sustainable manner, thereby securing the energy future in the long term. Currently, as of 2017, there are 21 nuclear power reactors in operation with a gross capacity of 6780 MWe; out of these, two are Boiling Water Reactor (BWR), two are Russian pressurised water reactor (VVER) and rest are Pressure Heavy Water Reactors (PHWR).

Four indigenous design 700 MWe PHWRs with a total capacity of 2800 MWe are under construction, two reactors of 700 MWe at each of the existing sites, Kakrapar in Gujarat state and Rawatbhata in Rajasthan state respectively. In addition to this Prototype Fast Breeder Reactor (PFBR) is in advanced stage of construction at Kalpakam, Tamilnadu.

1.3 Brief description of AHWR

The AHWR is a 300 MWe vertical, pressure tube type, boiling light water cooled, and heavy water moderated reactor (Sinha and Kakodkar, 2006). In AHWR, the reactor core is housed in calandria, a cylindrical stainless steel vessel containing heavy water, which acts as moderator and reflector. A vertical cross-sectional view of the AHWR reactor block is shown in Figure 1.1. The calandria, located below ground level, contains vertical coolant channels in which the boiling light water coolant picks up heat from fuel assemblies suspended inside the pressure tubes. Boiling light water is transported to the steam drum by Main Heat Transport (MHT) System. MHT system consists of a common circular inlet header from which several feeders branch out to the coolant channels in the core. The outlets from the coolant channels are connected to a number of tail pipes carrying steam-water mixture from the individual coolant channels to four steam drums. Steam is separated from the steam-water mixture in steam drums and is supplied to the turbine. Four downcomers connect each steam drum to the inlet header. Circulation of coolant flow in MHT system is maintained by natural circulation without any pump under operating and shutdown conditions. Thus, all scenarios initiating from non-availability of main pumps are, therefore, excluded. A simplified schematic diagram of the AHWR with and major systems is shown in Figure 1.2.

The reactor fuel cluster is shown in Figure 1.3. The fuel cluster is a cylindrical assembly of about 4300 mm in length and 118 mm nominal diameter. It has 54 fuel pins which are arranged in three concentric rings - 12 pins in the inner ring, 18 pins in the middle ring and 24 pins in the outer ring. The fuel pins contain (Th-²³³U) O₂ and (Th-Pu) O₂ pins with Zr-2 cladding and are assembled into a cluster by the top and bottom tie-plates, spacers and central rod acting as the tie-rod.

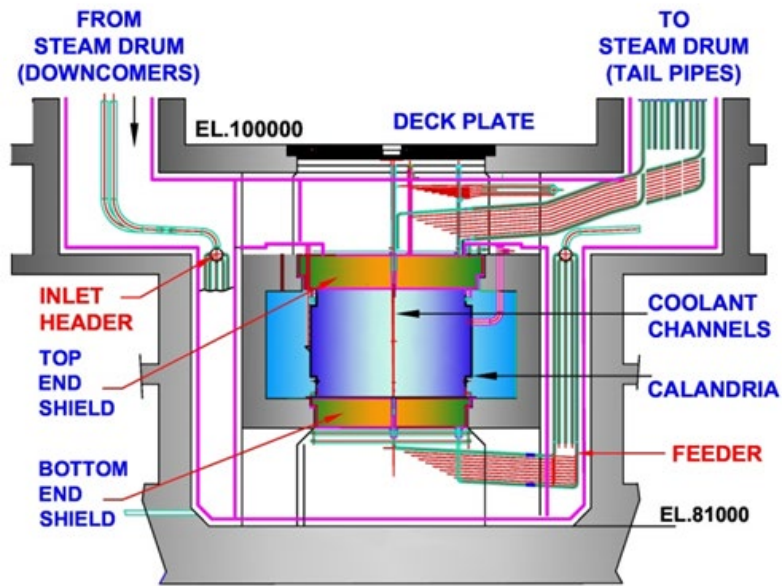


Figure 1.1: Vertical cross-sectional view of the AHWR reactor block

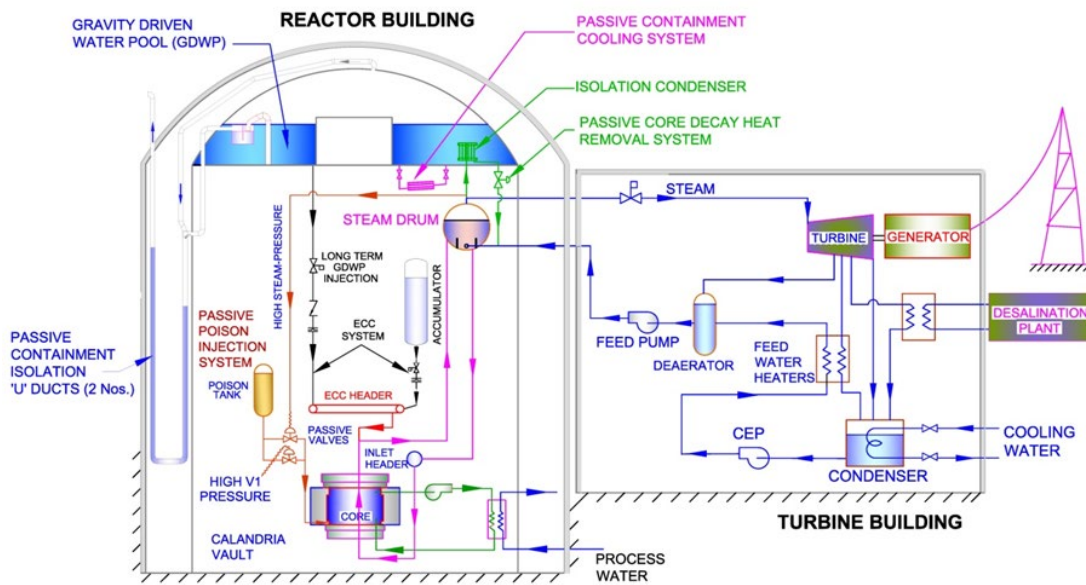


Figure 1.2: Simplified schematic diagram of the AHWR

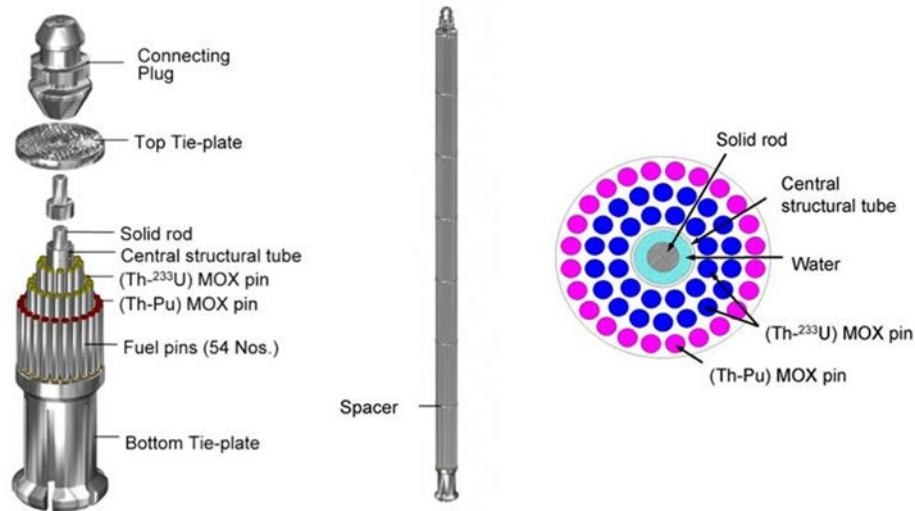


Figure 1.3: AHWR fuel cluster

1.4 Reactor Protection System

The design and operation of nuclear reactors ensure that the likely hood of malfunction, leading to unsafe condition is small, such failures are still postulated and safety systems are provided to minimise the impact of such failures. The reactor protection system has the capability to detect unsafe plant conditions and to initiate safety actions automatically to actuate the safety systems necessary for achieving and maintaining safe plant conditions. Shut Down System (SDS) is one of the safety systems which brings the reactor to safe shutdown state that is the subcritical state from any operational state including design basis accidents and can hold the reactor in a subcritical state even for the most reactive conditions of the reactor core. This function is usually achieved by adding a neutron absorbing material in the reactor core. Shut Down System may be required during major process system failures that cannot be safely handled by the Reactor Regulating System (RRS), or other safety related systems.

As shut down systems are so essential for reactor safety, the reactor cannot be operated if any of the shut down systems are not functional. Sufficient shutdown capability has to be available at all times to safely terminate any unit failure or combination of

failures. The shutdown systems protect the unit against two major types of process system failures:

- a) Loss of reactor control.
- b) Loss of reactor heat sink effectiveness.

Some of the possible causes of loss of reactor control can be:

- i. Removal of negative reactivity from the core (driving control rods out, etc).
- ii. Failure of the reactor regulating control program.

Some of the possible causes of loss of heat sink can be:

- i. Loss of coolant accident (LOCA).
- ii. Loss of Class IV power.
- iii. Loss of secondary heat sink (loss of boiler feedwater).

Apart from above clauses, the shut down system may also be invoked on demand as per requirement for shutdown by manual means.

1.4.1 Types of shut down systems

Considering the importance of shut down system, as per International Atomic Energy Agency Safety Standards on Safety of Nuclear Power Plants: Design (2016), at least two diverse and independent shut down systems are required for nuclear reactors. Shut down system shall be provided to ensure that there is a capability to shut down the reactor of the nuclear power plant in operational states and in accident conditions, and that the shutdown condition can be maintained even for the most reactive conditions of the reactor core.

At least one of the two different shut down systems shall be capable, on its own, of maintaining the reactor subcritical by an adequate margin and with high reliability, even for the most reactive conditions of the reactor core. In most reactors following types of shut down systems used are:

- a) Shut-Off Rods (SORs) - This shut down system uses shut-off rods having a strong neutron absorber encased in stainless steel, which drops under gravity or lifts by hydrostatic pressure, into the core. A vertical guide is located within the core to guide the rods. These rods are normally held above the core by electrically energised clutches, located on the reactivity mechanism desk. When this shut down system is actuated, the clutches holding the rods above the core de-energise, allowing the rods to fall into the core. The initial acceleration is assisted by springs, which are compressed by the retracted rods. This makes the reactor subcritical, and thus, the reactor is shut down.
- b) Liquid Poison Injection - The liquid poison injection system operates by injecting solution of neutron absorber, as poison into the moderator. The insertion of poison into the core renders the nuclear reactor subcritical from all operational states and accident conditions within the design basis.

It is possible to quickly reset the shutoff rod trip (if the cause of the trip is known and corrected) by bringing the SORs at initial position. However, recovery after a liquid poison injection trip is delayed, as the poison is to be separated from moderator/coolant by chemical means. This makes actuation of shut off rods a preferred choice for the reactor shut down. Therefore, in most designs, Shut off rod is called SDS-1 and liquid poison injection is called SDS-2

Each SDS is functionally as well as physically independent. Functional independence is achieved by designing the two shut down systems on two different

principles: mechanical insertion of a strong neutron absorber and chemical poisoning of the moderator by a neutron absorber. Physical independence in calandria is achieved by the vertical insertion of shut-off rods while the liquid poison is injected through horizontal tubes into the core.

To increase its reliability, the following three features are incorporated in a typical shut down system:

- a) Common cause failures: Complete separation of control and instrumentation routes of SDS along with independent services supplies like power supplies, instrument air etc. are routed through physically separate routes. This approach reduces the probability of the common cause failures. Concepts of diversity, redundancy, physical separation and functional independence have to be applied to achieve the necessary reliability of system.
- b) Single failure criterion: Shut down system is configured in a triplicated channel format (redundancy). Shutdown action is initiated when the set-point of any two of the three shutdown (trip) channels are exceeded by any unit variable or combination of variables. If a component fails in unsafe state (i.e. does not trip), there are still two channels which will cause a trip. In case of a spurious signal from one of the channel, the reactor does not trip, because one additional channel is required to trip.

This triplication has the following advantages:

- On-line testing and maintenance of individual channels is possible.
 - The unit will not shut down due to a single spurious trip signal.
 - One channel can fail without disabling the system.
- c) Quality components: The selection of quality components for the shutdown system also increases the probability that the system will function as designed.

1.4.2 Shut down system in various reactors

The design and implementation of shut down system is different in different reactors although the underlying principle remains same. A brief summary of philosophy employed for shut down systems of various commercial power reactors is given below:-

1. Pressurised Water Reactor (PWR)

In PWR, when reactor trip signal is received, the electromagnetic clutches holding up the control rods (working as shut off rods) are de-energized by an automatic cut-off of electric power. The rods then drop into the reactor core. Borated water (boric acid solution) can also be injected in core from the chemical and volume control system to shut down the reactor.

2. Boiling Water Reactor (BWR)

In a BWR, a rapid shut down is achieved by forcing the control rods (working as shut off rods) up into the core by hydrostatic pressure. The shutdown of the reactor can also be achieved by injection of aqueous solution of sodium pentaborate.

3. Pressure tube type heavy water moderated reactor

There are two fast and diverse shut down systems in pressure tube type heavy water moderated reactors. Shut Down System-1 (SDS-1) consists of mechanical shut off rods. Shut Down System-2 (SDS-2) is based on liquid poison injection into the moderator.

Insertion of the SORs is ensured by an electromagnetic clutch in the drive mechanism that releases on the loss of electrical power. Then a spring assisted gravity fall acts on the vertically oriented SORs.

In SDS-2, liquid poison is injected into the moderator. Gadolinium nitrate solution acts as a neutronic poison, which is injected in heavy water moderator through a set of nozzles located inside calandria vessel.

1.5 Shut Down System-2 of AHWR

In Advanced Heavy Water Reactor (AHWR) (Sinha and Kakodkar, 2006) two active, independent, functionally diverse, fast acting shut down systems are provided. Shut Down System-1 (SDS-1) consists of mechanical shut off rods and Shut Down System-2 (SDS-2) is based on liquid poison injection into the moderator. Each shut down system is fully capable of independently shutting down the reactor and keeping it under safe shutdown condition for a prolonged period. Following text gives description of SDS-2.

SDS-2 is based on liquid poison injection into the moderator. Poison injection into moderator inside calandria is expected to take place in a prescribed very short period to shut down the reactor. Based on the dispersion of poison, absorption of neutrons will take place and the reactor will shut down. The effectiveness of the system depends on the dispersion of poison in the moderator throughout the calandria in a short time. As SDS-2 is critical for the safety of the plant, detailed understanding of poison distribution in calandria following a trip signal.

SDS-2 consists of helium storage tank, an array of quick opening valves, poison tanks, connecting piping and injection tubes as shown in Figure 1.4. High pressure helium is stored in a tank known as helium storage tank, which is connected to the eight poison tanks through an array of quick opening valves. These valves are opened following a reactor trip signal and consequently, the high pressure helium forces the poison in poison tanks into the calandria through the injection tubes. There are eight injection tubes located inside calandria horizontally connected to respective poison tanks through connecting pipe

lines. These injection tubes contain injection nozzles of diameter 6 mm. There are four injection nozzles located centrally between calandria tubes forming a group of injection nozzles. Each injection tube has 20 such groups of injection nozzles. Hence there are total 640 injection nozzles in eight injection tubes for poison injection in calandria.

When there is no injection of poison, each tank is kept at the moderator cover gas pressure by connecting line between poison tanks and calandria. In these conditions, there is a natural boundary between the moderator and the liquid poison solution. This boundary is usually outside the core and is known as Poison Moderator Interface (PMI) as shown in Figure 1.4.

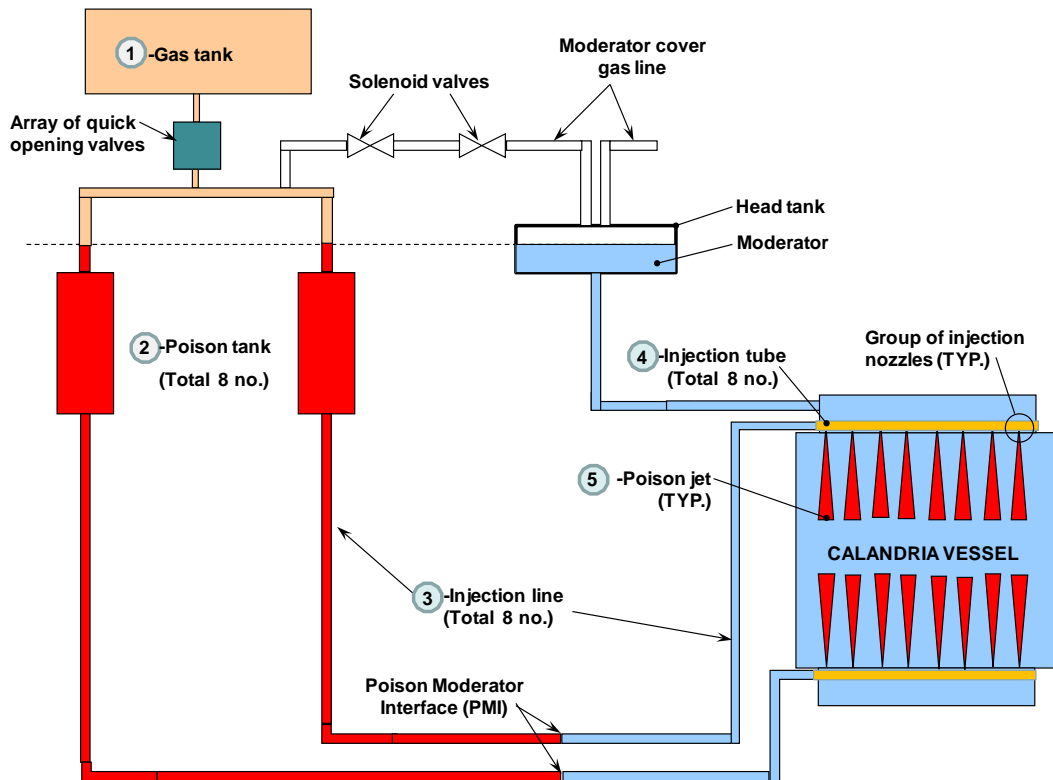


Figure 1.4: Schematic of Shut Down System -2 (SDS-2)

Injection nozzles permit the injection of liquid poison into the calandria as submerged jets which get merged to form continuous poison curtain in the moderator. AHWR calandria is a vertical cylindrical tank having a total height of 5 m, filled with heavy water. The calandria vessel comprises a main shell with a diameter of 6.9 m and a height 3.5 m.

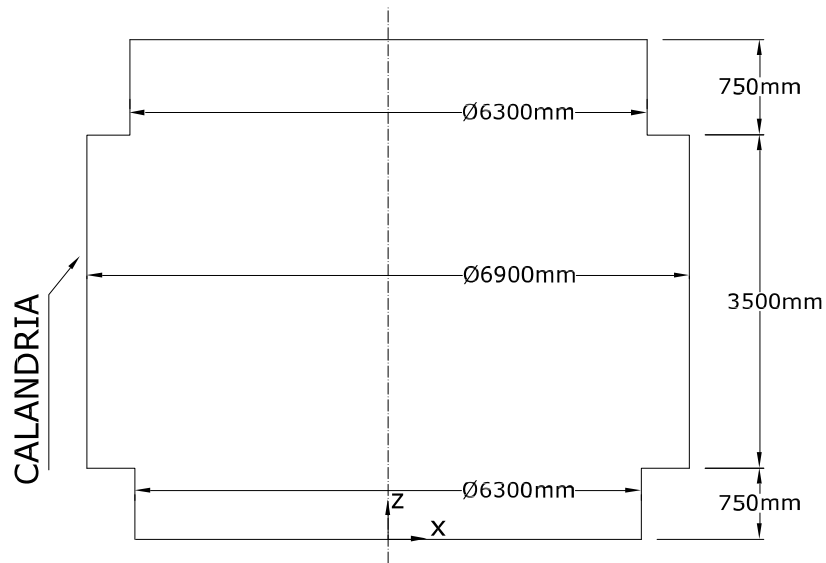
At each end of the main shell there is a smaller diameter sub-shell with a diameter of 6.3 m and height of 0.75 m and these regions are known as top and bottom reflectors. Inside the calandria, a total of 513 calandria tubes having diameter (d) of 0.168 m are arranged vertically in a square pitch (p) having p/d of 1.34 to form a lattice array as shown in Figure 1.5. Thus, starting from finding injection nozzles velocity distribution along the length of injection tube, estimating the poison distribution from 640 injection jets of diameter 6 mm having velocity around 45 m/s in 5 m high calandria having 513 calandria tubes is complex modelling problem. Along with this, the effect of moderator flow distribution with spatial distribution of heat generation should need to be accounted.

1.6 Challenges and Motivation for Present Work

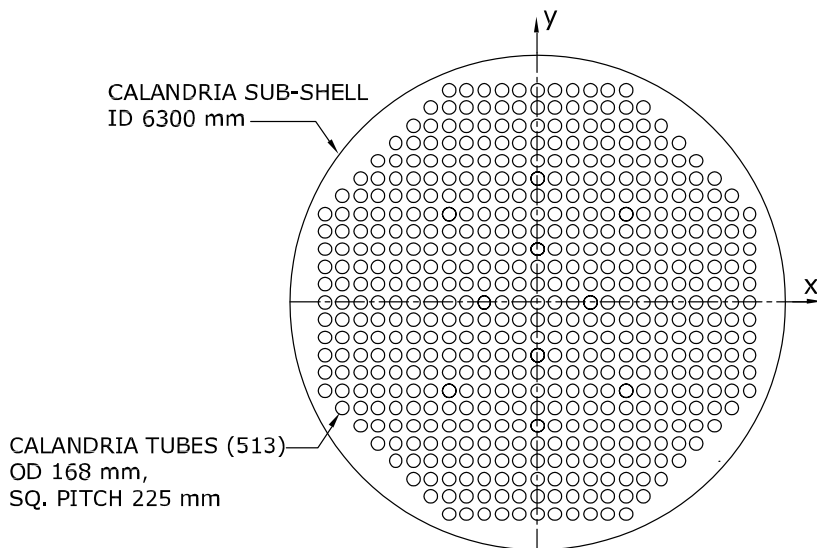
Shut down system is critical safety system of the reactor and its performance is paramount to safety review by the regulatory body. The distribution of poison inside calandria is critical so that desired reactivity worth is achieved. In SDS-1, poison insertion rate and its distribution in core estimated by locations of shut off rods and their drop rate. However, in SDS-2, the details of poison distribution in calandria are required to be estimated. This distribution will be used as input by reactor physics to estimate the negative reactivity insertion rate by liquid poison injection system. Estimation of liquid poison injection presents many challenges. Some of them are described below:-

Calandria Geometry: Internals of calandria are very complex. Calandria has hundreds of calandria tubes arranged in a square pitch (p) to form a lattice array as typically shown in Figure 1.5 (b).

Distribution of poison through perforated tube: A perforated tube is placed inside calandria for injecting poison at various locations in calandria. However, distribution of injected poison along the length of perforated tube is not uniform.



(a) Elevation without internals



(b) Moderator inlet header with calandria tubes

Figure 1.5: Details of AHWR calandria and calandria tubes

Submerged jet: From the perforated tube, liquid poison is injected as submerged jet which has different starting time and velocity along its length.

Number of submerged jets: Number of submerged jets in calandria can be from few hundreds to few thousands.

Interactions of jets: As submerged jet grows, it interacts with other submerged jets and calandria tubes. This makes flow pattern and poison distribution very complex.

Moderator flow distribution: Medium in which the submerged jets are injected is not stagnant. The medium is moderator and it is under circulation to remove nuclear heat generated in process of neutron thermalisation. This nuclear heat is not uniform and it is function of space and state of reactor. Thus, moderator flow and temperature distribution need to be estimated in such complex situation.

Experimental simulation: To simultaneously model all above phenomenon in the experiment is very difficult. Even if it is model, very large number of poison distribution measurements needs to be taken so that reactor physics calculation can done for reactivity worth. Taking such large number of measurements in such complex geometry is not practical.

CFD simulation: CFD simulation of liquid poison distribution with above mention phenomenon can give full distribution of liquid poison in calandria with time. For this – two species, complex geometry, large number of submerged jets, heat generation, etc. need to be modelled. These models need to be validated.

The design of SDS-2 of AHWR provides an opportunity to study such phenomenon. Thus, starting from finding injection nozzles velocity distribution along the length of injection tube, estimating the poison distribution from 640 injection jets of diameter 6mm having velocity around 45 m/s in 5 m high calandria having 513 calandria tubes is complex modelling problem. Along with this, the effect of moderator flow distribution with spatial distribution of heat generation should also be accounted. Based on the above mentioned challenges and present state of knowledge, objectives for this study are decided.

1.7 Objectives

As stated earlier, the SDS-2 consists of helium storage tank, an array of quick opening valves, poison tanks, injection tubes in calandria and associated piping between the poison tank and injection tube. The interface between poison and moderator lies in the pipe line between poison tank and injection tube. The injection of liquid poison into the moderator involves travelling of liquid poison from PMI to injection tube, exit of the poison from the nozzles on injection tubes, progression and spreading of poison jet with time, interaction of multiple jets among themselves and with calandria tubes and dispersion of liquid poison into the moderator.

The experimental data available for transient submerged jet progression with time are meagre. Moreover, there is no study available on the injection and dispersion of liquid poison into the moderator in the presence of calandria tubes, with heat generation and with flowing moderator in the calandria. The CFD studies performed by Rhee et al. (2007) on liquid poison injection for CANDU 6 reactor does not account the presence of calandria tubes, heat generation in the moderator. Further, the analysis was performed only for a sector of full geometry. Song et al. (2008) performed CFD studies on liquid poison injection in the moderator for Advanced CANDU Reactor (ACR) with limited number of calandria tubes. The CFD study was performed with quarter geometry due to symmetry.

In AHWR, due to tight lattice pitch, the spacing between calandria tubes is much less than the CANDU type reactors. Further, in AHWR, the emanating jet axes are parallel to calandria tube axis while in CANDU type reactor the jet axis is perpendicular to the calandria tube axis. Hence, to understand the shut down system-2 behaviour following studies have been undertaken with the following objectives:-

- Development of computer code to study the liquid poison injection and jet progression with time.

- Generation of experimental data for jet progression with and without considering calandria tubes.
- Validation of computer code developed for liquid poison injection and jet progression into the moderator.
- Study of moderator flow distribution inside the AHWR calandria with heat generation in the moderator and in the presence of calandria tubes.
- Study of interaction of multiple jets in presence of calandria tubes.
- Study of dispersion of liquid poison in the moderator flowing in the calandria and considering heat generation in the moderator.

1.8 Outline of Thesis

The thesis is organised into eight chapters. Chapter two provides a review of the literature relevant to present study like flow distribution from lateral holes in a sparger tube, transient submerged jet injection in water, moderator flow and temperature distribution, liquid poison injection in calandria. Based on the literature review, gap areas are identified on which further study is required to estimate distribution of liquid poison in AHWR calandria.

Chapter three deals with estimation injection velocity and poison initiation time from each injection nozzle that will be used as input parameters for CFD. A transient 1-D computer code (COPJET) is developed for the same. Computer code COPJET does the simulation of gas expansion, system piping, injection tubes and progress of the poison jet with time. A semi-empirical equation is formulated for progression of poison jet. Injection of the poison takes place after exhaustion of moderator present between PMI and injection tube. Due to this, poison front moves faster compared to impulsively started jet but slower than steady state jet due to inertia effect of partially developed jet flow. All these effects

are included in semi-empirical equation developed from the experimental studies available in the literature. The computer code developed has been validated with the results available in the literature.

Chapter four gives details of experimental studies are performed on transient poison injection in presence of calandria tubes. Based on the survey of published literature it was found that the experimental studies on jet injection in presence of tube bundle are not addressed sufficiently. The location and number of poison jets are design parameters, which can greatly affect dispersion and penetration of poison jets in calandria. The experiments are performed in the presence of tube bundle with poison jet. Two different orientations have been used to study poison jet progression. Results show that lateral spread of jet is more in cross bundle compared to axial bundle case. In axial bundle injection, the bundle has a tendency to maintain jet core in injection path whereas; cross bundle offers flow resistance and dissipate the jet energy faster. Hence, poison injection in axial bundle gives more progression of jet compared to cross bundle.

Chapter five gives details of the module which is developed in open source CFD code OpenFOAM to simulate time varying poison jet injection at nozzle inlets using source term. Calandria which has large number calandria tubes (513) and total 640 injection nozzles of diameter 6 mm each. In such complex nature of the problem, in order to facilitate the grid generation, source term approach is used for modelling inlet conditions. The inlet conditions have been taken care by defining the source terms in mass, momentum, energy and species equations. Modified model is validated with the experimental results obtained in chapter four. In addition to this, the experimental data of Johari et al. (1997) and velocity distribution in steady state jet are also used for validation. Thus, the scope of the present work is development and validation of the source term module for defining the poison jet injection through the nozzles.

Chapter six gives details of estimation of moderator flow and temperature distribution in vertical calandria vessel of the nuclear reactor using OpenFOAM. A large amount of heat (50MW) is generated within the moderator mainly due to slowing down of neutrons and attenuation of gamma radiations. To remove this energy, moderator is kept under continuous circulation through a heat removal system. Hence, to estimate the liquid poison distribution in AHWR calandria, moderator flow and its temperature field should be known. Validation of the CFD code has also been performed using the experimental data available in the literature. Simulations are performed for different cases of normal operating condition with and without heat generation. Studies are performed with spatial variation of heat generation. Effect of Archimedes number on temperature distribution has been also studied. The flow and temperature distribution of moderator has been used as input for further analysis of poison distribution in calandria.

Chapter seven gives details of CFD analysis of liquid poison injection and its dispersion into the moderator in calandria. Three cases are considered in poison distribution analysis. In the first case, poison distribution is simulated in stagnant moderator condition. In the second case, effect of moderator flow on poison distribution is studied. In the last case, effect of moderator flow with moderator heat generation on poison distribution is studied. In addition to this, effects of calandria tubes and effect of the neighbouring group of injection nozzles on poison jet progression are studied. Results of CFD simulations are compared with the results obtained from the analysis performed with computer code COPJET. Based on the above studies it is found that shut down system-2 of AHWR works effectively with the configuration considered in the studies.

In last chapter eight, conclusions drawn from the work done are given along with recommendation for future work.

Chapter 2

LITERATURE REVIEW

2.1 Introduction

In study of liquid poison distribution in AHWR calandria involve topics like flow distribution from lateral holes in a sparger tube, transient submerged jet injection in water, moderator flow and temperature distribution, liquid poison injection in calandria. Hence, a literature review has been taken up to understand the present state of knowledge on these topics. Based on the literature review, gap areas are identified on which further study is required to achieve our aim of estimating distribution of liquid poison in AHWR calandria.

2.2 Literature Review

For the literature review, the main subject is divided into sub topics (i) transient flow distribution from lateral holes in a sparger tube (ii) transient submerged jet injection in water (iii) Moderator flow and temperature distribution in calandria and (iv) Liquid poison injection and its dispersion in calandria of nuclear reactors. Following sections give details of present state of knowledge on these topics.

2.2.1 Flow distribution from lateral holes in an injection tube

The poison flow through injection tube depends on the total energy and frictional losses along the tube and the geometry of the holes (size, number, location, orientation,

etc). The injection tubes are modelled as dividing flow header for the analysis. In a diving flow header, the main fluid stream is decelerated due to loss of fluid through the lateral holes leading to rise in pressure in the flow direction provided the effect of friction is small. Acrivos et al. (1959) performed extensive experimental and theoretical studies to obtain pressure and flow distribution in the straight pipe with lateral branches in a steady state. They established momentum balance along the pipe by including frictional pressure drop and reduction in the kinetic head. The model takes the value of momentum recovery factor and orifice coefficient from their experimental data. Greskovich and O'Bara (1968) calculated the pressure distribution using summation technique, assuming the same velocity through all the holes. Bajura and Jones (1976) developed an analytical model, which takes into account the effect of momentum transport from the laterals. The model can be used for predicting flow distribution in different types of flow headers. Kulkarni et al. (2007) performed experiments and computational fluid dynamics (CFD) simulation on flow distribution in pipe and ring spargers. Singh and Rao (2009) gave a simplified analytical model for dividing flow header.

2.2.2 Transient submerged jet injection in water

Abramovich (1963) and Rajaratnam (1976) gave extensive experimental and theoretical details of steady state turbulent round jets of incompressible fluid. The turbulent jet has been divided into three regions namely initial region, transitional region and self similar or fully developed region. Initial region is characterised by a constant velocity potential core, the transitional region is developed as the jet grows and the mixing occurs and self similar region is formed as the axial velocity decays and the velocity profile is preserved. Both experimental and analytical models have been reported in the literature for the steady state flow. Ball et al. (2012) presented a critical review of both experimental and computational studies of steady state turbulent round jets. He gave a detailed comparison

of centreline axial mean velocity with axial distance for self-similar region reported by various authors. In addition to this, jet entrainment, effects of initial condition, length scale in jet and spectral analysis of jet are also discussed.

Unsteady jets have additional fourth region compared to steady state jet. This region is called termination zone, here the centreline velocity rapidly reduces to zero and it is called tip of the jet. Witre (1980) performed hot wire anemometer measurements for the centreline velocity of a suddenly started jet of air. The tip penetration of the jet has been shown to be proportional to the square root of time. A theoretical model has been developed that assumes the transient jet to be characterised as a spherical vortex interacting with a steady state jet. The model demonstrates that the ratio of nozzle radius to jet velocity defines a time constant that uniquely characterises the behaviour and similarity of impulsively started incompressible turbulent jets. Nawathe et al. (1991) performed experiments to measure the spread and growth rate of the poison jet. Experiments were performed on 3.2, 4, 5 and 8 mm nozzle diameters. The gas pressure for injecting water through the nozzle is varied from 1 to 2 MPa pressure. The experimental facility consisted of a rectangular tank (2 m high, 2 m long and 1 m wide) with two sides made up of acrylic sheets. This tank is filled with water after installing a suitable jet nozzle. The jet flow was visualised by enhanced contrast imaging using a coloured dye (blue ink) as the jet fluid and imaging the flow against a bright background. The dye solution was stored in a poison tank, which was connected to pressurised nitrogen tank through quick opening solenoid valve. In order to generate data on progression of the jet, Nawathe et al. (1991) used a video camera of 25 frames per second. As the dye concentration in the jet was not measured, the progression of poison jet was identified based on a subjective visual inspection of the image taken. The progression of the jet was given as the length occupied in the axial direction with time. Johari et al. (1997) performed an experimental

investigation on impulsively started turbulent jets. The jet penetration was recorded as a function of time in a series of flow visualization experiments. Jet tip celerity was found by differentiating the penetration data with respect to time. The experiments were carried out in an acrylic water tank of 1.2 x 1.2 m cross section and 1.5 m depth. Three nozzles with diameters of 6.35, 12.7 and 25.4 mm were used in the experiment. The Reynolds number was estimated in the range of 5×10^3 for the largest to 2×10^4 for the smallest nozzle. Both ordinary and fluorescent dyes were used for tagging the jet fluid. The internal structure of the jet was revealed by the Laser Induced Fluorescence (LIF) technique, which utilizes a photosensitive dye. All runs were recorded on videotape at recording rate of 30 frames per second.

Johari and Paduano (1997) experimentally studied mixing characteristics of a round, turbulent, unsteady jet. A gravity-driven flow was created by releasing dyed fluid from a vertical tube into a large water tank. The jet velocity was increased from zero to a maximum and then decreased continuously such that the each run lasted for about 1 s and had an average Reynolds number of 3×10^4 . The experiments were carried out in an acrylic water tank of 1.2 x 1.2 m cross section and 1.5 m depth. The flow was visualised by the LIF technique in which an argon-ion laser light sheet and a fluorescent dye (disodium fluorescein) were used. The LIF images were recorded on photographic film and videotape. The gravity-driven jet release mechanism consisted of a 1.22 m long acrylic tube with an internal diameter of 28 mm. The jet dilution was examined by an optical absorption technique that measured the line integral of concentration across the jet diameter. The jet dilution was quantified by a line absorption method and the notion of concentration thickness. Within the main body of the jet at the end of a run, the jet regions closer to the leading edge were diluted less than the steady jet by about 25%, whereas the jet mid-section was more diluted by the same amount.

2.2.3 Moderator flow and temperature distribution in calandria

In Shut Down System -2 (SDS-2), poison is injected in calandria that has moderator in flow condition. Moderator is kept in flow condition to remove the heat generated mainly due to neutron slowing down and attenuation of gamma radiations. Hence, to estimate the liquid poison distribution in AHWR calandria, moderator flow and its temperature field should be known. It is also necessary to know the effect of moderator flow and temperature distribution on liquid poison dispersion. Following is the literature review for moderator flow and temperature distribution in calandria of pressure tube type reactor.

Carlucci (1982) performed two dimensional moderator flow simulation for CANada Deuterium Uranium (CANDU) reactor. The equations of continuity and momentum in polar coordinates were solved. The author employed k- ϵ turbulence model with standard wall functions, volume porosity model to account for the presence of calandria tubes, Boussinesq approximation for handling buoyancy effect and polynomial fit for volumetric heat generation in calandria vessel. The effect of Archimedes number on the flow field was studied. Author found that the flow may be either buoyancy dominated or inlet jet momentum dominated depending on the Archimedes number (Ar). The temperature distribution was found to change significantly with a change in Ar .

Huget et al. (1989 and 1990) investigated experimentally the moderator flow and temperature distribution under different operating conditions. The geometry consisted of a thin slice of a CANDU reactor and the flow was considered two dimensional. The cross section of this facility was a one-fourth scale of the real calandria vessel, while the geometry and flow conditions were uniform in the axial direction. The velocities were measured using Laser Doppler Anemometer (LDA) while temperature measurements were performed at 40 locations using thermocouples. They also investigated velocity fields and

temperature distributions for each test case, using codes MODTURC (MODerator TURbulent Circulation) and MODTURC-CLAS (MODerator TURbulent Circulation Co-Located Advanced Solution). Porosity model was used in these codes for accounting the presence of calandria tubes. In porosity model, the tube resistance is accounted by incorporating the pressure loss term in the momentum equation. The loss coefficient can be either in-line tube bundle or cross flow tube bundle. In real geometry, flow is a combination of these two configurations. Hence, approximations for the presence of tubes and flow resistance may not predict flow and temperature behaviour very accurately.

Dharne and Gaitonde (1997) studied various configurations of inlet and outlet ports of calandria for Pressurised Heavy Water Reactors (PHWRs). They found that, in all the configurations, the placement of outlet nozzles at higher elevation compared to inlet nozzles results into lower local temperature pockets. This is because the upward flow of moderator from inlet to outlet is supported by buoyancy forces due to the heat gained by the moderator.

Koroyannakis (1983) experimentally examined the flow phenomena formed by inlet flows and internal heating of a fluid in a calandria-like cylindrical vessel of Sheridan Park Engineering Laboratory (SPEL) experimental facility. Volumetric heat generation was achieved by “electrolyte heating” method. A chemical flow visualization technique was employed to determine the predominant flow regime inside the vessel. Detailed temperature profiles inside the vessel were obtained using an optical fibre probe. They observed all the three types of flow patterns: (a) buoyancy dominated, (b) inlet jet momentum dominated and (c) mixed type inside the test vessel and the occurrence of any type was dependent on the flow rate and heat load.

Yoon et al. (2004) carried out 3D CFD analysis of the CANDU-6 moderator circulation under normal operating condition. CFD code CFX-4.4 was used to solve continuity, momentum and energy equations. Calandria tubes were modelled by porous media approach. The flow was assumed steady, incompressible and single phase. The standard k- ϵ turbulence model along with logarithmic wall function was used. Authors used multi-block structured grid consisting of angular, radial and axial divisions. Volumetric heat generation in the moderator was approximated by polynomial fit in axial and radial direction. CFD results predicted the flow reversal angle of inlet jet and steep temperature change around them. It also predicted the maximum moderator temperature.

Kim et al. (2006) carried out CFD analysis of moderator flow in CANDU reactor. The authors performed CFD simulation of SPEL experimental facility using Fluent 6.0 CFD code, to validate the models used. They later applied the model to CANDU reactor for steady state and transient conditions. In a steady state simulation, the volumetric heat generation was taken as uniform. Their results showed that the flow in reactor might vary from purely inlet jet momentum dominated to purely buoyancy dominated depending upon the inlet velocity and the heat load. A safety map for the moderator flow regime is proposed. Authors give a plot between Archimedes number and Reynolds number which shows buoyancy dominated flow for $Ar > 0.40$ and inlet jet momentum dominated for $Ar < 0.06$.

Prabhakaran et al. (2012) carried out CFD analysis of moderator flow and temperature distribution in calandria of 700MWe PHWR for flow-induced vibration. PHWR calandria has 12 moderator inlets near the horizontal centre line of the calandria and four moderator outlets at the bottom of the calandria vessel. The moderator is injected inside the calandria through diffusers, having a rectangular cross section of gradually

increasing size. The diffusers are designed such that the moderator jets travel all along in the reflector zone to the top of the calandria and then flow vertically down to outlet nozzles. Due to the axial and radial symmetry of the calandria, only one-fourth model has been considered for CFD analysis. All the horizontal fuel channels (196 channels) in the one-fourth model in the calandria vessel were modelled to analyse as a real geometry, since they, acting as flow resistance, play an important role to affect the heat transfer and the flow field. The fluid flow was assumed incompressible and single phase. They employed the standard $k-\epsilon$ turbulence model and the buoyancy effects were accounted by the Boussinesq approximation. To solve the governing equations, CFD code CFD-ACE+ was used. A good agreement was obtained between the predicted flow and temperature distribution in calandria. Table 2.1 gives a brief summary of the published work.

2.2.3.1 Analogy between calandria having tubes and flow through tube bundles

As large number of tubes affects the flow distribution in calandria, a literature survey has been done on numerical simulations of flow passing through tube bundles. Simonin and Barcouda (1988) performed experimental and numerical studies of turbulent cross-flow in a tube bundle. The measurements were made using an LDA technique. The transverse and longitudinal pitch-to-diameter ratios were 2.074 and 1.037 respectively. For the numerical study, they used a $k-\epsilon$ model to predict the mean velocities and turbulent kinetic energy. It was reported that the predicted mean velocities were in good agreement with the measured values. Watterson et al. (1999) performed numerical simulation for the turbulent, incompressible flow around a staggered array of tubes for which experimental results are available. Authors used a low-Reynolds number $k-\epsilon$ model. For their comparisons, they modelled flow with a Reynolds number of 21,000 based on the approach velocity. It was reported that the predicted mean values were in good agreement and the Reynolds stresses

showed agreement with the measured values. Rollet-Miet et al. (1999) employed Large Eddy Simulation (LES) and a $k-\varepsilon$ turbulence models. They reported that the mean velocity profiles were well predicted using both turbulence models. Hassan and Barsamian (2003) performed LES of a three-dimensional tube bundle at Reynolds number of 21700, based on the inlet velocity and the tube diameter. The numerical results were compared with available experimental data and found to be consistent. The ‘flapping’ effect in the tube wake was captured. This investigation indicates that the LES technique can be utilized as a tool in predicting the unsteady behaviour of flow in some industrial applications. Paul et al. (2007 and 2008) performed measurements and numerical predictions of turbulent cross-flow in a staggered tube bundle. The bundle consists of transverse and longitudinal pitch-to-diameter ratios of 3.8 and 2.1, respectively. The experiments were conducted using a particle image velocimetry technique, in a flow of water in a channel at a Reynolds number of 9300 based on the inlet velocity and the tube diameter. The steady and isothermal RANS equations were used to predict the turbulent flow using $k-\varepsilon$, a standard $k-\omega$, a $k-\omega$ based shear stress transport and an epsilon based second moment closure turbulence models. The results show that none of the turbulence models were able to consistently reproduce the mean and turbulent quantities reasonably well. The omega-based models predicted the mean velocities better in the developing region while the epsilon-based models gave better results in the region where the flow is becoming spatially periodic.

Table 2.1: Summary of previous work

Author	Carlucci (1982)	Koroyannakis et al. (1983)	Huget et al. (1989, 1990)	Dharne & Gaitonde (1997)	Yoon et al.(2004)	Kim et al. (2006)	Prabhakaran et al. (2012)	
Geometry	Typical CANDU reactor vessel	$D_{Tank}=0.737m$, $L_{Tank}=0.254m$, $OD_{Tube}=38$ mm, $N_{Tube}=52$, $W_{inlet}=12.6mm$, $L_{inlet}=150$ mm, $W_{outlet}=77mm$, $L_{outlet}=150mm$,	$D_{Tank}=2$ m, $L_{Tank}=0.2m$, $OD_{Tube}=33$ mm, $N_{Tube}=440$, $W_{inlet}=12$ mm, $L_{inlet}=0.2m$, $W_{outlet}=15$ mm, $L_{outlet}=0.2m$,	Indian PHWR (MAPS and KAPS)	CANDU 6	CANDU 6 $D_{Tank}=7.6m$, $L_{Tank}=6m$, $OD_{Tube}=131$ mm, $N_{Tube}=380$	700 MWe Indian PHWR , $D_{Tank}=7.8$ m, $L_{Tank}=5.9$ m, $OD_{Tube}=132$ mm , $N_{Tube}=392$	
Moderator Heat Generation	Varies proportional to the channel power in the core region and constant in the reflector region	Electrode heating by AC power supply	DC supply to rods for resistance heating and AC for electrode heating	Uniform Volumetric heat generation	Volumetric heat generation by two polynomial fit equation for axial and radial direction.	Uniform Volumetric heat generation	Uniform Volumetric heat generation	
Temperature	-	Measured using Optical fibre probe.	Measured by 40 T type Thermocouples	-	-	-	-	
Velocity	-	Chemical flow visualization	Measured by LDA and flow visualization by tracer technique using a pH indicator	-	-	-	-	
CFD Simulation	2D/3D	2D	-	2D	3D	3D	3D	
	Calandria Tube model	a	-	a	a	b	b	
	Code and Grid	Radial and circumferential coordinates grid having 1020 cells	-	MODTURCLAS with non-orthogonal mesh. (735 cells)	MFLO code with Cartesian co-ordinate grid. (8125 cells)	CFX 4.4 using cylindrical coordinate grid (19504 cells)	FLUENT code (0.83 million cells)	CFD-ACE+ (3 million cells)
	Turbulence model	Std. k- ϵ	-	Std. k- ϵ	DNG	Std. k- ϵ	Std. k- ϵ	Std. k- ϵ
	Grid Independence	Yes	-	Sensitivity of the solution to the mesh size is checked	DNG	Grid independency has not been achieved	DNG	DNG
Velocity and temperature field	Yes	-	Yes	YES	Yes	Yes	Yes	
Comparison with experiment	Yes	-	YES	Yes	DNG	Yes	Yes	
Limitations	1, 2, 3	-	1, 2, 3, 4	2, 3, 4, 5	2, 6	4	4	

BA - Boussinesq approximation

DNG-Data not given in paper

Calandria Tube modelled in CFD

- a) Porosity model for modelling calandria tubes
- b) Calandria tubes matrix are modelled

Limitations

- 1) 2D approximation.
- 2) Porosity model too much simplification of calandria internals, hence lacks local effects.
- 3) Grid size is too small to capture detail flow and temperature pattern.
- 4) Uniform heat generation.
- 5) Cartesian co-ordinate grid to capture cylindrical calandria.
- 6) Grid independency has not been achieved.

2.2.4 Liquid poison injection in calandria

Rhee et al. (2007) analysed the poison concentration distribution during a highly pressurized poison injection under a transient condition of a CANDU reactor using CFD code CFX-4.4. In order to facilitate the grid generation, the source terms were used as boundary conditions instead of using the inlet boundary conditions. For validation of the proposed models, the jet front heights were compared with those of three poison injection experiments: (a) SDS-2 phase-1 experiments performed for 540-MWe pressurized heavy water reactors by Nawathe et al. (1991) (b) the generic CANDU-6 poison injection SPEL test conducted by AECL in Canada, and (c) the 850-MWe CANDU poison injection SPEL test. All the comparisons show that the proposed model can predict the poison jet front height growth consistently with a reasonable accuracy. In their studies, authors only modelled 90° sector of calandria with half of the lattice pitch without calandria tubes. Moreover, effect of moderator flow and its temperature distribution in calandria is not considered for poison concentration distribution.

Song et al. (2008) simulated the transient behaviour of poison injection in the moderator for Advanced CANDU Reactor (ACR-1000), using a commercial CFD software ANSYS-CFX 10.0. The model used was for the isothermal, transient and 3-D poison injection in the moderator. The CFD simulation was validated against the measurements of jet length obtained from the CANDU-6 Liquid Injection Shutdown System (LISS) tests at AECL. The poison injection in the ACR-1000 design was then simulated to obtain a better understanding of the jet growth and poison distribution in the moderator in the presence of calandria tubes. The ACR-1000 design utilizes a smaller reactor core and a tighter calandria tube lattice pitch than the CANDU-6 design. One quarter of the injection node was simulated due to symmetry. The CFD results demonstrate the effects of calandria tubes on the jet growth, which are beneficial for the optimization of the LISS and injection

nozzle design. However, the effect of moderator flow and its temperature distribution in calandria is not considered for poison concentration distribution.

2.3 Gap Areas

Based on above sections following gap areas are identified on which further study is required to achieve our aim of estimating distribution of liquid poison in AHWR calandria.

2.3.1 Transient flow distribution from lateral holes in injection tube

The published literature shows that all the developed models cater to flow distribution through distribution header for steady state cases. However, in AHWR, poison injection is done in few seconds. Hence, to design injection tube in AHWR, formulation for transient flow distribution through header has to be done. Moreover, poison moderator interface in the pipe has to be modelled as well as initiation of poison injection from different holes in injection tube.

2.3.2 Transient submerged jet injection in water

The design of SDS-2 system involves optimisation of number and size of poison injection nozzles, which depends on the spread of poison jets. The spread of poison jet depends on its length. Hence, for the initial design of the system, mathematical model should be available to predict the poison jet length. Moreover, in AHWR, liquid poison and moderator are separated by Poison Moderator Interface (PMI) inside the connecting pipe between poison tank and injection tube as shown in Figure 1.3. After the system actuation, poison is injected into the calandria tank. However, during the initial period of injection, moderator present between PMI and injection nozzle flows into the calandria. Actual injection of the poison follows injection of moderator into the calandria. This causes time delay for actual entry of poison into calandria vessel after system is actuated.

Therefore, the poison injection cannot be modelled as impulsively started jet or as steady state jet as the flow is still developing. Survey of the published literature shows no formulation is available for predicting the progression of poison jet under such conditions.

2.3.3 Moderator flow in calandria

All the published work with calandria tube modelled assumes uniform volumetric heat generation; geometry of AHWR is different from CANDU type reactor. In AHWR, calandria tank is vertical whereas it is horizontal in CANDU type reactor. In addition, the ratio of lattice pitch by calandria tube diameter is 1.34, compared to the CANDU 6 where the pitch to diameter ratio is 2.2. Hence, it is necessary that moderator temperature and flow fields should be generated for AHWR configuration by taking into account the spatial distribution of volumetric heat generation.

2.3.4 Liquid poison injection in calandria

As discussed, in AHWR, where the ratio of lattice pitch by calandria tube diameter is 1.34, the effect of calandria tube on the propagation of poison jet dominates as compared to the CANDU 6 where the pitch to diameter ratio is 2.2. Hence, in CFD studies related to CANDU (Rhee et al., 2007) liquid poison injection assumes negligible effect of calandria tubes and modelled only a sector of full geometry. Published literature shows in the case of Advanced Candu Reactor (ACR) (Song et al., 2008), where the ratio of calandria tube pitch to diameter is in same order as AHWR, a limited number of calandria tubes were included in the CFD simulations to cover the jet growth region and only one quarter of the injection node was simulated due to symmetry. Moreover, in ACR, the jet axis is perpendicular to calandria tube axis, compared to near parallel axis of jets and calandria tubes in AHWR. The published literature also shows that the experimental studies on jet injection in presence of tube bundle have not been addressed. Hence, experimental and

CFD simulations are needed to estimate flow and mixing characteristics inside a vertical calandria for different operating conditions and in the presence of calandria tubes.

2.4 Conclusions

Based on the literature review it can be concluded that following issues need to be addressed to estimate the liquid poison distribution in AHWR calandria.

- Formulation for transient flow distribution from lateral holes in an injection tube.
- Development of semi-empirical equation for predicting the progression of poison jet considering the effect of dead time.
- Generation of moderator flow and temperature fields by considering spatial distribution of volumetric heat generation.
- Transient study of liquid poison distribution in AHWR calandria with calandria tubes and moderator flow.

Chapter 3

ANALYTICAL MODEL FOR LIQUID POISON INJECTION SYSTEM

3.1 Introduction

In AHWR, SDS-2 operates on the principle of direct injection of poison into bulk moderator by means of high pressure helium in a very short time. The poison proposed to be used is gadolinium nitrate solution mixed in heavy water. A schematic of SDS-2 is given in Figure 1.4. The system consists of helium storage tank, poison tanks, connecting piping and perforated injection tubes. The injection tubes are horizontally located inside calandria. These injection tubes have a number of holes on their cylindrical surfaces referred as injection nozzles. The liquid poison is stored in eight tanks, known as poison tanks. Each tank is connected to an injection tube separately. High pressure helium is stored in a tank known as helium storage tank, which is connected to the poison tanks through an array of quick opening valves. These valves are opened following an SDS-2 trip signal and consequently, the high pressure helium forces the gadolinium nitrate solution into the calandria through the injection tubes.

The design of the injection tube involves optimisation of number and size of the lateral nozzles. Injection tubes act as a dividing-flow header. In this header, the main fluid

stream is decelerated due to the loss of fluid through the lateral nozzles. Therefore, non-uniformity may happen in the velocity of jet issued from nozzles depending on frictional pressure drop in the pipe and pressure drop across the lateral nozzles. It is necessary to know the flow distribution in the injection tube for evaluating the system performance. It is also important to know the progression and spreading of the jet with time to evaluate the dispersion of poison in the moderator.

Acrivos et al. (1959), Greskovich and O'Bara (1968), Singh and Rao (2009) and Bajura and Jones (1976) developed a steady state analytical model for dividing flow header, which takes into account the effect of momentum transport from the laterals. The model can be used for predicting flow distribution in different types of flow headers. However, in the present case, poison injection is a transient phenomenon. Hence, a transient model should be developed for dividing flow header.

The liquid poison and moderator are separated by Poison Moderator Interface (PMI) inside connecting pipe between poison tank and perforated injection tube as shown in Figure 1.4. The time required for poison to travel from PMI to calandria is termed as dead time (t_{dead}). It is necessary to estimate the dead time to arrive at the progression of poison jet with time into the calandria. Initiation of poison injection is also different for different nozzles in injection tube and increase along the length of the injection tube. Thus, PMI and poison injection timing along injection tube has to be modelled.

Distribution of poison depends on progression and spread of poison jets. The spread of poison jet, in turn, depends on its length. Hence, for the initial design of the system, mathematical model should be available to predict the poison jet length. After the system actuation, poison is injected into the calandria tank. However, during the initial period of injection, moderator present between PMI and injection nozzle flows into the calandria. Actual injection of the poison follows injection of moderator into the calandria. This

causes time delay for actual entry of poison into calandria vessel after system is actuated. Survey of published literature shows there is no formulation available for predicting the progression of poison jet under such condition. Hence, a mathematical model has to be developed for the same.

A computer code COPJET is developed for transient simulation of gas expansion, system piping, injection tubes and progress of the poison jet with time. Separate transient momentum equations along with continuity equation are solved for system piping and injection tube. Variation of friction factor with Reynolds number is considered in the model. Variation in mass flow rate, helium tank pressure, jet velocity and progression of poison jet with time has been estimated. This chapter deals with the system description, model development, numerical solution and validation of COPJET computer code developed.

3.2 Development of Analytical Model

3.2.1 Flow geometry

Calandria of AHWR is a vertical cylindrical tank filled with heavy water (Sinha and Kakodkar, 2006). The calandria vessel comprises a main cylindrical shell of 6.9 m diameter and net height of 5 m as shown in Figure 3.1. At either end of the main shell, sub-shell of 6.3 m diameter and 0.75 m height is provided. These sub-shells form top and bottom reflector regions of the reactor core. There are eight liquid poison tanks in SDS-2. Each tank is connected to injection tube through the piping circuit penetrating the calandria horizontally as shown in Figure 1.4. Four injection tubes are located at 0.75 m and other four injection tubes are located at 4.25 m elevation from the calandria bottom. The injection tube inner diameter is 38.1 mm. These injection tubes contain circular openings called injection nozzles. There are four injection nozzles located centrally between

calandria tubes forming a group of injection nozzles as shown in Figure 3.2. Each injection tube has 20 such groups of injection nozzles. Hence, there are total 640 injection nozzles of diameter 6 mm in eight injection tubes for poison injection in calandria. The direction of injection is towards the centre of calandria. Out of four injection nozzles, the axis of two central nozzles is parallel to calandria vertical axis and the other two are inclined at $\pm 20^\circ$ angle to the axis of calandria. Axial nozzles provide penetration and inclined nozzles provide a lateral spread of poison.

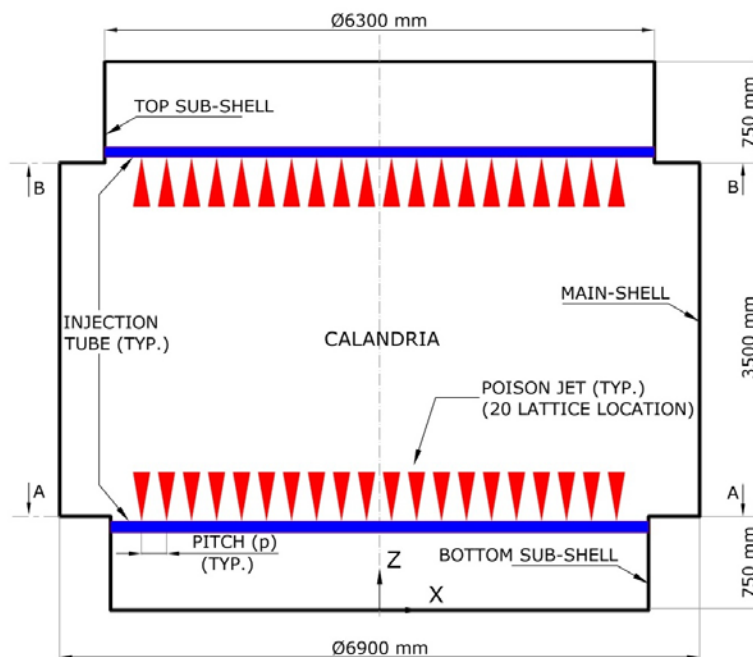


Figure 3.1: Schematic of SDS-2 injection tubes (Elevation view without internals)

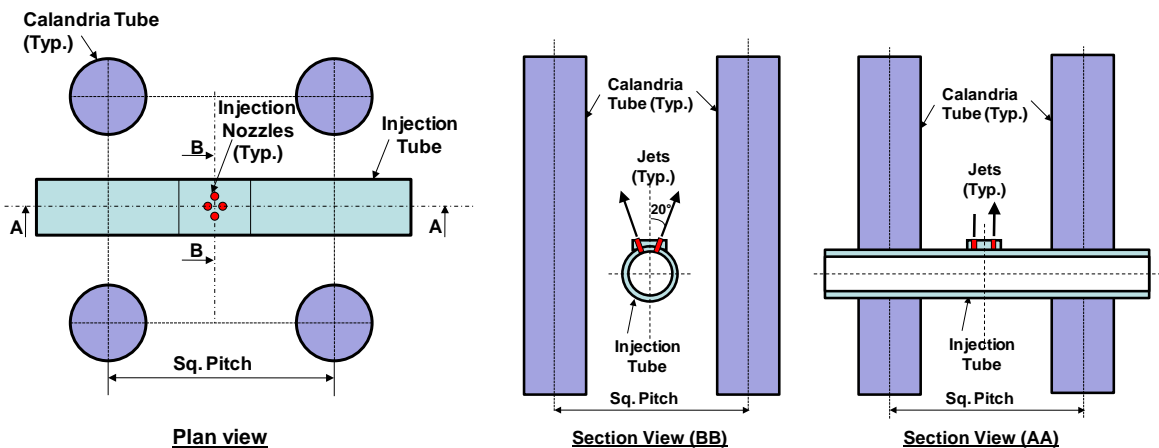


Figure 3.2: Schematic of a group of jet nozzles at a typical lattice location

3.2.2 Assumptions in analytical model

The following assumptions have been made in the formulation of the analytical model:

1. Fluid is single phase, isothermal and incompressible.
2. Fluid properties are constant.
3. Flow is 1-D throughout the transient.
4. Effect of calandria tubes on the progression of jet is not considered.
5. Effect of other jets on the progression of jet is not considered.
6. Diffusion of PMI is neglected.

As poison jet injection is in axial direction with respect to calandria tubes they will not offer high resistance and will guide the jet flow. It is assumed that effect of resistance offered and flow guided by calandria tubes will nearly cancel out, and resultant effect is negligible. Hence effect of calandria tubes on progression of jet is not considered. As neighbouring jets will assist in progression of jet hence assumption of neglecting effect of neighbouring jets on progression of jet is conservative. As PMI travels through piping it diffuses in both sides of interface hence assumption of neglecting diffusion of PMI is conservative.

3.2.3 Governing equations

Transient 1-D computer code, COPJET for liquid poison injection is developed which consists of four modules. These modules are gas expansion, system piping, injection tube and poison jet progression. In first the module, the gas expansion is modelled. In second and third modules, transient momentum and continuity equations are modelled. In the fourth module a semi-empirical formula is used, which is developed from experimental data. Following sections describe the analytical models used in the various modules discussed above.

3.2.3.1 Gas expansion module

In this module, high pressure helium gas is modelled as ideal gas and expansion treated is considered to be adiabatic as transient is very fast. Following relationship is used for gas expansion.

$$P_g V_g^\gamma = \text{constant} \quad (3.1)$$

Where, P_g is gas pressure and V_g is gas volume in gas tank and poison tank. The above equation is used for gas space in gas and poison tanks.

3.2.3.2 System piping module

In this module, flow is considered incompressible, isothermal and one dimensional. The domain of this module covers poison tank and system piping.

Continuity equation for incompressible flow

$$\frac{\partial u}{\partial x} = 0 \quad (3.2)$$

Momentum equation

$$\frac{\partial(\rho u)}{\partial t} + \frac{\partial(\rho u^2)}{\partial x} = \rho g_x - \frac{\partial p}{\partial x} + \frac{\partial p_f}{\partial x} \quad (3.3)$$

Where, ∂p_f is frictional pressure loss in pipe (Benedict, 1980) within elemental length of ∂x is

$$\partial p_f = - \left(\frac{f \partial x}{D} \right) \frac{\rho u^2}{2} \quad (3.4)$$

Using continuity and frictional pressure loss equations, momentum equation can be written as

$$\rho \frac{\partial u}{\partial t} = \rho g_x - \frac{\partial p}{\partial x} - \left(\frac{f}{D}\right) \frac{\rho u^2}{2} \quad (3.5)$$

Substituting $u = \dot{m}/(\rho A)$,

$$\frac{1}{A} \frac{d\dot{m}}{dt} = \rho g_x - \frac{\partial p}{\partial x} - \left(\frac{f}{D}\right) \frac{\dot{m}^2}{2\rho A^2} \quad (3.6)$$

Here, full derivative is used as \dot{m} is function of only time and constant with space.

Integrating above equation (3.6) over specified domain,

$$\int \frac{1}{A} \frac{d\dot{m}}{dt} dx + \int \left(\frac{f}{D}\right) \frac{\dot{m}^2}{2\rho A^2} dx - \int \rho g_x dx - \int \partial p = 0 \quad (3.7)$$

$$\frac{d\dot{m}}{dt} \int \frac{dx}{A} + \frac{\dot{m}^2}{2\rho} \int \frac{1}{A^2} \left(\frac{f dx}{D}\right) - \rho \int g_x dx - \int \partial p = 0 \quad (3.8)$$

Finally, integrals are expressed in summation form for different segments of piping from $i = 1$ to n and using loss coefficient $K = fL/D$, $g_x dx = -g dh$. Where, L is pipe length, D is pipe diameter, A is pipe flow area and h is pipe height.

$$\frac{d\dot{m}}{dt} \sum_{i=1}^n \left(\frac{L}{A}\right)_i + \frac{\dot{m}^2}{2\rho} \sum_{i=1}^n \left(\frac{K}{A^2}\right)_i - \rho g \Delta h_{1n} - \Delta p_{1n} = 0 \quad (3.9)$$

Where, Δh_{1n} is the height difference between start of first and end of last pipe segment and Δp_{1n} is pressure difference between start and end point of the piping system.

3.2.3.3 Injection tube module

The design of the injection tube involves optimisation of number and size of the injection nozzles. Injection tube acts as a dividing flow header, where the main fluid stream is decelerated due to the loss of fluid through the lateral nozzles. Therefore, non-uniformity may happen in the velocity of jet issued from nozzles depending on frictional

pressure drop that occurs in the pipe and across the lateral nozzles. The flow distribution from the lateral nozzles should be known for the estimation of system performance. Figure 3.3 shows a typical injection tube. Momentum and mass conservation equations are considered for injection tube as described below where subscript *IT* is for injection tube, *n* for lateral nozzles and A_n is flow area of nozzles per unit length.

Continuity equation for incompressible flow is applied as

$$\begin{aligned} &\text{Change in mass flow rate in injection tube per unit length} + \\ &\text{Change in mass flow rate through nozzles per unit length} = 0 \end{aligned} \quad (3.10)$$

$$\frac{\partial(A_{IT}u_{IT})}{\partial x} \cdot dx + A_n v_n \cdot dx = 0 \quad (3.11)$$

$$v_n = -\frac{1}{A_n} \frac{\partial(A_{IT}u_{IT})}{\partial x} = -\left(\frac{A_{IT}}{A_n}\right) \frac{\partial u_{IT}}{\partial x} \quad (3.12)$$

Axial momentum equation,

$$\frac{\partial(\rho u_{IT})}{\partial t} + \frac{\partial(p_r)}{\partial x} = \rho g_x - \frac{\partial p_{IT}}{\partial x} + \frac{\partial p_f}{\partial x} \quad (3.13)$$

Where, p_r is pressure recovery due to conversion of velocity head into pressure head and p_f is frictional pressure.

Since, kinetic head of the flow decreases along the axis of injection tube due to discharge from the lateral nozzles, it results into pressure recovery. The ideal pressure recovery (∂p_{r_ideal}) across a nozzle is given by the following correlation

$$\partial p_{r_ideal} = \partial (\rho u_{IT}^2) \quad (3.14)$$

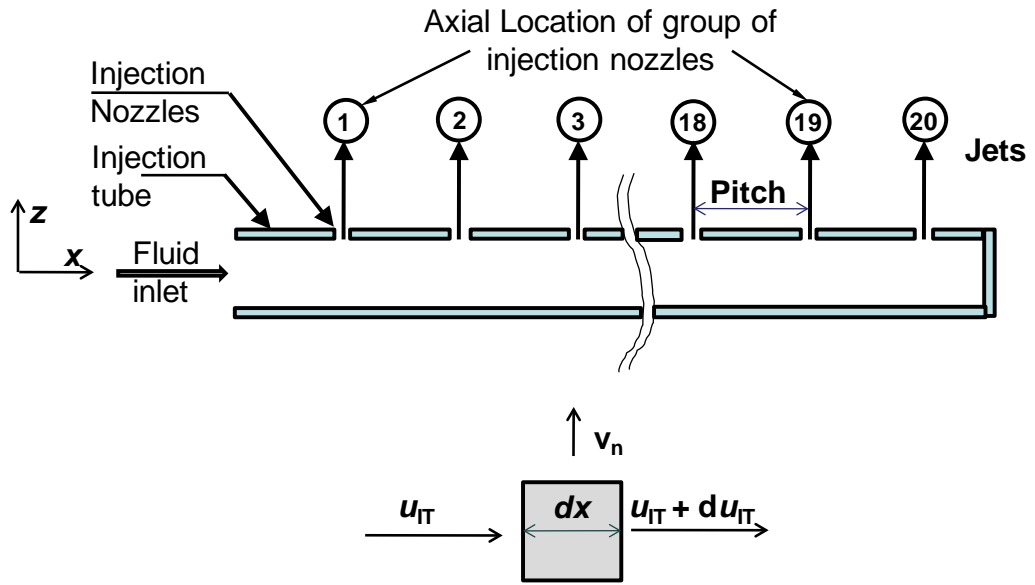


Figure 3.3: Schematic of injection tube

However, in actual conditions, the non-idealities do not permit complete conversion of velocity head into pressure head. Hence, momentum recovery factor (k'), which takes into account all the non-idealities in conversion of velocity head into pressure head is introduced into axial momentum equation. Real pressure recovery (∂p_{r_real}) can be estimated using equation (3.14) as below

$$\partial p_{r_real} = k' \partial p_{r_ideal} \quad (3.15)$$

$$\partial p_{r_real} = k' \partial (\rho u_{IT}^2) \quad (3.16)$$

Value of $2k'$ is taken as 1.05 as recommended by Bajura and Jones (1976). Using equation (3.16), equation (3.13) is modified as

$$\frac{\partial(\rho u_{IT})}{\partial t} + k' \frac{\partial(\rho u_{IT}^2)}{\partial x} = \rho g_x - \frac{\partial p_{IT}}{\partial x} + \frac{\partial p_f}{\partial x} \quad (3.17)$$

Where, $\partial p_f = -\left(\frac{f \partial x}{D}\right) \frac{\rho u^2}{2}$ and as injection tube is horizontal $g_x = 0$

$$\frac{\partial(\rho u_{IT})}{\partial t} + k' \frac{\partial(\rho u_{IT}^2)}{\partial x} + \frac{\partial p_{IT}}{\partial x} + \left(\frac{f}{D}\right) \frac{\rho u_{IT}^2}{2} = 0 \quad (3.18)$$

Let the constant pressure outside the injection tube be p_o . Then pressure loss across nozzles (Benedict, 1980) is given by

$$p_{IT} - p_o = K_n \left(\frac{\rho v_n^2}{2} \right) \quad (3.19)$$

Where, K_n is the local loss coefficient for injection nozzle.

Putting the value of v_n from eq.(3.12) in eq.(3.19)

$$p_{IT} - p_o = \frac{\rho K_n}{2} \left(\frac{A_{IT}}{A_n} \right)^2 \cdot \left(\frac{\partial u_{IT}}{\partial x} \right)^2 \quad (3.20)$$

Variation of pressure in injection tube along the length is obtained by differentiating the above equation.

$$\frac{\partial p_{IT}}{\partial x} = \rho K_n \left(\frac{A_{IT}}{A_n} \right)^2 \cdot \frac{\partial u_{IT}}{\partial x} \frac{\partial^2 u_{IT}}{\partial x^2} \quad (3.21)$$

Substituting the value of $\partial p_{IT}/\partial x$ from above equation into equation (3.18)

$$\frac{\partial u_{IT}}{\partial t} + 2k' u_{IT} \frac{\partial u_{IT}}{\partial x} + K_n \left(\frac{A_{IT}}{A_n} \right)^2 \cdot \frac{\partial u_{IT}}{\partial x} \frac{\partial^2 u_{IT}}{\partial x^2} + \left(\frac{f}{2D} \right) u_{IT}^2 = 0 \quad (3.22)$$

In all the above equations, the friction factor used is the non iterative correlation of Churchill (1977) which is valid in all three regions namely laminar, transition and turbulent.

$$f = 8 \left[\left(\frac{8}{Re} \right)^{12} + \frac{1}{(A+B)^{1.5}} \right]^{1/12} \quad (3.23)$$

$$\text{Where, } A = \left[-2.457 \ln \left(\left(\frac{\varepsilon/d}{3.7} \right) + \left(\frac{7}{Re} \right)^{0.9} \right) \right]^{16} \quad (3.24)$$

$$B = \left(\frac{37530}{Re} \right)^{16} \quad (3.25)$$

3.2.3.4 Poison jet progression module

In the fourth module, a semi-empirical formula is developed from the experimental data of Nawathe et al. (1991) and Johari et al. (1997). For steady state jet, centre line velocity (Abramovich, 1963) at distance z is given by equation (3.26) where z is the axis of turbulent jet.

$$\frac{U_c}{U_o} = \frac{c_1}{c_2 \left(\frac{z}{d_n} \right) + c_3} \quad (3.26)$$

Where, c_1 , c_2 & c_3 are constants and d_n is nozzles diameter. Using $v = dz/dt$ in equation (3.26) and integrating from $t = 0$ to t and $y = 0$ to z , the equation (3.26) becomes

$$\frac{c_2}{2c_1} \frac{z^2}{d_n} + \frac{c_3}{c_1} z = U_o t \quad (3.27)$$

Dividing the above equation by d_n

$$\frac{c_2}{2c_1} \left(\frac{z}{d_n} \right)^2 + \frac{c_3}{c_1} \left(\frac{z}{d_n} \right) = \frac{U_o t}{d_n} \quad (3.28)$$

Substituting, $z^* = z/d_n$, $t^* = (U_o t)/d_n$, as non-dimensional progression of poison jet and time in above equation. It can be seen that d_n is the length scale and d_n/U_o is the time scale.

$$\frac{c_2}{2c_1} z^{*2} + \frac{c_3}{c_1} z^* = t^* \quad (3.29)$$

If equation (3.29) is applied for steady state turbulent jet, it will give displacement of a particle introduced in jet with time. For steady state jet $c_1 = 0.96$, $c_2 = 0.16$ and $c_3 = 0.29$ (Abramovich, 1963). Thus, equation (3.29) for steady state jet becomes

$$\frac{1}{12} z^{*2} + \frac{1}{3.31} z^* = t^* \quad (3.30)$$

For generating constants of equation (3.29) for progression of unsteady poison jet, experimental data generated by Nawathe et al. (1991) and Johari et al. (1997) are used. Table 3.1 gives details of jet diameter and Reynolds number at which experiments were done.

Table 3.1: Experimental conditions for impulsively started turbulent jets

Author	Jet Diameter	Reynolds number
Nawathe et al. (1991)	3.2 mm	34000, 44000, 53000
	4 mm	33000, 36000, 44000
	5 mm	38000, 44000, 50000
	8 mm	50000, 62000, 76000
Johari et al. (1997)	6.35 mm	20000
	12.7 mm	15000
	25.4 mm	5000

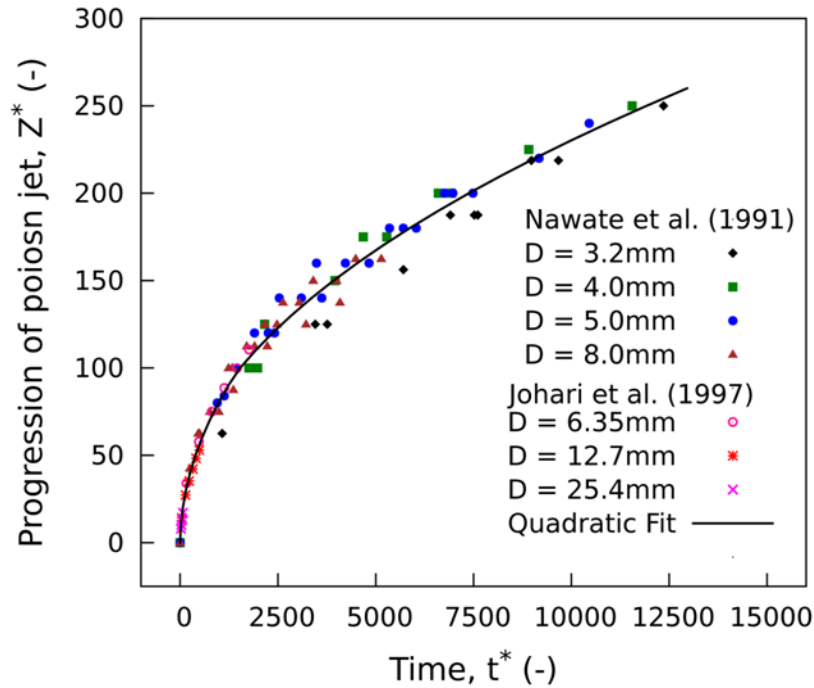


Figure 3.4: Progression of impulsively started poison jet with time

When polynomial curve fitting is done through the data points as shown in Figure 3.4, following quadratic equation in non-dimensional form emerges.

$$\begin{aligned}
 t^* &= 0.5592 z^* + 0.1461 z^{*2} && (z^* < 100) \\
 &= -6.1473 z^* + 0.2153 z^{*2} && (100 \leq z^* < 250) \quad (3.31)
 \end{aligned}$$

This semi-empirical correlation is used for estimating the progression of poison jet with time. This equation is applicable for values of $z^* < 250$.

In the present case of AHWR, liquid poison and moderator are separated by Poison Moderator Interface (PMI) inside the connecting pipe between poison tank and injection tube as indicated in Figure 1.4. After the system actuation, poison is injected into the calandria tank. However, during initial period of injection, moderator present between PMI and injection nozzle flows into the calandria. Actual injection of the poison takes place after exhaustion of moderator present between PMI and injection tube. This causes time delay for actual entry of poison into calandria vessel after system is actuated. The time

required for poison to travel from PMI to calandria is defined as dead time (t_{dead}). The initial moderator injection acts as an impulsively started jet, which is suddenly started jet from rest. By the time, poison reaches the injection nozzle i.e. after dead time (t_{dead}), the flow acts as a partially developed jet flow. Due to this, poison front moves faster compared to impulsively started jet but slower than steady state jet due to inertia effect of partially developed jet flow. Figure 3.5 gives the graphical representation of effect of dead time on poison jet progression. From Figure 3.5 it can be seen that actual poison jet (curve A) is faster than impulsively started jet at $t = t_{dead}$ (curve B) and slower than impulsively started jet at $t = 0$ (curve C) and steady state jet started at $t = t_{dead}$ (curve D). Thus, equation (3.30) for Steady State Jet (SSJ) started at $t = t_{dead}$ and equation (3.31) for Impulsively Started Jet (ISJ) started at $t = 0$ defines upper bound for Poison Jet (PJ) progression. Equation (3.31) for the Impulsively Started Jet (ISJ) started at $t = t_{dead}$ defines lower bound for Poison Jet (PJ) progression. Actual poison jet will be between these two bounds which will depend on dead time (t_{dead}) and poison injection time (t_p).

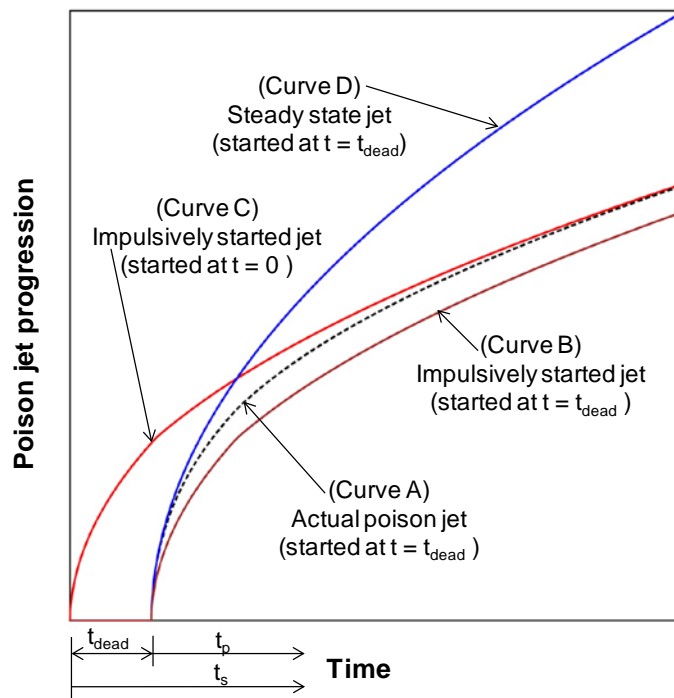


Figure 3.5: Effect of dead time of poison jet progression

Hence the equation for progression of poison jet with delay injection can be written as following assuming linear interpolation.

$$z_{PJ}^* = \min \left[z_{SSJ}^*(t_p) \cdot \left(1 - \frac{t_p}{t_s}\right) + z_{ISJ}^*(t_p) \cdot \left(\frac{t_p}{t_s}\right), z_{ISJ}^*(t_s) \right] \quad (3.32)$$

Where

t_p = poison injection time (s)

$t_s = t_p + t_{\text{dead}}$

Equation (3.32) satisfies limiting cases given in Table 3.2.

Table 3.2: Limiting cases for progression of poison jet with delay injection

Limiting Case	t_p/t_s	z_{PJ}^*
$t_{\text{dead}} = 0$ i.e. ($t_p = t_s$)	1	$z_{ISJ}^*(t_p \text{ or } t_s)$
$t_p \rightarrow t_s$	1	$z_{ISJ}^*(t_p)$
$t_p = 0$	0	$z_{SSJ}^*(t_p)$

3.2.4 Initial and boundary condition

For the gas expansion equation (3.1) initial condition are $P_g = P_i$ (initial gas tank pressure) and $V_g = V_i$ (initial volume of gas in tank). V_g will increase and P_g will decrease with time as the poison gets injected into calandria.

For the system piping equation (3.9) initial condition is $\dot{m}(x, 0) = 0$ and $\Delta p_{1n} = (P_i - P_{\text{sp_it}})$ where $P_{\text{sp_it}}$ is pressure at junction of system piping and injection tube. Pressure difference Δp_{1n} is maximum when injection starts and decreases as the poison gets injected into calandria.

For the dividing flow header equation (3.22) initial condition and boundary conditions are $u_{IT}(x, 0) = 0$, $u_{IT}(0, t) = \dot{m}(t)/(\rho A_{IT})$, $u_{IT}(L, t) = 0$

For poison jet equation (3.22), the poison jet progression is only function of non-dimensionalised time.

3.2.5 Method of solution

Equation (3.1) is explicitly solved for pressure as gas expands due to injection of poison from poison tank to calandria.

Time step is taken such that it meets both stability criterion and Courant number limit. Equation (3.9) is explicitly solved for $d\dot{m}/dt$ assuming P_{sp_it} , from this new mass flow rate (\dot{m}) is estimated. In equation (3.22), velocity at $x = 0$ is $u_{IT} = \dot{m}(t)/(\rho A_{IT})$ and at $x = L$ velocity is $u_{IT} = 0$, using these, the boundary condition and initial condition of $u_{IT}(x, 0) = 0$, the equation (3.22) is explicitly solved. From the distribution of u_{IT} along injection tube, pressure distribution in injection tube is estimated using equation (3.19), thus pressure at start of injection tube (P_{sp_it}) is estimated. At the junction, continuity of pressure (P_{sp_it}) is maintained by iteration between equations (3.9) and (3.22), with convergence at 10^{-4} .

From the solution of equation (3.22), velocity distribution through lateral nozzles is estimated by using equation (3.12). Using velocity distribution through lateral nozzles and injection time, poison jet progression is estimated using equation (3.32) explicitly.

3.2.6 Model validation

The computer code COPJET is validated for the lateral flow distribution and progression of poison jet with the data available in literature.

3.2.6.1 Lateral flow distribution

Validation of injection tube module for lateral flow distribution was done with steady state experimental data reported by Acrivos et al. (1959). They performed experiments to obtain pressure and flow distribution in the straight manifolds. The

manifold used was a 6 ft long brass pipe having inner diameter of 1.025". This brass pipe was provided with 24 side ports at interval of 3". The side ports were made from 9" long copper tube having inner diameter of 0.317". Fluid pressure inside the manifold was observed by means of 32 pressure taps that were soldered to the bottom of the manifold at 3" interval. Inlet velocity of air was measured to be 47.2 ft/s by orifice located at 28.5" upstream from the first side port. The quantity of air leaving the side ports was measured by Pitot tubes. As this data is for steady state, the solution of equation (3.22) has been obtained numerically by ignoring transient term and compared with experimental data as shown in Figure 3.6. The result shows that flow rate from the side ports increases in the direction of flow in the main channel. This is due to pressure rise owing to deceleration of the fluid due to dividing manifold.

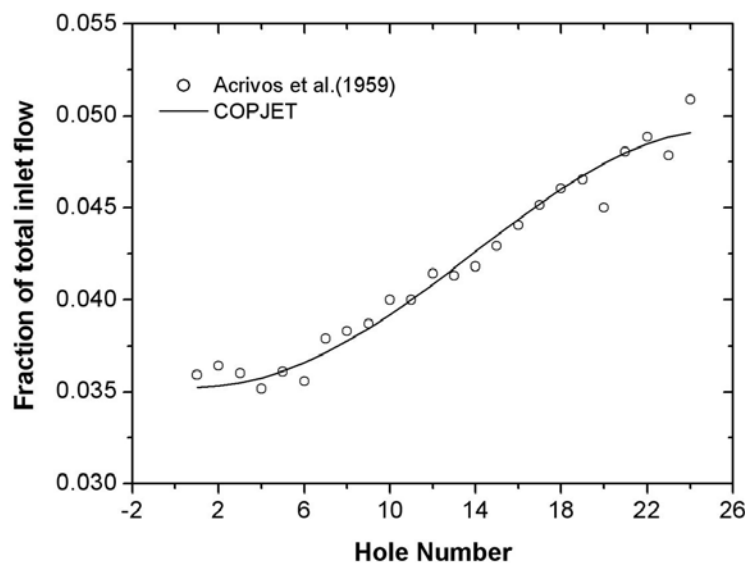


Figure 3.6: Comparison of predicted lateral flow distribution with experimental data

3.2.6.2 Poison jet progression

Validation of the computer code COPJET for progression of poison jet as a function of time was carried out with the poison jet experiments of a generic CANDU-6 reactor. Poison jet experiments are performed by AECL and reported by Rhee et al. (2007).

Geometric and process details of CANDU-6 are taken from Chae et al. (2001a, b) as given in following text.

SDS-2 of CANDU-6 on actuation injects liquid poison (gadolinium nitrate solution in heavy water) into bulk moderator inside calandria through 6 perforated injection tubes using high pressure helium to shut down the reactor. The maximum injection velocity of the liquid poison is 27.8 m/s and the mass fraction of the poison is 8000 ppm. Poison injection tubes were provided with outer diameter of 55.9 mm and thickness of 2.5 mm. There were four rows of nozzles along its length. The nozzle diameter in the poison injection tube is 3.2 mm. The holes are arranged in groups of 16 nozzles such that they are placed centrally between calandria tubes. There were 21 such groups in each poison injection tube.

Rhee et al. (2007) reported experimental results only for progression of poison jet from the first group of holes. The progress of the poison jet growth was captured by a high-speed camera. As the poison concentration was not measured in this experiment, the progression of poison jet was identified based on a visual inspection of the pictures. Rhee et al. (2007) performed CFD simulation of AECL experiment using CFX code. Progression of jet corresponding to 200 ppm and 500 ppm concentration was compared with experimental data. In the present study, the progression of the jet has been determined by using computer code COPJET. Figure 3.7 shows that computer code COPJET prediction is in close agreement with AECL experimental data and CFD analysis carried out by Rhee et al. (2007).

3.3 Results and discussions

The validated computer code, COPJET was used to simulate the SDS-2 poison injection behaviour in AHWR. Different parameters like mass flow rate, gas tank pressure,

dead time for different nozzles in the injection tube, velocities from nozzles along the injection tube and progression of poison jet are predicted using COPJET. The process parameters used for this analysis using COPJET are given in Table 3.3. Following subsections give details of poison starting time along injection tube, mass flow rate, gas tank pressure, poison jet progression and how these results can be used as input for reactor physics analysis.

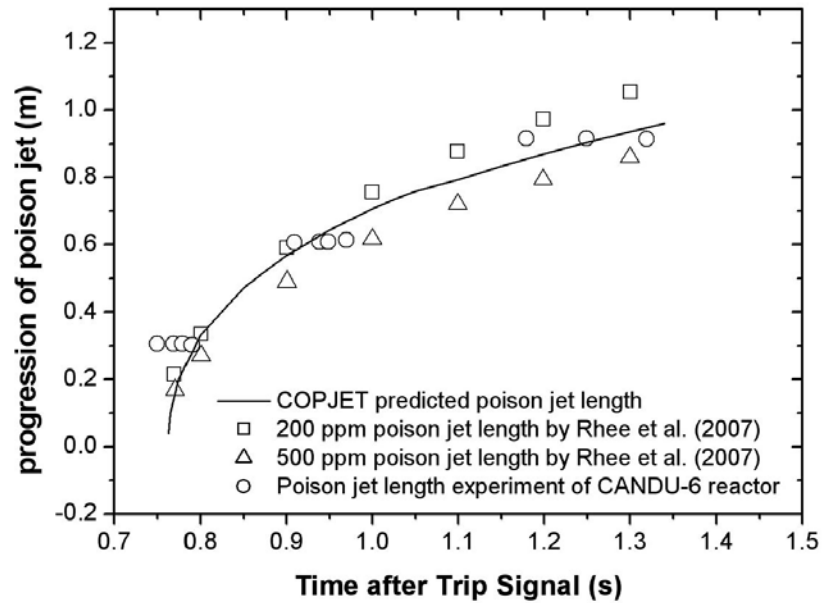


Figure 3.7: Comparison of COPJET predicted progression of poison jet with experiment data and CFD simulation

3.3.1 Time delay in poison injection

To estimate poison jet front length from a particular axial location in injection tube with time, it is necessary to estimate the time at which poison injection starts (t_{st}) from that nozzle. The injection tube has groups of injection nozzles along the length as shown in Figure 3.3. Therefore, different axial location of injection nozzles will have different time delay (t_d) in poison injection with respect to first axial location. Hence, t_{st} is estimated as

$$(t_{st})_i = t_{dead} + (t_d)_i \quad (3.33)$$

Table 3.3: Process parameters for analysis of SDS-2 poison injection

Parameter	Value
Number of gas tank	1
Initial gas tank pressure	80 bar
Number of poison tanks	8
Number of injection tubes	8
Injection tube inner diameter	38 mm
Injection nozzle diameter	6 mm
Number of holes per injection tube	80
Pitch between two calandria tubes	225 mm
Temperature	Ambient

Where, i indicate the location number of nozzle and t_{dead} is the time for poison to reach first group of injection nozzles in injection tube from PMI as shown in Figure 1.3. t_{dead} is estimated by equation (3.35). Where, $volume_{dead}$ is moderator volume between PMI and first group of injection nozzle.

Poison injection starting time $(t_{st})_i$ is estimated by equating moderator volume displaced by PMI movement from injection nozzle group $(i-1)$ to i with moderator volume injected from i to last injection nozzle group as given in equation (3.34). Figure 3.8 shows moderator volume between $i-1$ and i location, which must be injected from i and later nozzles for movement of PMI from $i-1$ to i . Here, $(t_{st})_2$ is estimated using $(t_{st})_1$ which is t_{dead} . Similarly, $(t_{st})_3$ is estimated using $(t_{st})_2$ and so on.

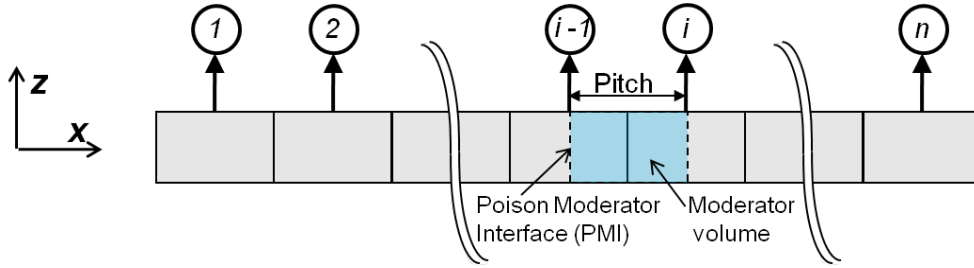


Figure 3.8: Schematic of injection tube with injection nozzle group number

$$Pitch \cdot A_{IT} = \int_{(t_{st})_{i-1}}^{(t_{st})_i} \int_{x_i}^{x_N} (v_n)_i A_h dx dt \quad (3.34)$$

$$Volume_{dead} = \int_0^{t_{dead}} \int_{x_1}^{x_N} (v_n)_i A_h dx dt \quad (3.35)$$

Considering the input data of AHWR provided in Table 3.3, the estimated dead time (t_{dead}) is 0.85 s. Figure 3.9 depicts the poison injection starting time for different nozzle location.

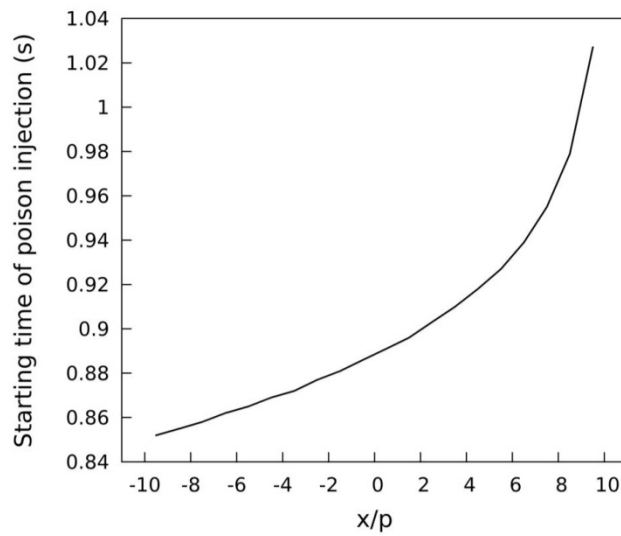


Figure 3.9: Poison injection starting time for different nozzle location

3.3.2 Mass flow rate and gas tank pressure

Figure 3.10 gives the variation of pressure in gas tank and mass flow rate of poison from poison tank with time. It can be seen that mass flow rate reaches maximum value after 0.28 s after injection starts in the calandria. After reaching its maximum value, mass flow rate decreases due to reduction in gas tank pressure.

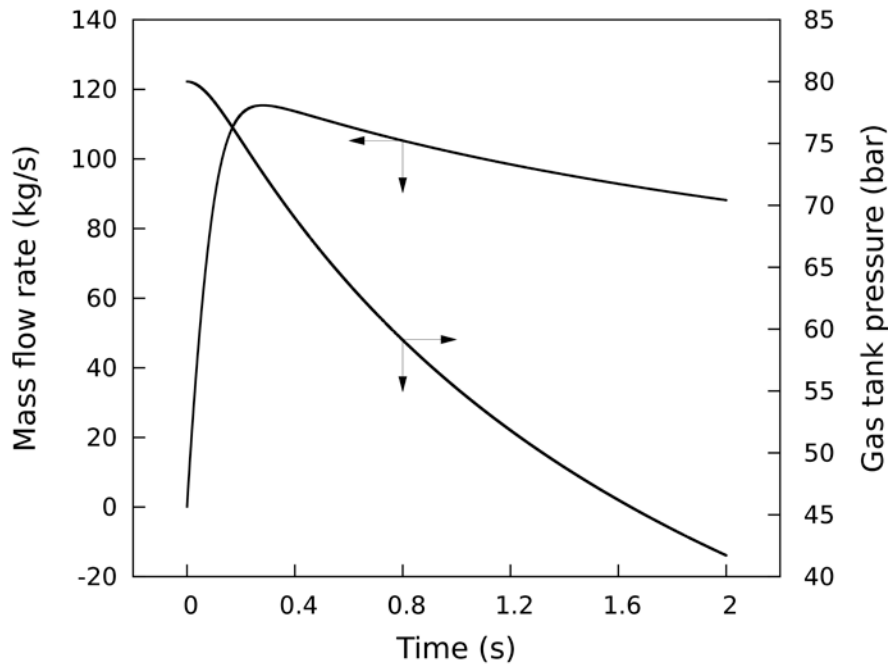


Figure 3.10: Variation of mass flow rate and gas tank pressure with time

3.3.3 Poison jet progression

The variation of progression of poison jet with time is shown in Figure 3.11. At 0.9 s poison injection did not start from the full length of injection tube as poison has not covered the full length of injection tube as shown in Figure 3.9. It can be also seen that after 1.2 s the jet reaches nearly same length for all the injection nozzle groups of the injection tube. This is due to increase in the jet velocity along the length of the injection tube. At 2 s, poison jet reached nearly 2 m from the injection location. Figure 3.12 shows injection velocity for 11th group of injection nozzle. It shows maximum injection velocity of 45 m/s and poison injection start time of 0.89 s.

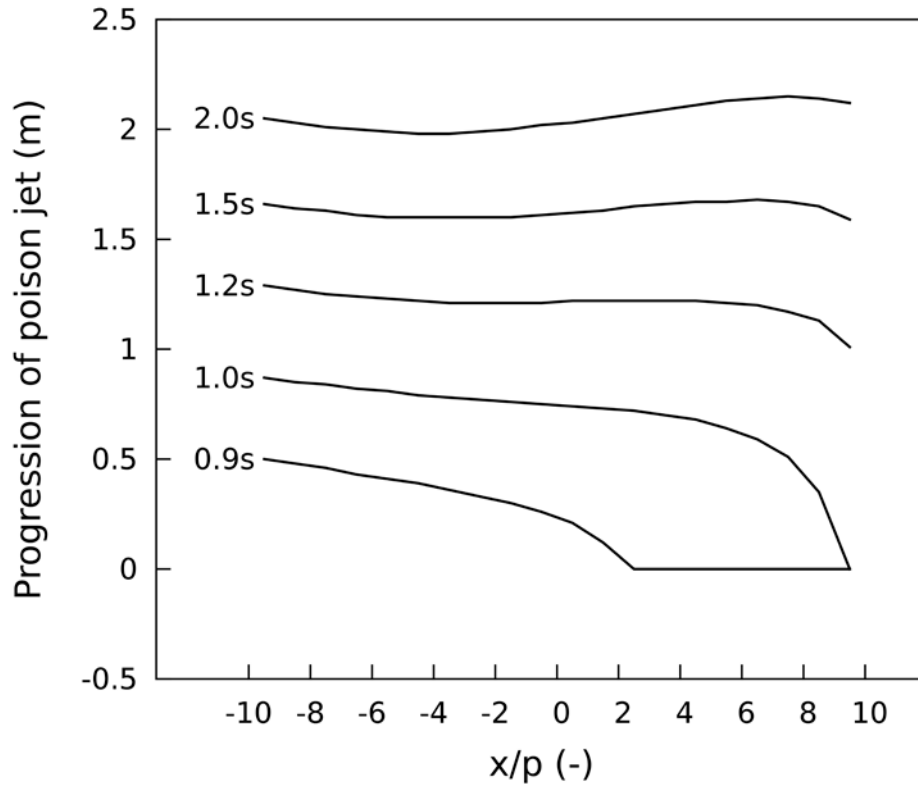


Figure 3.11: Progression of poison jet at different time

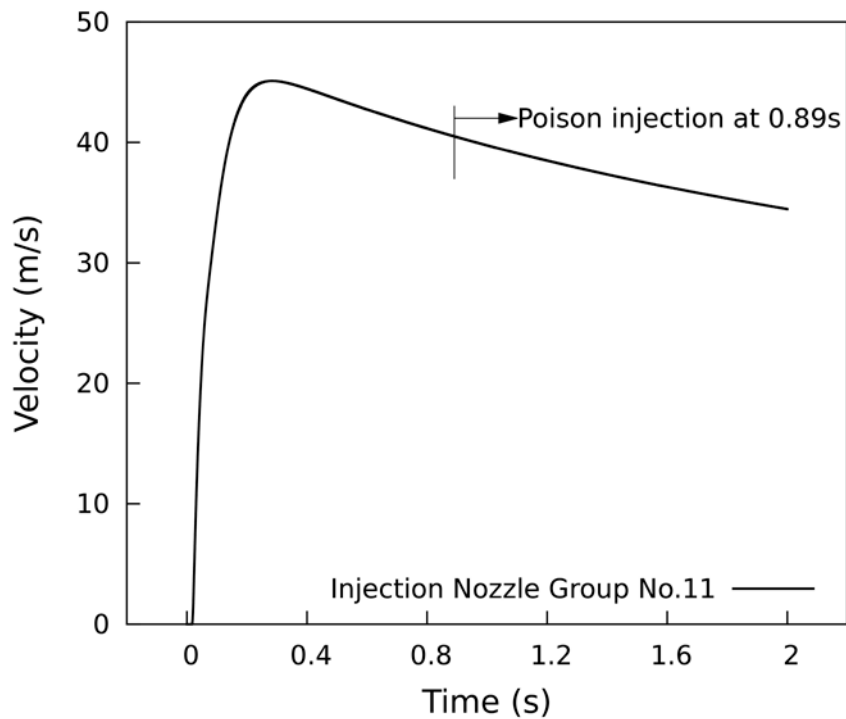


Figure 3.12: Injection velocity for 11th group of injection nozzle

3.3.4 Input for reactor physics analysis

COPJET code predicted jet length and amount of poison injected will be used for calculating the reactivity worth of the SDS-2 by methodology developed by Balakrishnan et al. (1992). In this methodology, poison concentration in jet cone is assumed one dimensional with concentration distribution of $C(z) = C_o(z)/z^k$, where z is progression of poison jet and k is constant. The value of constant k is estimated by following equation of poison in the jet cone.

$$V(z).C_o(z) = \int_0^z C(z).\pi z^2.\tan^2\theta.dz \quad (3.36)$$

Where, $V(z)$ is volume of the poison injected from the nozzle for poison jet of z and half jet angle of θ . Concentration distribution of poison is estimated from this methodology will be used as input in reactor physics code for calculating reactivity worth.

3.4 Conclusions

A computer code, COPJET is developed for predicting transient liquid poison injection behaviour in AHWR. In this model, a semi-empirical equation in non-dimensional form is incorporated for modelling jet injection into the moderator. The equation is derived by using experimental data available on impulsively started jet in literature and standard relation available on steady state jet. The computer code COPJET is validated against the data available in the literature for lateral flow distribution and progression of poison jet. The prediction shows good agreement with experimental data and CFD analysis reported. The results generated by COPJET code can be used for further analysis of reactivity worth.

Chapter 4

EXPERIMENTAL STUDIES ON POISON INJECTION

4.1 Introduction

Shut Down System 2 (SDS-2) operates on the principle of direct injection of poison (gadolinium nitrate solution in heavy water) into bulk moderator in a very short time by means of high pressure helium. This injection is in the form of submerged transient jets. High neutron absorption cross section of Gadolinium solution (Glasstone and Seisanski, 2004), makes the reactor subcritical resulting in shut down of the reactor. As a poison jet emerges in the moderator the surrounding heavy water also gets entrained and mixing takes place. The effectiveness of the system depends on the dispersion of poison in the moderator throughout the calandria in a short time. Based on the distribution in the moderator of poison, the absorption of neutrons occurs thus stops the fission reaction.

In AHWR, the calandria and calandria tubes axes are vertically oriented as compared to CANDU type pressurized heavy water reactor. Moreover, calandria tube pitch to diameter ratio in AHWR is 1.34, hence the effect of calandria tube on the propagation of poison jet will be more as compared to the CANDU type reactors. Due to these differences in configuration, in AHWR injection tubes have different layout as compared to CANDU type reactors. Published literature shows that the experimental studies on jet injection in

presence of tube bundle are not addressed. Hence, experimental studies are needed for poison jet injection in the presence of tube bundle. Location of poison jets with respect to calandria tubes is one of the design parameters, which greatly affect dispersion and penetration of poison jets in calandria. Hence, experiments will be done for different orientation of tube bundle with respect to poison jet.

4.2 Experiments

Experiments on poison jet injection have been performed in the presence of tube bundle. A scaled model has been designed to study the jet behaviour. Experiments have been performed with different orientations of the tube bundle. Details of scaling philosophy, experimental set-up and experimental technique are explained in the following sections.

4.2.1 Scaling philosophy

The experiment setup is designed to study the turbulent submerged jet in a water tank. The purpose of the study is to generate experimental data which can be used for theoretical model validation. For similarity analysis, non-dimensional parameters are found out which can affect the jet growth using Buckingham's pi theorem. Axi-symmetric transient jet progression depends on the following parameters: Time (t), fluid density (ρ), fluid dynamic viscosity (μ), diffusion coefficient (D_{AB}), radial velocity (v_r), axial velocity (v_z), jet inlet velocity (U_o), jet inlet diameter (d), radial coordinate (r), axial coordinate (z), jet fluid concentration (C), jet fluid inlet concentration (C_o), tube bundle pitch (p), tube diameter (D)

Total number of parameters, $n = 14$

There are basic unit namely mass, length, time and concentration for the 14 parameters stated above $j = 4$

So, numbers of Π terms are $(n - j) = (14 - 4) = 10$

ρ , U_o , d and C_o are selected as repeated variables.

Now for finding first Π term

$$\begin{aligned}\Pi_1 &= t \times \rho^{a_1} \times U_o^{b_1} \times d^{c_1} \times C_o^{d_1} \\ &= [T^1] [ML^{-3}]^{a_1} [LT^{-1}]^{b_1} [L]^{c_1} [C]^{d_1} = [M^0 L^0 T^0 C^0]\end{aligned}$$

By comparing powers of M, L, T and C we get

$$a_1 = 0, b_1 = 1, c_1 = -1 \text{ and } d_1 = 0$$

So, Π_1 becomes

$$\Pi_1 = \frac{tU_o}{d}$$

Similarly, other pi terms are found as

$$\Pi_2 = \frac{\rho U_o d}{\mu} = \text{Re (Reynolds number)},$$

$$\Pi_3 = \frac{D_{AB}}{U_o d},$$

$$\Pi_4 = \frac{v_r}{U_o}, \quad \Pi_5 = \frac{v_z}{U_o},$$

$$\Pi_6 = \frac{r}{d}, \quad \Pi_7 = \frac{z}{d},$$

$$\Pi_8 = \frac{C}{C_o},$$

$$\Pi_9 = \frac{p}{d}, \quad \Pi_{10} = \frac{D}{d},$$

Now Π_3 changes to $1/(\Pi_2 \times \Pi_3)$

$$\Pi_3 = \frac{\mu}{\rho D_{AB}} = Sc \text{ (Schmidt number)}$$

and Π_9 and Π_{10} can be combined as

$$\Pi_9 = \frac{\Pi_9}{\Pi_{10}} = \frac{p}{D}$$

So, jet progression is written as the following function

$$\frac{z}{d} = f\left(\frac{tU_o}{d}, \frac{r}{d}, \frac{v_r}{U_o}, \frac{v_z}{U_o}, \frac{\rho U_o d}{\mu}, \frac{\mu}{\rho D_{AB}}, \frac{C}{C_o}, \frac{p}{D}, \frac{D}{d}\right)$$

$$z^* = f\left(t^*, r^*, v_r^*, v_z^*, Re, Sc, C^*, \frac{p}{D}, \frac{D}{d}\right)$$

For similarity of solution in model and prototype, Reynolds number needs to be identical for model and prototype. If the scaled model selected is 1/3.3 then, for meeting this requirement, jet inlet velocity in model needs to be around $45 \times 3.3 \approx 150$ m/s, as the jet inlet velocity in prototype is about 45 m/s. However, performing experiments with such high velocity is not feasible. Hence, in model, inlet jet velocity is maintained such that Reynolds number is in turbulence regime like prototype.

Now to understand the effect of different Reynolds number in model and prototype, Reynolds Averaged Navier-Stokes (RANS) equations (Rajaratnam, 1976) in cylindrical coordinate (r, ϕ, z) for axi-symmetric turbulent jet case was converted into non-dimensional form. The RANS equations in the cylindrical system for axi-symmetric flow could be written by neglecting the body force terms:

Continuity equation

$$\frac{\partial}{\partial r} r v_r + r \frac{\partial}{\partial z} v_z = 0 \tag{4.1}$$

Momentum equation in radial direction

$$\begin{aligned} & \frac{\partial v_r}{\partial t} + v_r \frac{\partial v_r}{\partial r} + v_z \frac{\partial v_r}{\partial z} \\ &= -\frac{1}{\rho} \frac{\partial p}{\partial r} + \nu \left(\frac{\partial^2 v_r}{\partial r^2} + \frac{1}{r} \frac{\partial v_r}{\partial r} - \frac{v_r}{r^2} + \frac{\partial^2 v_r}{\partial z^2} \right) - \left(\frac{\partial}{\partial r} \overline{v_r'^2} + \frac{\partial}{\partial z} \overline{v_r' v_z'} + \frac{\overline{v_r'^2}}{r} - \frac{\overline{v_\phi'^2}}{r} \right) \end{aligned} \quad (4.2)$$

Momentum equation in axial direction

$$\begin{aligned} & \frac{\partial v_z}{\partial t} + v_r \frac{\partial v_z}{\partial r} + v_z \frac{\partial v_z}{\partial z} \\ &= -\frac{1}{\rho} \frac{\partial p}{\partial z} + \nu \left(\frac{\partial^2 v_z}{\partial r^2} + \frac{1}{r} \frac{\partial v_z}{\partial r} + \frac{\partial^2 v_z}{\partial z^2} \right) - \left(\frac{\partial}{\partial r} \overline{v_r' v_z'} + \frac{\partial}{\partial z} \overline{v_z'^2} + \frac{\overline{v_r' v_z'}}{r} \right) \end{aligned} \quad (4.3)$$

Mass Transport Equation

$$\frac{\partial C}{\partial t} + \frac{v_r}{r} \frac{\partial(rC)}{\partial r} + v_z \frac{\partial C}{\partial z} = \left(D_{AB} + \frac{\nu_t}{Sc_t} \right) \left(\frac{\partial^2 C}{\partial r^2} + \frac{1}{r} \frac{\partial C}{\partial r} + \frac{\partial^2 C}{\partial z^2} \right) + S \quad (4.4)$$

The orders of parameter for axi-symmetric jet are as

$r \sim \delta$ (order radius of the jet is same as spread of jet)

$z \sim L$ (order of z axis is same as jet length)

$v_z \sim U_o$ (order of axial velocity is same as jet inlet velocity)

Since axial velocity is very high compared to radial velocity ($v_z \gg v_r$)

So, from continuity equation it is found that

$$\frac{\partial}{\partial z} \ll \frac{\partial}{\partial r} \quad \text{and} \quad \frac{\partial^2}{\partial z^2} \ll \ll \frac{\partial^2}{\partial r^2}$$

Jet flow is in fully turbulent region hence, Reynolds stresses are dominant over viscous stress. Viscous terms in right side can be neglected compared to turbulent stress terms.

So, dominant term in right side term of equation (4.3) is $\frac{\overline{\partial v_r v_z}}{\partial r}$ and $\frac{\overline{v_r v_z}}{r}$ having order of $\sim \frac{\overline{v_r v_z}}{\delta}$

The order of second advection term in axial momentum equation (4.3) is $v_z \frac{\partial v_z}{\partial z} \sim \frac{U_o^2}{L}$

The magnitude of Reynolds stress can be estimated by noting that advective and turbulent stress terms should be of the same order within the jet flow, so

$$\frac{\overline{v_r v_z}}{\delta} \sim \frac{U_o^2}{L} \text{ or } \overline{v_r v_z} \sim \frac{\delta}{L} U_o^2$$

Now, Order of v_r can be found from the continuity equation

$$\frac{\delta \times v_r}{\delta} \sim \frac{\delta \times U_o}{L} \Rightarrow v_r \sim \frac{\delta}{L} U_o \text{ and order of time } t \text{ is } \frac{L}{U_o}$$

Now, by putting order of magnitude of all terms in momentum equations and mass transfer equations and assuming turbulent stresses in all direction are same orders,

Order of magnitude for momentum equation in radial direction (4.2)

$$\begin{aligned} \frac{\partial v_r}{\partial t} + v_r \frac{\partial v_r}{\partial r} + v_z \frac{\partial v_r}{\partial z} &= -\frac{1}{\rho} \frac{\partial p}{\partial r} - \left(\frac{\partial \overline{v_r^2}}{\partial r} + \frac{\partial \overline{v_r v_z}}{\partial z} \right) \\ \downarrow \quad \quad \downarrow & \\ \frac{\delta}{L} \left(\frac{U_o^2}{L} \right) \quad \frac{\delta}{L} \left(\frac{U_o^2}{L} \right) \quad \frac{\delta}{L} \left(\frac{U_o^2}{L} \right) \quad \frac{1}{\rho} \frac{\partial p}{\partial r} \quad \left(\frac{U_o^2}{L} \right) \quad \frac{\delta}{L} \left(\frac{U_o^2}{L} \right) & \end{aligned} \quad (4.5)$$

Order of magnitude for momentum equation in axial direction (4.3)

$$\begin{aligned}
 \frac{\partial v_z}{\partial t} + v_r \frac{\partial v_z}{\partial r} + v_z \frac{\partial v_z}{\partial z} &= -\frac{1}{\rho} \frac{\partial p}{\partial z} - \left(\frac{\partial \overline{v_r v_z}}{\partial r} + \frac{\partial \overline{v_z^2}}{\partial z} + \frac{\overline{v_r v_z}}{r} \right) \\
 \downarrow \quad \quad \downarrow & \\
 \left(\frac{U_o^2}{L} \right) \quad \left(\frac{U_o^2}{L} \right) \quad \left(\frac{U_o^2}{L} \right) \quad \frac{1}{\rho} \frac{\partial p}{\partial z} \quad \left(\frac{U_o^2}{L} \right) \quad \delta \left(\frac{U_o^2}{L} \right) \quad \left(\frac{U_o^2}{L} \right) &
 \end{aligned} \tag{4.6}$$

After comparing the order of magnitude and neglecting the smaller value terms, momentum equation in radial (4.2) and axial (4.3) direction becomes

$$0 = -\frac{1}{\rho} \frac{\partial p}{\partial r} - \left(\frac{\partial \overline{v_r^2}}{\partial r} \right) \tag{4.7}$$

$$\frac{\partial v_z}{\partial t} + v_r \frac{\partial v_z}{\partial r} + v_z \frac{\partial v_z}{\partial z} = -\frac{1}{\rho} \frac{\partial p}{\partial z} - \left(\frac{\partial \overline{v_r v_z}}{\partial r} + \frac{\partial \overline{v_z^2}}{\partial z} + \frac{\overline{v_r v_z}}{r} \right) \tag{4.8}$$

By integrating the momentum equations in radial direction from r to ∞ , expression for pressure can be found as

$$p = p_\infty - \rho \overline{v_r^2} \tag{4.9}$$

By putting this expression in momentum equation in axial direction (4.8)

$$\frac{\partial v_z}{\partial t} + v_r \frac{\partial v_z}{\partial r} + v_z \frac{\partial v_z}{\partial z} = -\frac{1}{\rho} \frac{\partial p_\infty}{\partial z} - \left(\frac{\partial \overline{v_r v_z}}{\partial r} + \frac{\partial \left(\overline{v_z^2} - \overline{v_r^2} \right)}{\partial z} + \frac{\overline{v_r v_z}}{r} \right) \tag{4.10}$$

Second term in right side is very small, since turbulent stresses are of equal order. The pressure in ambient fluid far from jet field is nearly constant, hence $\partial p_\infty / \partial z = 0$.

So equations of motion for jet reduces to the following forms

Continuity equation (4.1) becomes,

$$\frac{\partial}{\partial r} r v_r + r \frac{\partial}{\partial z} v_z = 0 \quad (4.11)$$

Momentum equation in axial direction (4.10) becomes,

$$\frac{\partial v_z}{\partial t} + v_r \frac{\partial v_z}{\partial r} + v_z \frac{\partial v_z}{\partial z} = - \left(\frac{\partial}{\partial r} \overline{v_r' v_z'} + \frac{\overline{v_r' v_z'}}{r} \right) \quad (4.12)$$

$$\frac{\partial v_z}{\partial t} + v_r \frac{\partial v_z}{\partial r} + v_z \frac{\partial v_z}{\partial z} = - \frac{1}{r} \left(\frac{\partial}{\partial r} r \overline{v_r' v_z'} \right) \quad (4.13)$$

The mass transport equation (4.4) reduces for jet flow as

$$\frac{\partial C}{\partial t} + \frac{v_r}{r} \frac{\partial (rC)}{\partial r} + v_z \frac{\partial C}{\partial z} = \left(\frac{v}{Sc} + \frac{v_t}{Sc_t} \right) \left(\frac{\partial^2 C}{\partial r^2} + \frac{1}{r} \frac{\partial C}{\partial r} \right) \quad (4.14)$$

Now, for converting these equations of motion to non-dimensional form, following non-dimensional variables are used:

$$r^* = \frac{r}{\delta} \sim 1, \quad z^* = \frac{z}{L} \sim 1$$

$$v_r^* = \frac{v_r}{\frac{\delta}{L} U_0}, \quad v_z^* = \frac{v_z}{U_0}, \quad \overline{v_r' v_z'^*} = \frac{\overline{v_r' v_z'}}{\frac{\delta}{L} U_0^2},$$

$$C^* = \frac{C}{c_0}$$

$$\text{and } t^* = \frac{t U_0}{L}$$

Now, these non-dimensional quantity are substituted in equations of motion, so equations becomes

Continuity equation (4.11) becomes,

$$\frac{\partial}{\partial r^*} r^* v_r^* + r^* \frac{\partial}{\partial z^*} v_z^* = 0 \quad (4.15)$$

Momentum equation in axial direction (4.13) becomes,

$$\frac{\partial v_z^*}{\partial t^*} + v_r^* \frac{\partial v_z^*}{\partial r^*} + v_z^* \frac{\partial v_z^*}{\partial z^*} = -\frac{1}{r^*} \left(\frac{\partial}{\partial r^*} r^* \overline{v_r' v_z'} \right) \quad (4.16)$$

In mass transport equation for high Reynolds number

$$\frac{v}{Sc} \ll \frac{v_t}{Sc_t},$$

$$v_t \sim \text{velocity scale} \cdot \text{length scale} \\ \sim U_o L$$

The mass transport equation (4.14) becomes,

$$\begin{aligned} \frac{C_o U_o}{L} \left(\frac{\partial C^*}{\partial t^*} + \frac{v_r^*}{r^*} \frac{\partial (r^* C^*)}{\partial r^*} + v_z^* \frac{\partial C^*}{\partial z^*} \right) &= \frac{v_t}{Sc_t} \frac{C_o}{\delta^2} \left(\frac{\partial^2 C^*}{\partial r^{*2}} + \frac{1}{r^*} \frac{\partial C^*}{\partial r^*} \right) \\ \frac{C_o U_o}{L} \left(\frac{\partial C^*}{\partial t^*} + \frac{v_r^*}{r^*} \frac{\partial (r^* C^*)}{\partial r^*} + v_z^* \frac{\partial C^*}{\partial z^*} \right) &= \frac{U_o L C_o}{Sc_t} \frac{1}{\delta^2} \left(\frac{\partial^2 C^*}{\partial r^{*2}} + \frac{1}{r^*} \frac{\partial C^*}{\partial r^*} \right) \\ \frac{\partial C^*}{\partial t^*} + \frac{v_r^*}{r^*} \frac{\partial (r^* C^*)}{\partial r^*} + v_z^* \frac{\partial C^*}{\partial z^*} &= \frac{L}{C_o U_o} \frac{U_o L C_o}{Sc_t} \frac{1}{\delta^2} \left(\frac{\partial^2 C^*}{\partial r^{*2}} + \frac{1}{r^*} \frac{\partial C^*}{\partial r^*} \right) \\ \Rightarrow \frac{L}{C_o U_o} \frac{U_o L C_o}{Sc_t} \frac{1}{\delta^2} &= \frac{1}{Sc_t} \left(\frac{L}{\delta} \right)^2 \end{aligned}$$

where, $\frac{\delta}{L}$ is tangent of half jet angle ($\sim 8^\circ$) and Sc_t is 0.7

Hence the final form of the mass transport equation (4.14) becomes,

$$\frac{\partial C^*}{\partial t^*} + \frac{v_r^*}{r^*} \frac{\partial (r^* C^*)}{\partial r^*} + v_z^* \frac{\partial C^*}{\partial z^*} = \frac{1}{Sc_t} \left(\frac{L}{\delta} \right)^2 \left(\frac{\partial^2 C^*}{\partial r^{*2}} + \frac{1}{r^*} \frac{\partial C^*}{\partial r^*} \right) \quad (4.17)$$

These equations now consist of non-dimensional parameter each of order one and independent of Reynolds number. So, model and prototype Reynolds number need not to be same for jet flow analysis for high Reynolds number jet. These equations give the similar solution for both model and prototype for same non-dimensional parameters included in equations and requires only geometric similarity.

4.2.2 Experimental facility

Two sets of experiments were carried out. In the first set of experiments, 1/3.3 scaled model was fabricated for poison distribution in the presence of calandria tubes and in the second set of experiments, full scale test facility was fabricated for poison jet progression in the presence of calandria tubes. A few calandria tubes were used for the studies in full scale test facility. Actual condition of injection velocity is applied at the jet inlet.

4.2.2.1 Model with scaled dimensions

The experimental setup consists of a transparent tank having a base dimension of 500 x 500 mm and a height of 500 mm. The tank is filled with water. Schematic of the experimental setup is shown in Figure 4.1. Flow through injection nozzle is adjusted using bypass valve (V-1). A three way solenoid valve is used to shift flow direction back to dye tank and injection nozzle. Before the start of the experiment, the pump is started with solenoid valve directing flow back to tank and line up to injection nozzle filled with dye. For starting the experiments, high speed camera is switched on and flow through solenoid valve is directed to the injection nozzle.

Experiments were performed with and without tube bundle. Two types of tube bundles were employed in the experiments: first was an axial bundle and the other was a cross bundle. In the axial bundle, tube axes were parallel to jet axis whereas, in the cross bundle, tube axes were perpendicular to the jet axis. The schematic arrangement of axial and cross bundle is shown in Figure 4.2. For axial tube bundle configuration, an array of 2 x 2 tube

was installed and for cross tube bundle configuration, an array of 5 x 2 tube was installed.

Figure 4.3 shows the arrangement of both the bundles in a transparent water tank.

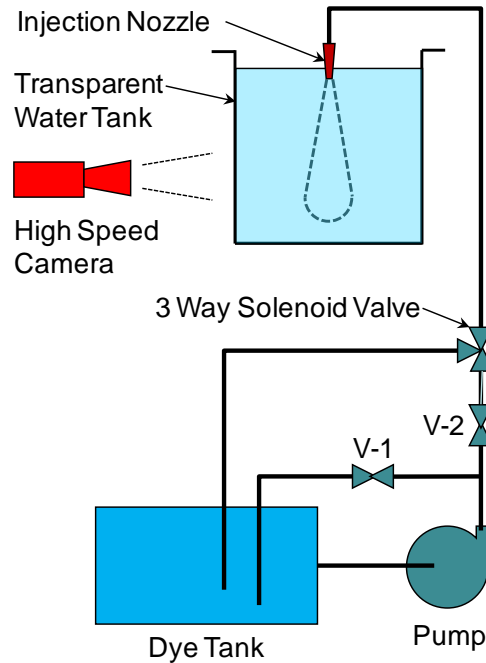
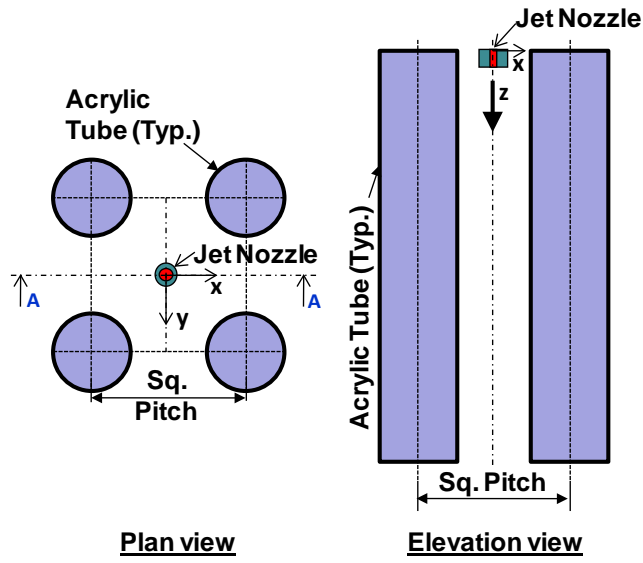
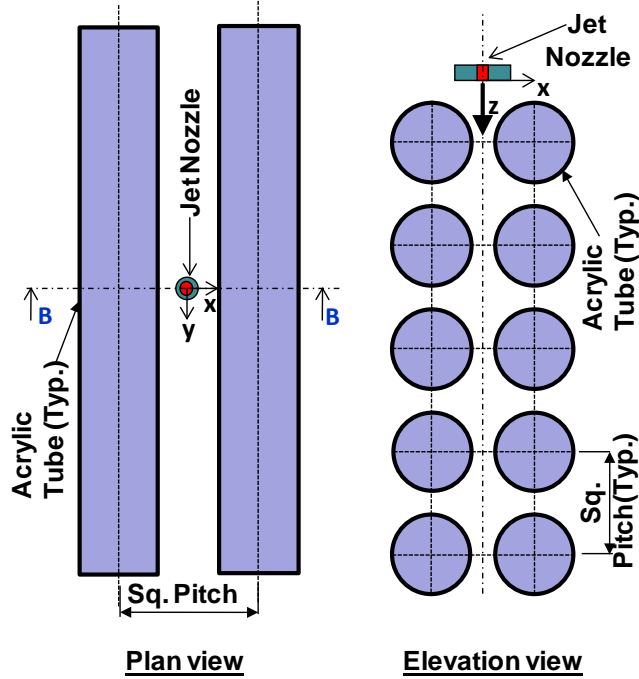


Figure 4.1: Schematic layout of experimental setup

AHWR has calandria tube of outer diameter 168 mm arranged in a square pitch of 225 mm. This gives the pitch to diameter (p/d) ratio as 1.34. In this experiment, the diameter of acrylic tube is 50.8 mm hence to maintain p/d ratio same as the prototype, a pitch of 68 mm was selected. Prototype SDS-2 have nozzle diameter in the range of 6-7 mm based on the number of jets and poison volume to be injected, hence model should have nozzle diameter in between 1.8 to 2.1 mm and 2mm nozzle diameter was selected for the experiments. Experiments were performed at inlet jet velocity of 7.5 m/s ($Re = 15040$) which is in turbulent regime.

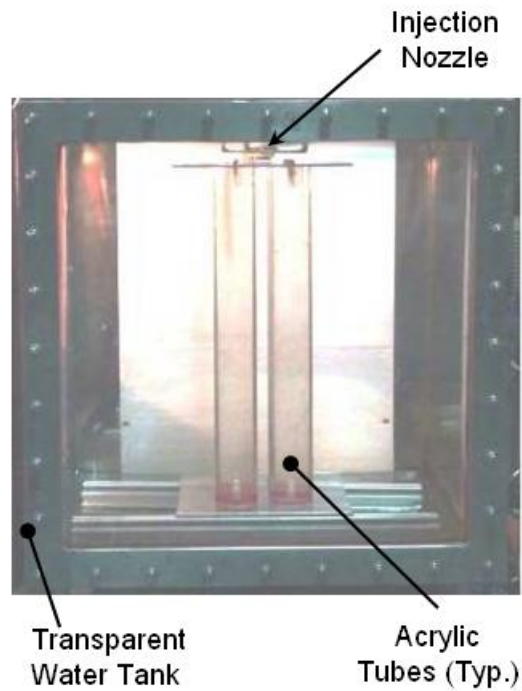


(a) Axial bundle arrangement

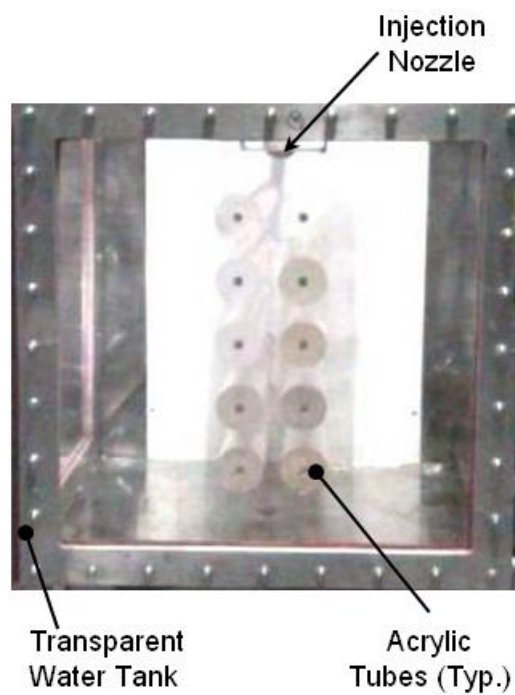


(b) Cross bundle arrangement

Figure 4.2: Schematic arrangement of acrylic tubes for (a) axial bundle and (b) cross bundle in scaled facility



(a) Axial bundle arrangement



(b) Cross bundle arrangement

Figure 4.3: Tube bundle arrangement in transparent water tank

4.2.2.2 Model with full scale dimensions

An experimental setup of a full scale injection nozzle with full scale calandria tubes is fabricated to study submerged jet growth. The nozzle diameter of 6 mm is used. Axis of installed jet nozzle was perpendicular to the tube bundle axis. In the setup, 4 x 4 array of calandria tubes are used. Figure 4.4 gives the details of the experimental setup.

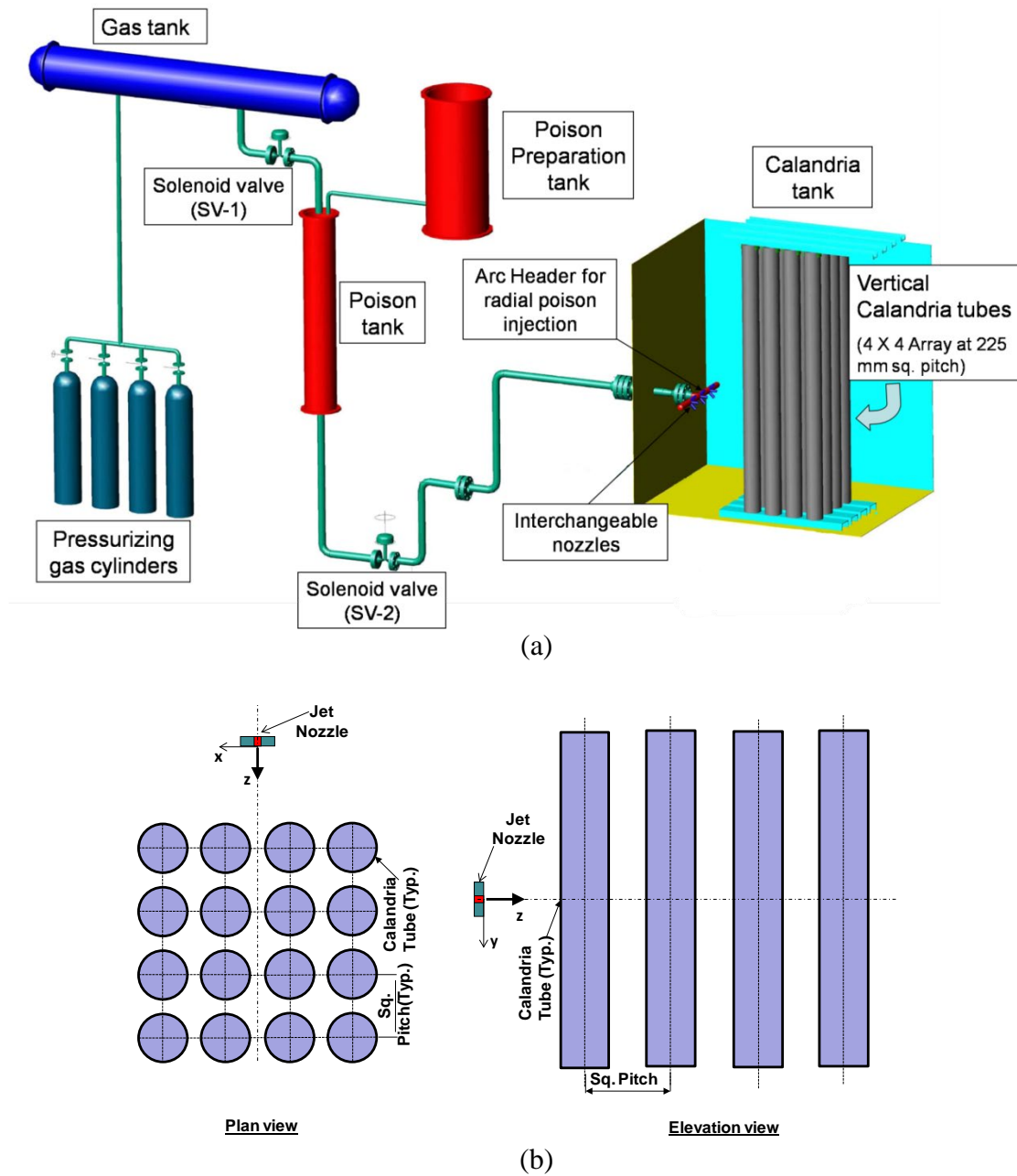


Figure 4.4: Schematic of full scale experimental setup for jet injection

In AHWR, liquid poison and moderator are separated by Poison Moderator Interface (PMI) inside connecting pipe between poison tank and injection tube as shown in Figure 1.3. After the system actuation, poison is injected into the calandria tank. However, during the initial period of injection, moderator present between PMI and injection nozzle flows into the calandria. Actual injection of the poison occurs after the injection of moderator into the calandria. This causes time delay for actual entry of poison into calandria vessel after the system is actuated. The time required for poison to travel from PMI to calandria is defined as the dead time (t_{dead}). In the experimental setup, there is a solenoid valve which separates poison from the water in the tank.

4.2.3 Experimental techniques

4.2.3.1 Dye injection

In all the experiments, solution of potassium permanganate ($KMnO_4$) was used as a dye for flow visualization of jet injection. In this technique, jet of coloured dye was injected into water filled in a transparent tank. The movement of dye was recorded with the camera.

4.2.3.2 Camera

The jet injection was captured by a video camera operated at the frame rate of 125 per second and 25 per second in the scaled facility and the full scaled test facility respectively. Captured frames were in RGB (Red Green Blue) format.

4.2.4 Data Processing

To estimate the jet progression from the captured frames, they were first cropped to the region of interest and the background was subtracted from all the frames. To obtain black and white images, they were converted into black and white indexed images. This process makes the jet colour black and the rest of the images become white in colour. Figure 4.5 shows the comparison between the cropped images before the post processing and after

post processing. It was observed that the post-processed image represents the actual jet profile, and hence was used for estimating poison jet propagation in water.

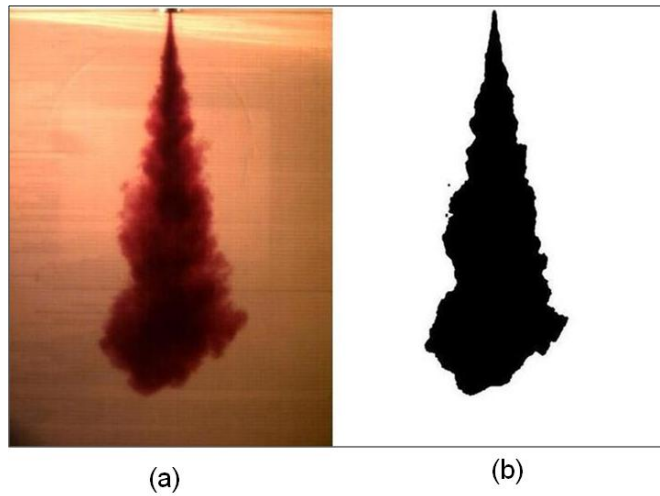


Figure 4.5: Image captured by high speed camera (a) actual image (b) processed image

4.3 Results and Discussions

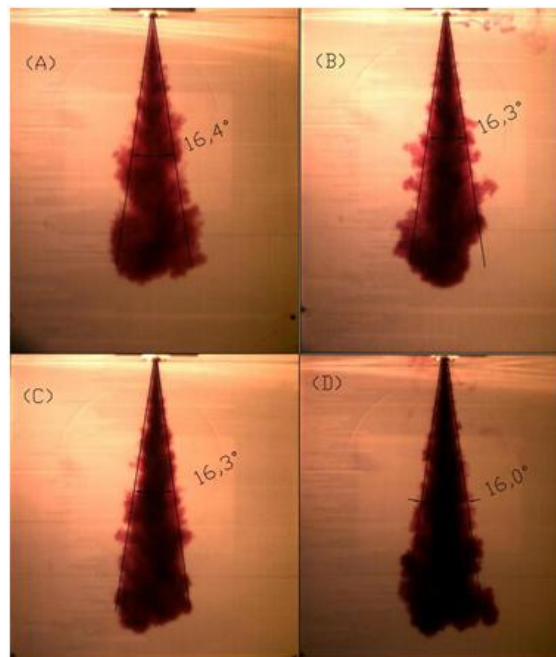
The results from experiments performed in scaled model are discussed in the following sections.

4.3.1 Free jet

As the circular jet enters the ambient fluid it spreads in a conical shape. In SDS-2, poison distribution depends on poison jet spread. Jet spreading was analysed for different jet inlet Reynolds numbers. Spreading of jets for different inlet Reynolds numbers is shown in Figure 4.6. It was found that for all the free jets, the spread angle is nearly the same and equal to 16° . This is within the range of spread angle $14^\circ - 17^\circ$ reported in the literature for free water jets. The spread of angle for water jet was reported 14° by Binnie (1942), 17° by Horn and Thrino (1956) and 17° by Johari and Paduano (1997).

Figure 4.7 shows progression of 2 mm diameter jet having velocity 7.5 m/s ($Re = 15000$) initiated by opening of a solenoid valve, with interval of 0.2 s. From Figures 4.7 (a)

to (d), it can be seen that rate of jet progression reduces with time. Figure 4.8 shows the progression of free jet with time.



(A) $Re = 7600$, (B) $Re = 15040$, (C) $Re = 22880$ and (D) $Re = 24600$

Figure 4.6: Jet spread angle of free jet for different Reynolds number

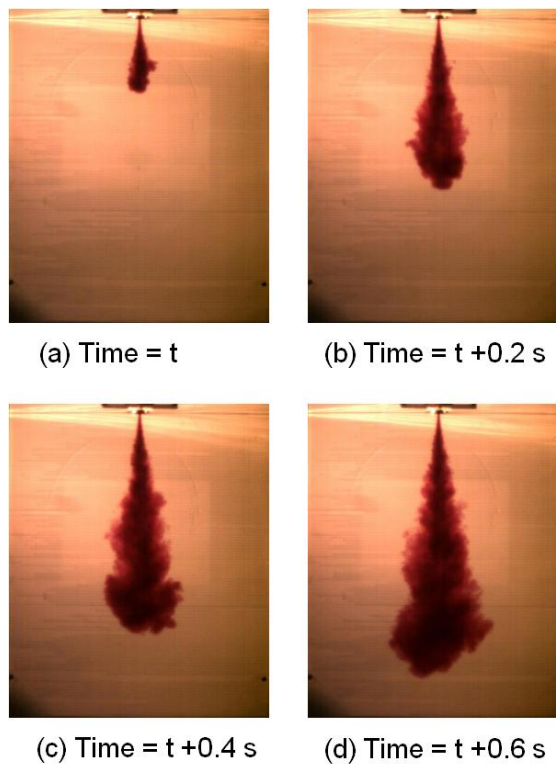


Figure 4.7: Progression of 2 mm diameter free jet with time ($Re = 15000$)

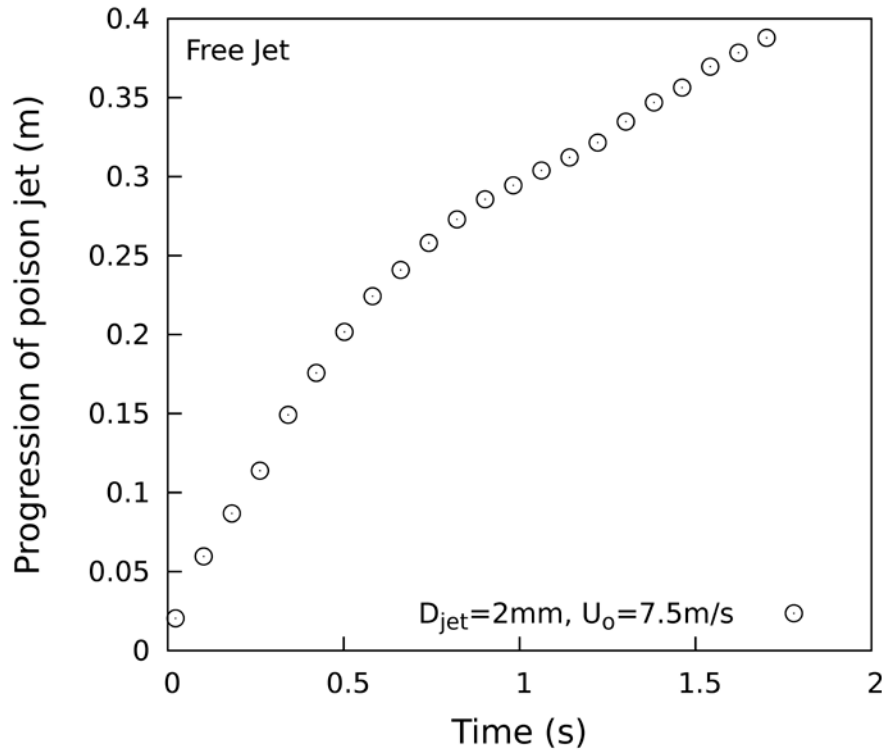


Figure 4.8: Progression of free jet with time

4.3.2 Jet with tube bundle

4.3.2.1 Axial tube bundle in scaled model

Experiments for impulsively started jet with axial tube bundle were performed for geometry described in sub-section 4.3.2.1. Figure 4.2 (a) and Figure 4.3 (a) shows the schematic of jet injection in the tube bundle having same direction of axis to the jet axis. The jet was initiated by sudden charging of a solenoid valve, which was connected with 2 mm diameter nozzle having velocity of 7.5 m/s. Experiments were also performed with 4 mm diameter nozzle and with 1.9 m/s jet velocity. It can be seen from Figure 4.9, that the lateral spread of jet is less as compared to the free jet and this may be due to the tendency of axial tubes which do not allow jet to spread radially. By referring Figures 4.9 (a) to (d) it can be said that the rate of jet progression reduces with time. Figure 4.9 shows distortion in the captured image and this may be due to lens effect of acrylic tubes in water. Figure 4.10 shows the progression of poison jet through axial bundle. When progression of poison jet

is plotted in no-dimensional form both curves of Figure 4.10 nearly overlaps as shown in Figure 4.11. Hence the behaviour of jets of different diameters remains similar.

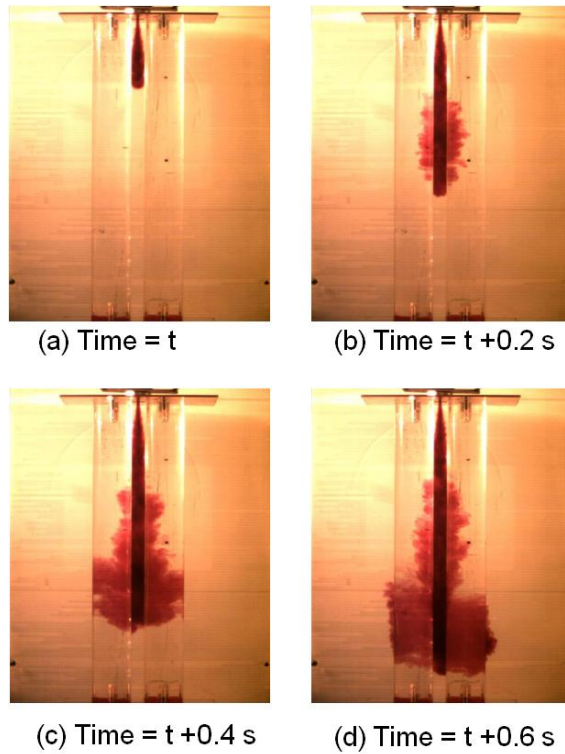


Figure 4.9: Progression of 2 mm diameter jet in axial bundle with time ($Re = 15000$)

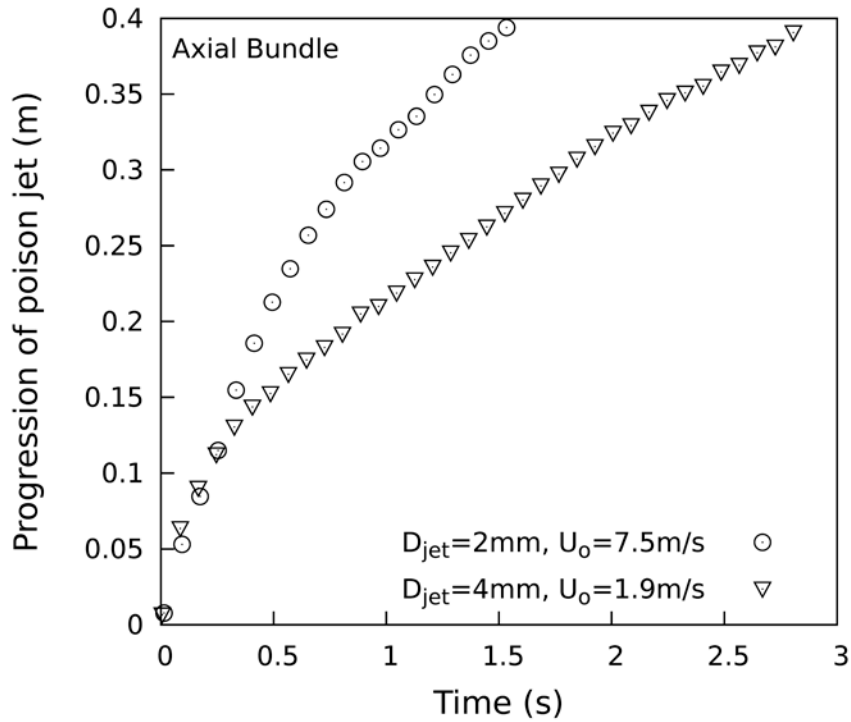


Figure 4.10: Progression of poison jet through axial bundle

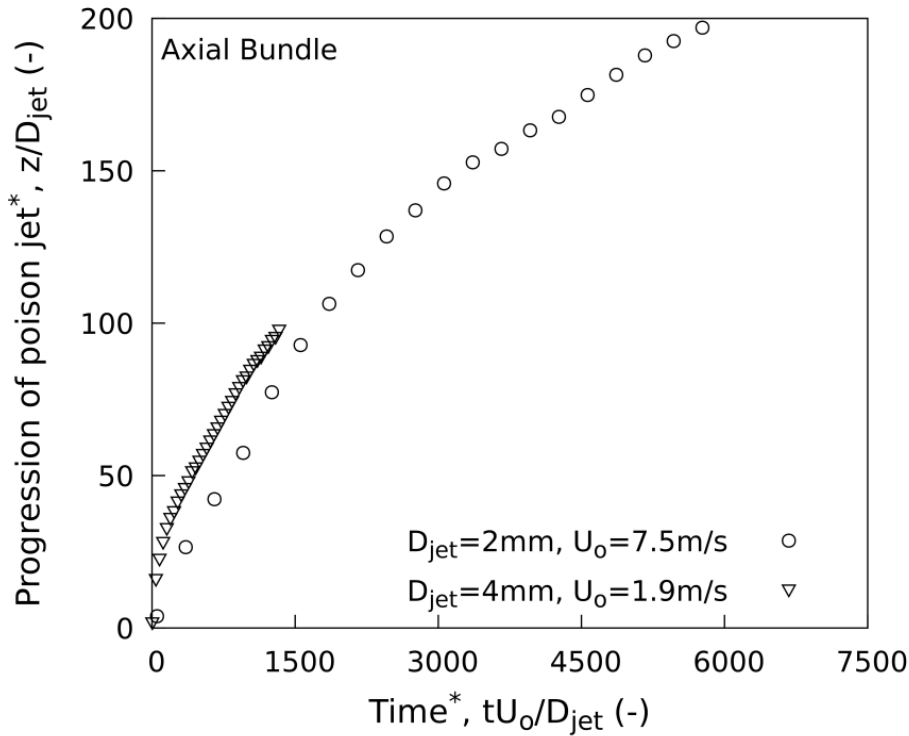


Figure 4.11: Non-dimensional progression of poison jet through axial bundle

4.3.2.2 Cross tube bundle in scaled model

Experiments for impulsively started jet with cross tube bundle were performed for geometry described in sub-section 4.3.2.1. Figure 4.2 (b) and 4.3 (b) shows the schematic of jet injection in the tube bundle having axis perpendicular to the jet axis. The jet was initiated by the sudden charging of a solenoid valve, which was connected with 2 mm diameter nozzle. The jet velocity of 7.5 m/s was maintained during the experiments. In addition to experiments with 2 mm diameter nozzle, experiments were also performed with 4 mm diameter nozzle. The jet velocity was maintained at 1.90 m/s during the experiments. Figure 4.12 shows that lateral spread of jet initially increase and then reduce with jet progression. Jet energy dissipates faster in case of cross bundle arrangement due to higher flow resistance. Figure 4.13 shows the progression of poison jet through cross bundle. When progression of poison jet is plotted in no-dimensional form both curves of Figure

4.13 nearly overlaps as shown in Figure 4.14. Hence the behaviour of jets of different diameters remains similar.

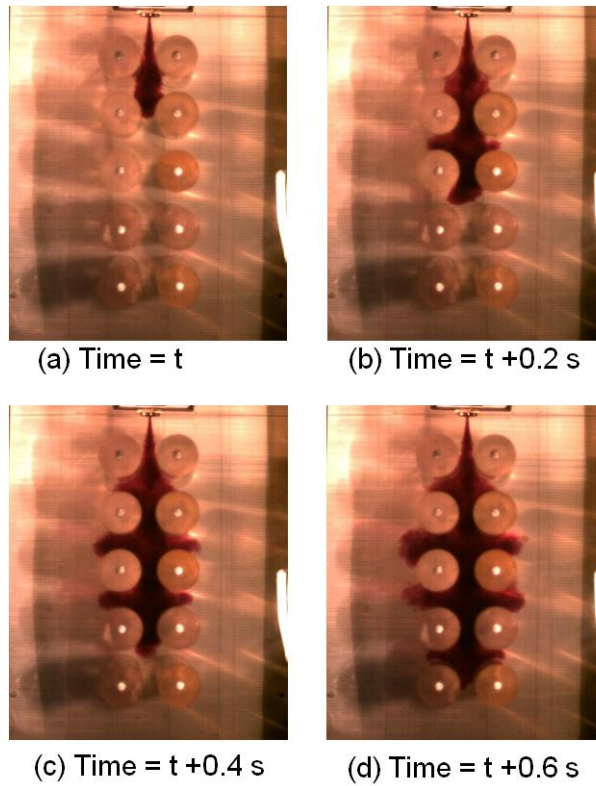


Figure 4.12: Progression of 2 mm diameter jet in cross bundle with time ($Re = 15000$)

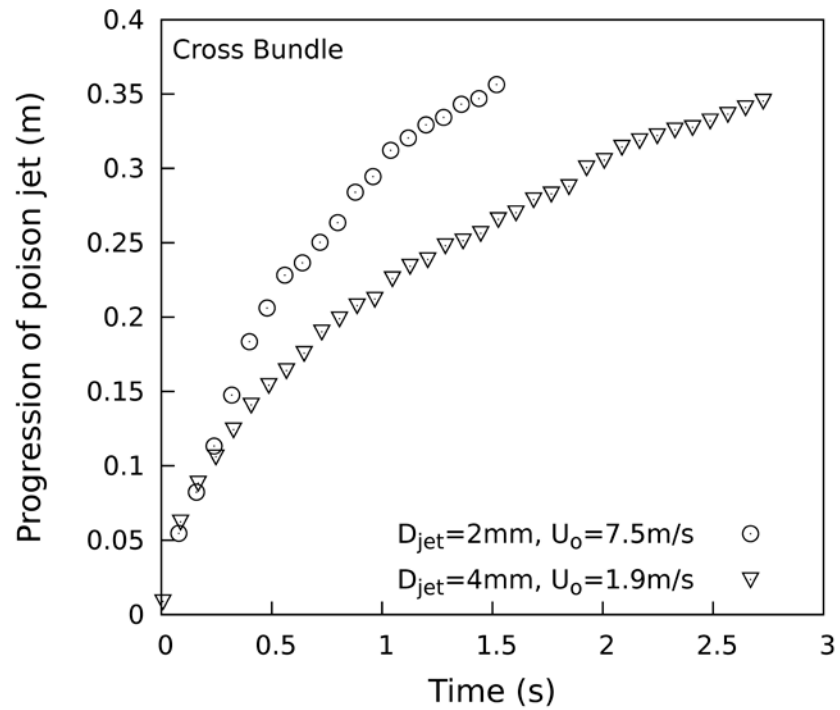


Figure 4.13: Progression of poison jet through cross bundle

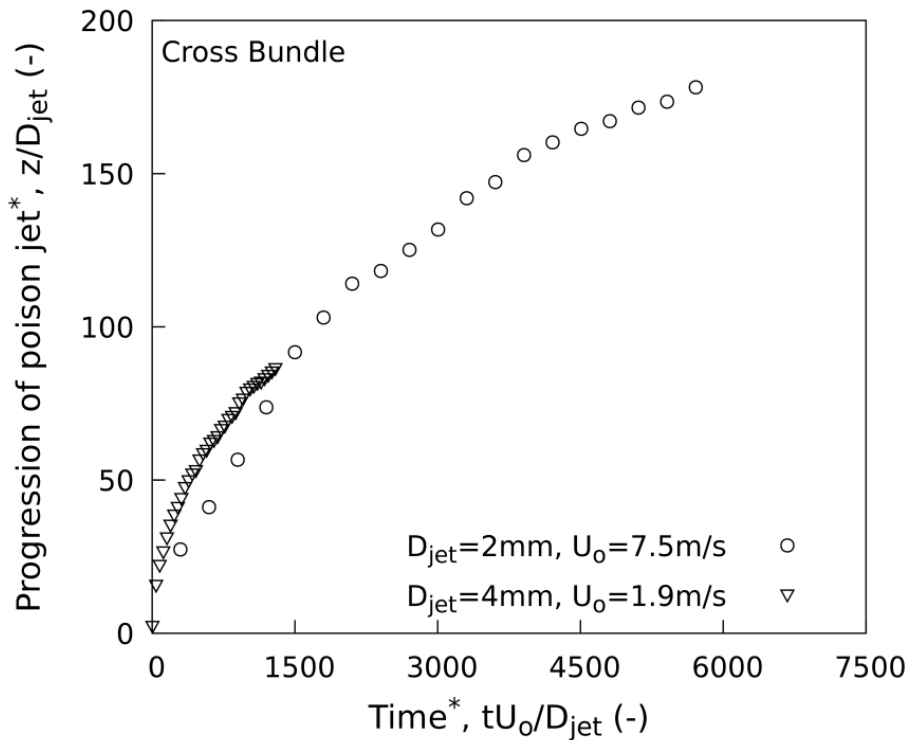


Figure 4.14: Non-dimensional progression of poison jet through cross bundle

4.3.2.3 Full scale experimental setup

Experiments were performed on the full sized nozzle in presence of calandria tubes. The experimental setup is defined in sub-section 4.3.2.2 and as shown in Figure 4.4. To simulate poison moderator interface in the experiment facility, poison tank was filled with dye that reached up to the solenoid valve (SV-2). Water remained filled between SV-2 and calandria. Experiments were carried out with gas tank pressure at 30 bar. The dead time estimated from the experiment was 0.56 s. When solenoid valves (SV-1 and SV-2) are opened, injection into the calandria was initiated. During initial injection, only water flow takes place through nozzle. After water comes out from the nozzle, the flow of dye takes place. Figure 4.15 shows instance when poison jet is crossing first row of calandria tubes. At time 1.8 s, the poison front reaches the fourth row of calandria tubes. Figure 4.16 shows the progression of poison jet with time.



Figure 4.15: Full scale poison jet facility-Jet cross first row of calandria tubes

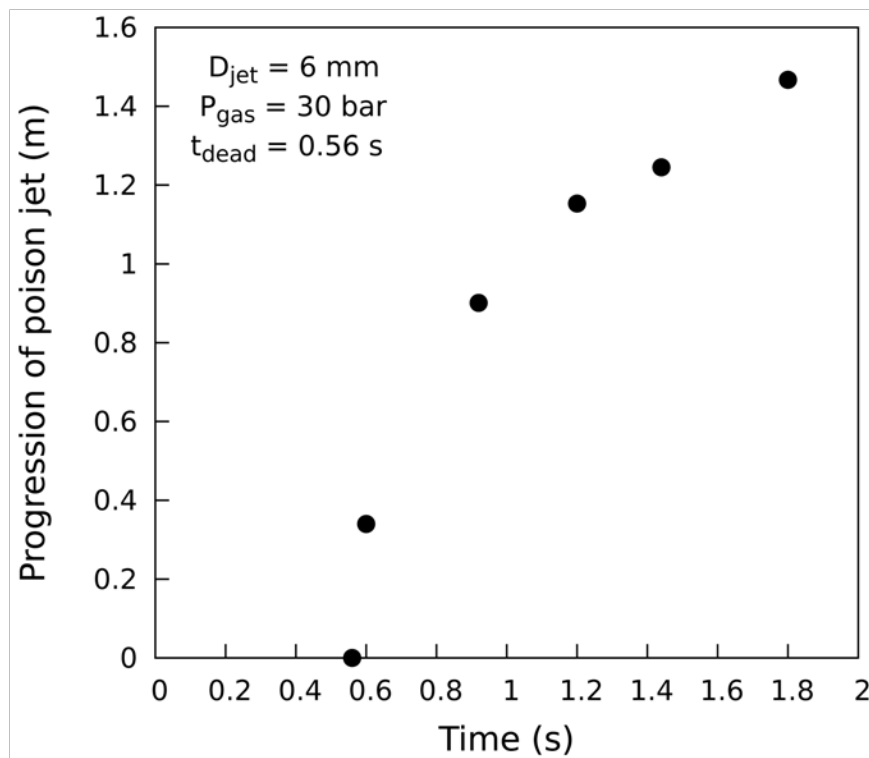


Figure 4.16: Progression of poison jet in full scale experimental setup

4.4 Conclusions

Experiments have been performed for liquid poison injection for the validation of CFD model. Experimental results from the scaled model show that progression of jet injected in the axial bundle is more as compared to cross bundle. However, the lateral spread of jet is more in cross bundle compared to the axial bundle. In axial bundle

Conclusions

injection, bundle has a tendency to maintain jet core in injection path whereas; cross bundle offers flow resistance and dissipate the jet energy faster.

Chapter 5

SOURCE TERM MODULE FOR POISON JET IN CFD

5.1 Introduction

To assess the poison jet behaviour, the experimental techniques are very expensive particularly at the time of optimization of design. Hence, for such situations, Computational Fluid Dynamics (CFD) simulations prove to be an important tool. The CFD simulations can provide poison distribution with time in the calandria, which are very useful in analysing the performance of SDS-2. In the calandria, moderator is in continuous circulation to remove the heat generated due to neutron thermalisation. Large numbers of calandria tubes (513) are present in calandria, which makes the moderator flow distribution analysis complex. In addition to this, calandria has a total eight poison tubes having total 640 injection nozzles of diameter 6 mm. During the analysis, it is necessary to model all poison injection nozzles, which are of very small size as compared to domain size of calandria. In such a complex nature of the problem, in order to facilitate the grid generation, a different treatment is necessary to model poison jets. To analyse the problem, OpenFOAM has been used. The code was modified to account mass, momentum, energy and species coming out from injection nozzles. The inlet conditions have been taken care by defining the source terms in mass, momentum, energy and species equations. In this

chapter, the source term for defining the inlet condition has been discussed. For validation purpose, the experimental results obtained in the scaled model and full scale model as explained in chapter four have been used. In addition to these, the experimental data of Johari et al. (1997) and velocity distribution in steady state jet are used for validation. Thus, the scope of the present chapter is development and validation of the source term module for poison jet.

5.2 Computational Fluid Dynamics

5.2.1 Flow geometry

Flow geometries described in sub section 4.3.2 are taken for the CFD analysis.

5.2.2 Governing equations

Table 5.1 lists the governing equations used in the CFD code OpenFOAM 2.2.2 (2013) to model the transient, incompressible, single phase and multi species flow in calandria. Chae et al. (2001b) used standard k- ϵ turbulence model in the numerical study on transient high-speed free jet into a confined enclosure using source term. They have validated the model and found good agreement with experimental results. Apart from this, Carlucci (1982), Huget et al. (1989, 1990), Yoon et al. (2004), Kim et al. (2006), Prabhakaran et al. (2012) also used standard k- ϵ turbulence model for moderator flow distribution in calandria and found good agreement with experimental results. Based on this, standard k- ϵ turbulence model is used for simultaneous modelling of poison jet injection and moderator flow distribution in present simulation.

5.2.3 Model assumptions

The following assumptions have been made:

1. Incompressible single phase fluid.
2. Average density in control volume is estimated by species fraction weighted density.

3. Fluid properties are constant except density in the formulation.
4. An adiabatic boundary condition at the calandria walls was employed.

5.2.4 Method of solution

CFD simulations have been performed using the open source CFD code OpenFOAM 2.2.2 (2013). Modified solver for mixing of two incompressible fluids (*twoLiquidMixingFoam*) is utilized for the incompressible Unsteady Reynolds Average Navier Stokes (URANS) modelling based on the finite-volume method (FVM) factorized method and the predictor–corrector algorithm (Issa, 1986). The dynamic adjustable time stepping technique is used to guarantee the local Courant number less than 1.

In a complex problem in order to facilitate the grid generation, the source terms are used instead of using inlet boundary condition normally given in the computer code. Standard solver OpenFOAM does not have source term option. Table 5.1 gives the mass, momentum, energy and species equations. These equations are modified to take mass, momentum, energy and species as a source term for inlet condition using Patankar (1980) methodology. This methodology says that any desired value of variable can be assigned to the solution at grid point by setting coefficients of linearised source term. General discretise equation for mass, momentum, energy and species can be written as $a_p \phi_p = \sum a_{nb} \phi_{nb} + b$ where ϕ_p is variable at grid point p, subscript nb is neighboring grid points of p and a is coefficient. In general discretization equation, source term S is added, $a_p \phi_p - \sum a_{nb} \phi_{nb} + b = S$. This source term (S) is linearised as $S = S_c + S_p \phi_p$ where $S_c = 10^{30} \phi_{p,desired}$ and $S_p = -10^{30}$. Here, 10^{30} denotes a number large enough to make the other terms in the discretisation equation negligible. The consequence is $S_c + S_p \phi_p \approx 0$. Thus, $\phi_p = -(S_c/S_p) = \phi_{p,desired}$.

Pressure, velocity, energy and species equations are solved. For discretisation of convection term, second order upwind scheme is used and for discretisation of diffusion and gradient term, central differencing scheme is used. Solutions are considered to be fully converged, when the sum of scaled residuals is below 10^{-3} .

Table 5.1: Governing equations for CFD

Continuity	$\frac{\partial \rho}{\partial t} + \nabla \cdot (\rho \langle u_k \rangle) = 0$	(5.1)
------------	--	-------

Momentum	$\frac{\partial (\rho \langle u_k \rangle)}{\partial t} + \nabla \cdot (\rho \langle u_k \rangle \langle u_k \rangle) = -\nabla \langle pr \rangle + \nabla \cdot \bar{\tau}_k + \rho \bar{g}$ $\bar{\tau}_k = (\mu + \mu_t)(\nabla \langle u_k \rangle + (\nabla \langle u_k \rangle)^T) - \frac{2}{3} \nabla \langle u_k \rangle I$	(5.2)
----------	---	-------

Turbulent kinetic energy	$\frac{\partial (\rho k)}{\partial t} + \nabla \cdot (\langle u_k \rangle \rho k) = \nabla \cdot \left[\left(\mu + \frac{\mu_t}{\sigma_k} \right) \nabla k \right] + G_k - \rho \varepsilon$	(5.3)
--------------------------	--	-------

Turbulent kinetic energy dissipation rate	$\frac{\partial (\rho \varepsilon)}{\partial t} + \nabla \cdot (\langle u_k \rangle \rho \varepsilon) = \nabla \cdot \left[\left(\mu + \frac{\mu_t}{\sigma_\varepsilon} \right) \nabla \varepsilon \right] + C_{\varepsilon 1} \frac{\varepsilon}{k} G_k - C_{\varepsilon 2} \rho \frac{\varepsilon^2}{k}$	(5.4)
---	--	-------

Species transport	$\frac{\partial (\rho Y_A)}{\partial t} + \nabla \cdot (\langle u_k \rangle \rho Y_A) = \nabla \cdot \left[\left(\rho D_{AB} + \frac{\mu_t}{Sc_t} \right) \nabla Y_A \right]$	(5.5)
-------------------	---	-------

Energy	$\frac{\partial (\rho T)}{\partial t} + \nabla \cdot (\rho \langle u_k \rangle T) = \nabla \cdot \left[\frac{kc_{eff}}{c_p} (\nabla \langle u_k T \rangle + (\nabla \langle u_k T \rangle)^T) \right] + \frac{shgvol}{c_p}$	(5.6)
--------	--	-------

$$G_k = \bar{\tau}_{ik} \frac{\partial \langle u_k \rangle}{\partial x_k}, \quad \mu_t = C_\mu \frac{k^2}{\varepsilon}$$

$$C_\mu = 0.09, \sigma_k = 1, \sigma_\varepsilon = 1.3, C_{\varepsilon 1} = 1.44, C_{\varepsilon 2} = 1.92$$

$$shgvol = f(x, y, z)$$

5.2.5 Boundary conditions

In the model, the calandria tubes and calandria vessel surfaces are considered as adiabatic with no slip boundary condition. Standard wall function is used at all the wall surfaces. Time varying uniform inlet jet velocity at poison injection nozzles is given as

source term instead of using the inlet velocity as boundary condition, as explained in the previous section.

5.3 Results and Discussions

As discussed earlier, the model employed in OpenFOAM is validated with experimental results and with the data available in the literature. The results obtained are discussed in the following sections.

CFD code OpenFOAM has been used for 3D simulation of poison jet. Before CFD analysis for AHWR geometry, OpenFOAM is validated with results of experiments performed for impulsively started jets in scaled and full scale experimental facilities. In addition to this, experimental results by Johari et al. (1997) and literature data of steady state jet are used for validation. Following sections give details of validation.

5.3.1 Steady state jet without tube bundle

3D CFD analysis for steady state jet without tube bundle is performed. The jet of 10 mm diameter with inlet velocity of 1 m/s is considered in the analysis. The grid independence for the case was investigated by considering three different grids (1) 45 thousand, (2) 100 thousand and (3) 200 thousand. During grid independence, velocity distribution along the jet axis has been taken for comparison purpose. Figure 5.1 shows comparison of predicted centre line velocity profile (non-dimensionalised by inlet velocity, U_0) for different grids. It is found that with 200 thousand grid, the centre line velocity is 6% more compared to the velocity with 100 thousand grids at location $z/D_{jet}=100$. Based on grid independence study, grid of size 200 thousand is taken for validation of model. Figure 5.2 shows comparison of the centre line velocity determined in CFD analysis with velocity obtained from correlation given by Abramovich (1963). It can be seen from Figure 5.2 that a very good agreement is obtained.

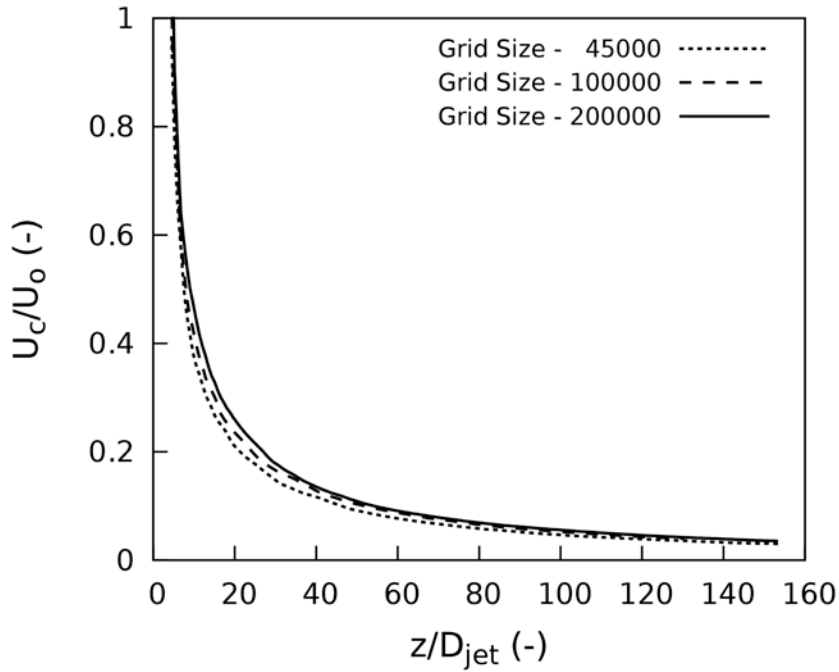


Figure 5.1: Effect of grid size on CFD predicted axial velocity of steady state jet

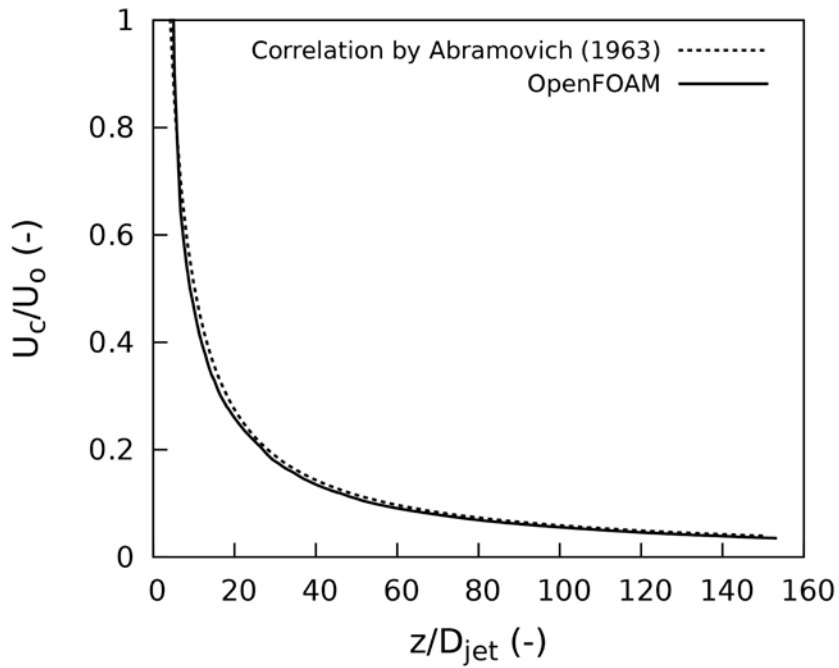


Figure 5.2: Comparison of CFD predicted axial velocity with correlation given by Abramovich (1963) for steady state jet

Figure 5.3 shows comparison of the radial distribution of axial velocity determined in CFD analysis with experimental data of Trupel (1915) published in Abramovich (1963) is compared at various axial locations (z/D_{jet} 20, 50 and 100). In Figure 5.3 the radial distance

is non- dimensionalised by dividing with $r_{1/2}$, where $r_{1/2}$ is the radial distance at which velocity is half of the centre line velocity. Profile in Figure 5.3 is called self similar profile and it is typical for jet. It can be seen from Figure 5.3 that a very good agreement is obtained.

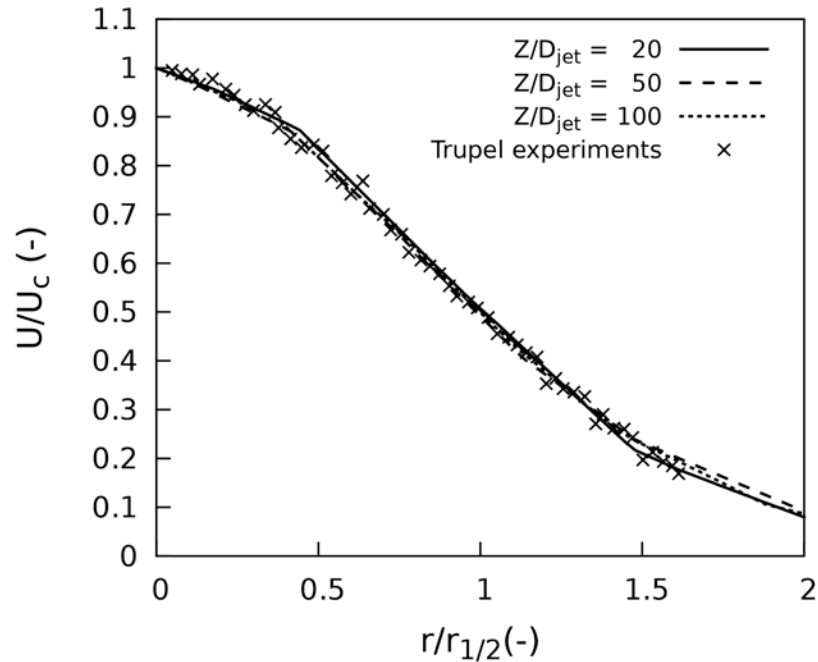


Figure 5.3: Comparison of CFD predicted radial velocity with Trupel steady state jet experiments (1915)

5.3.2 Impulsively started jet without tube bundle

5.3.2.1 Validation with experimental data of scaled facility

3D CFD analysis for impulsively started jet without tube bundle is performed for geometry described in sub-section 4.3.2.1. The jet having the velocity 7.5 m/s is initiated by opening of a solenoid valve, which is connected, with the nozzle of 2 mm diameter. The grid independence for the case is investigated by considering three different grids (1) 78 thousand, (2) 124 thousand and (3) 154 thousand. To check the grid independence, progression of poison jet along the axis with time is considered. The location along the jet axis having concentration of 1% of the initial concentration (C_0) is taken as progression of poison jet using the analogy of boundary layer thickness. Figure 5.4 shows the comparison

of predicted jet progression for different grid sizes. For grid size of 154 thousand, the predicted progression of poison jet is 1.14% more than 124 thousand grid sizes. Based on grid independence study, a grid of size 154 thousand is taken for validation of the model.

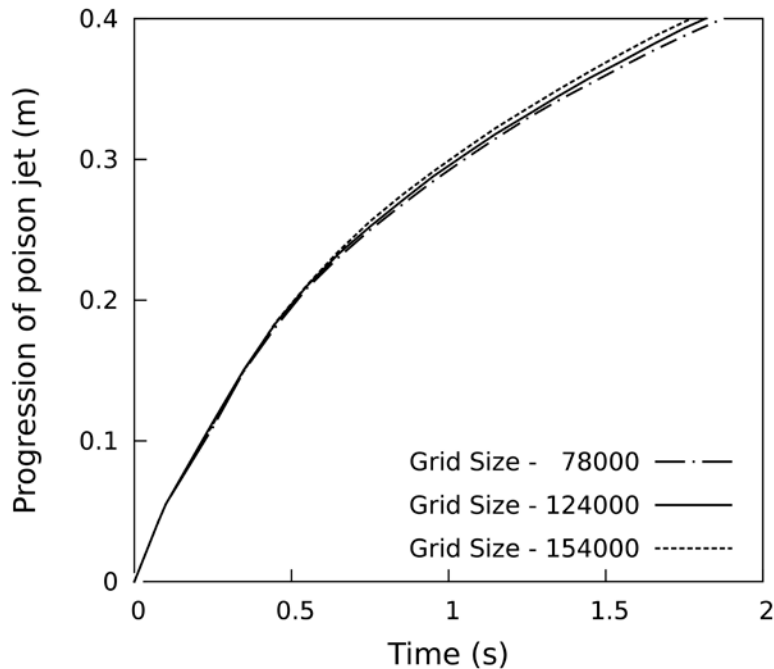


Figure 5.4: Effect of grid size on CFD predicted progression of poison jet for 2mm free jet

To define the domain of poison jet, cut-off concentration of 1% initial concentration is taken. Further to assess the effect of cut-off concentration fraction on the predicted progression of poison jet, three cut-off concentrations are taken. Progression of poison jet for 0.5%, 1% and 2% cut-off concentration is shown in Figure 5.5. Results show that in the initial stage of jet, progression of poison for all the three concentrations is same, as the tip of the jet is not diffused significantly. In the later stage of jet progression, variation can be observed in Figure 5.5 in the predicted progression of jet. This variation in progression of jet is due to the diffusion effect. However, differences were found to be -1.3% and 3.4% in predicted progression of poison jet for 0.5% and 2% cut-off concentration respectively compared to 1% cut-off concentration. Based on this, 1% of initial concentration (C_0) is taken as cut-off concentration for predicting progression of poison. Figure 5.6 shows

comparison of predicted jet length with experimental results. Maximum deviation in result is 3.2% at 1.3s.

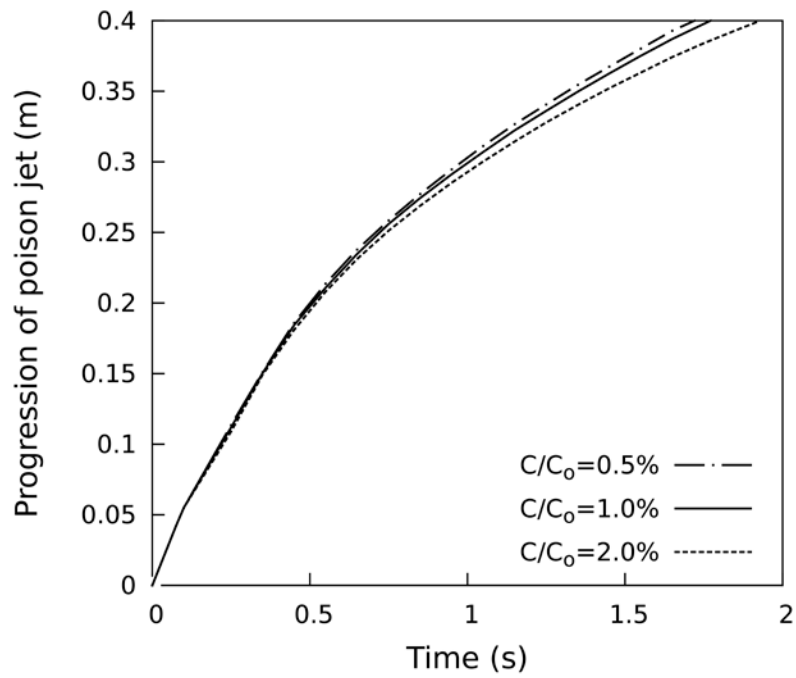


Figure 5.5: Effect of cut-off concentration on progression of poison jet for 2mm free jet

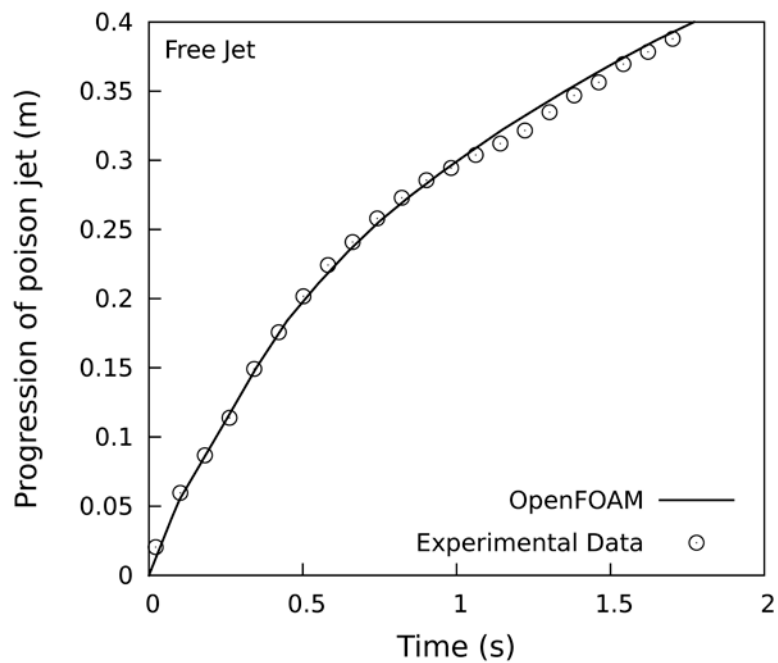


Figure 5.6: Comparison of CFD predicted progression of poison jet with experiment for 2 mm free jet

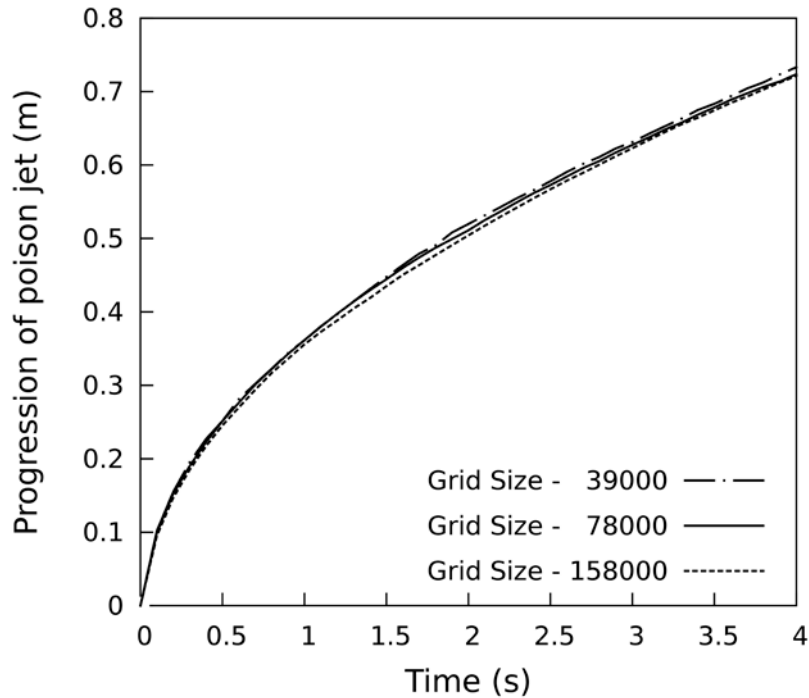


Figure 5.7: Effect of grid size on CFD predicted progression of poison jet for 6.35 mm free jet

5.3.2.2 Validation with experimental data from literature

The structure and mixing of impulsively started jets have been studied by Johari et al. (1997) in a water tank utilizing Laser-Induced Fluorescence (LIF) technique and acid-base reaction. The experiments were carried out in a water tank of 1.2 x 1.2 m cross section and 1.5m depth. The jet is initiated by the sudden charging of a solenoid valve, which is connected to a nozzle of 6.35 mm diameter. The Reynolds number, based on the average jet velocity at nozzle exit is 20,000. The jet growth is studied by extracting the jet tip from the video images. CFD analysis is performed for this case and grid independence for the case is investigated by considering three different grids (1) 39 thousand, (2) 78 thousand and (3) 158 thousand as shown in Figure 5.7. The difference between the progressions of poison jet is 0.82% and -0.3% at 4 s for grid size of 39 thousand and 158 thousand respectively as compared to grid size of 78 thousand. Based on the grid independence study, grid of size 78 thousand is selected for model validation. Figure 5.8 shows comparison of progression of poison jet predicted by CFD with experimental data of Johari

et al. (1997) for free jet of 6.35 mm diameter having velocity of 3.1 m/s. It can be seen that the predicted progression of jet at 4 s is deviated by -2% as compared to the experimental data.

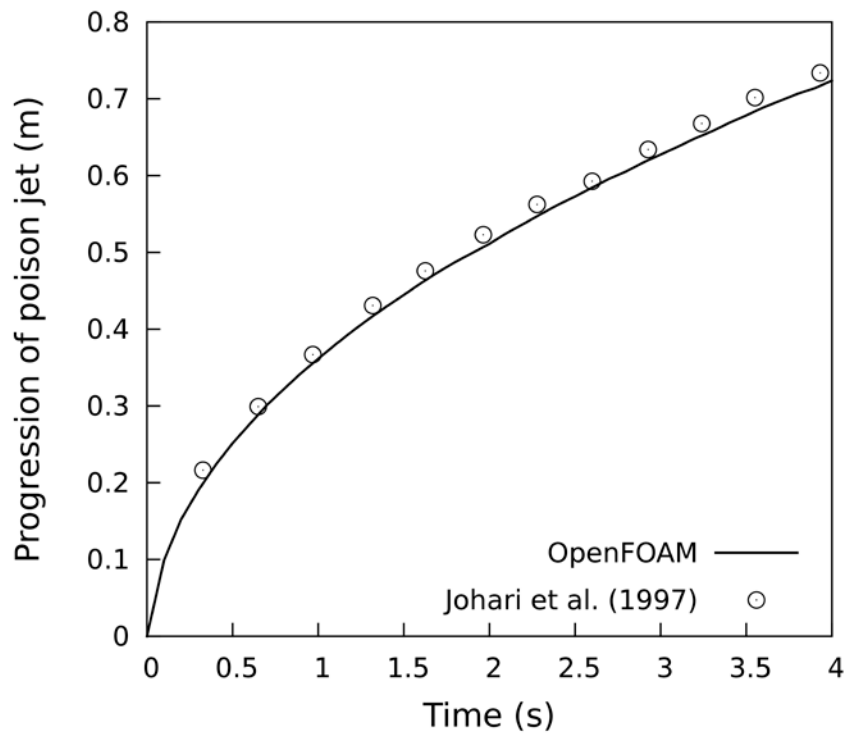


Figure 5.8: Comparison of CFD predicted progression of poison jet with experiment results of Johari et al. (1997) for 6.35 mm free jet

5.3.3 Impulsively started jet with tube bundle

5.3.3.1 Axial tube bundle in scaled facility

3D CFD analysis for impulsively started jet with axial tube bundle is performed for geometry described in sub-section 4.3.2.1. The jet is initiated by the sudden charging of a solenoid valve, which is connected, with 2 mm nozzle diameter having a velocity of 7.5 m/s. The grid independence for the case is investigated by considering three different grids (1) 56 thousand, (2) 124 thousand and (3) 215 thousand. Based on grid independence study, a grid size of 124 thousand is taken for model validation. Figure 5.9 shows comparison of predicted jet length with experimental results. Maximum deviation in predicted result is -8.5% at 0.7s compared experimental data. In addition to experiments of

2 mm diameter jet, experiments were also performed with 4 mm diameter nozzle with 1.9 m/s jet velocity. Experiments were performed with same axial bundle configuration. It can be seen from Figure 5.9 that deviation in predicted progression of poison jet is -2.5% at 2.8 s. Figures 5.10 and 5.11 show the comparison of CFD predicted poison jet contour with experimental data for 2 mm diameter jet at section plane AA of Figure 4.2 (a). Figure 5.10 (b) shows distortion in captured image, due to lens effect of acrylic tubes in water. Figure 5.10 (c) shows the super imposed image of post processed experimental contour with CFD concentration profile of $C/C_o = 1\%$. A good agreement can be observed between experimental contour and CFD concentration profile.

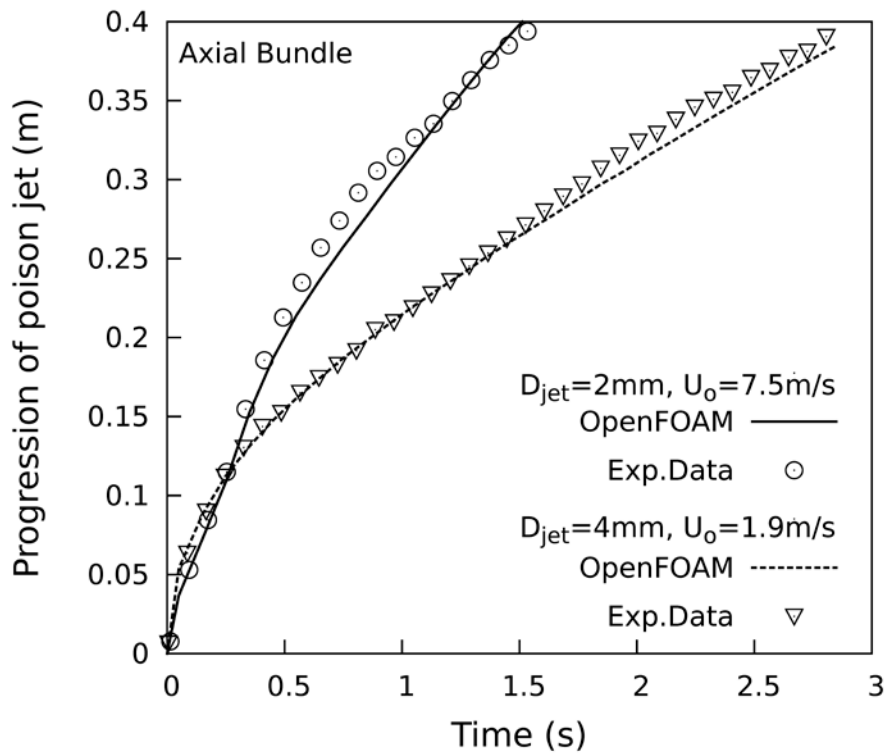


Figure 5.9: Comparison of CFD predicted progression of poison jet with experiment for axial bundle in scaled facility

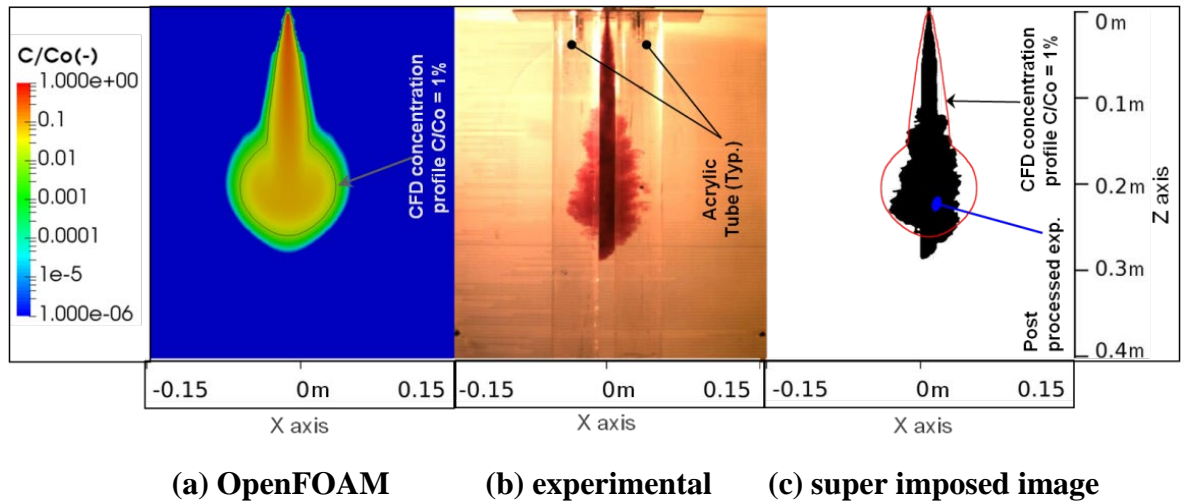


Figure 5.10: Comparison of CFD predicted progression of poison jet with experiment for 2 mm axial jet at $t= 0.7$ s

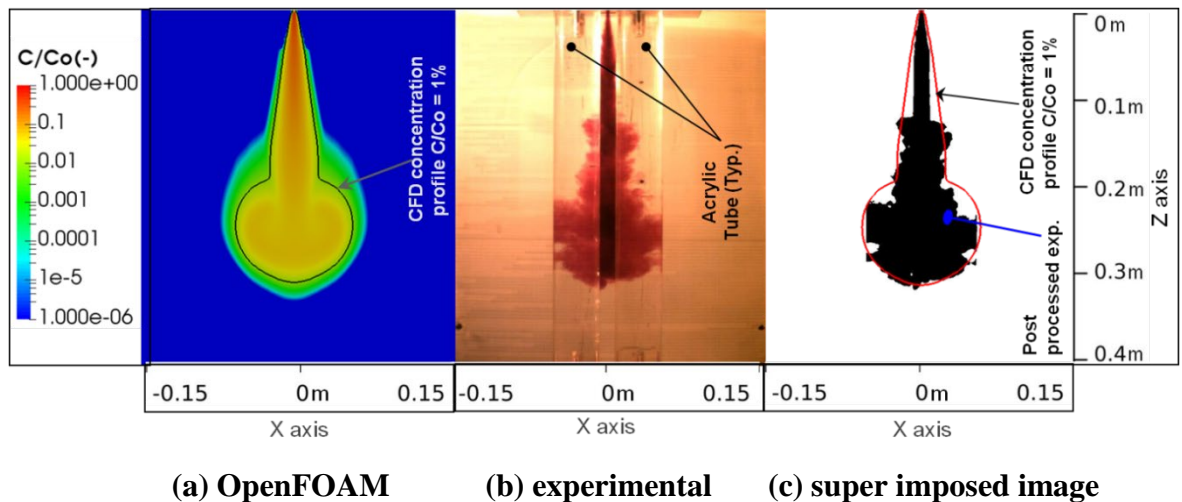


Figure 5.11: Comparison of CFD predicted progression of poison jet with experiment for 2 mm axial jet at $t=1$ s

5.3.3.2 Cross tube bundle in scaled facility

3D CFD analysis for impulsively started jet with cross tube bundle is performed for the geometry described in sub-section 4.3.2.1. The jet is initiated by the sudden charging of a solenoid valve, which is connected with 2 mm nozzle diameter and having a velocity of 7.5 m/s. For analysis, the grid independence for the case is investigated by considering three different grids (1) 134 thousand, (2) 223 thousand and (3) 272 thousand. Based on grid independence study, grid size of 223 thousand is selected for model validation. Figure 5.12

shows the comparison of predicted jet length with experimental results. Deviation in predicted results is 2.8% at 1.5 s as compared to experimental data. In addition to experiments of 2 mm diameter nozzle at 7.5 m/s, experiment was also performed with 4 mm diameter nozzle at 1.90 m/s initial velocity in same cross bundle. Maximum deviation in predicted progression of poison jet is -3% at 2.2 s. Figures 5.13 and 5.14 show the comparison of CFD predicted poison jet contour with the experimental results for 2 mm diameter jet. Figure 5.13 (c) shows the super imposed image of post processed experimental contour with CFD concentration profile of $C/Co = 1\%$.

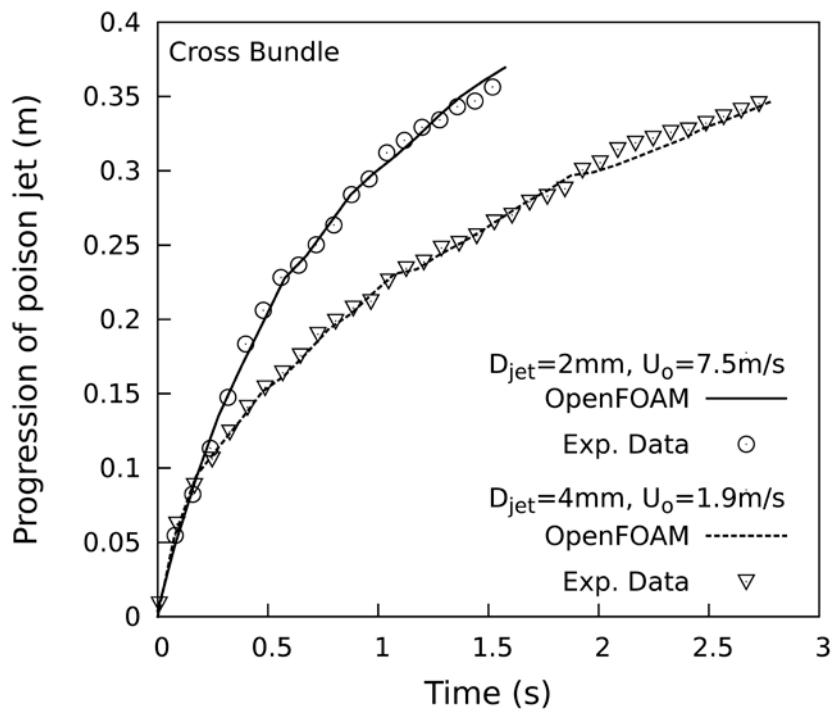


Figure 5.12: Comparison of CFD predicted progression of poison jet with experiment for cross bundle in scaled facility

From Figures 5.9 and 5.12, it can be seen that the progression of poison jet for the axial bundle is 10% and 11% more than the cross bundle for 2 mm diameter and 4 mm diameter nozzles, respectively. Results show that the jet has more penetration in axial bundle compared to cross bundle. By post processing CFD results for 2 mm diameter nozzle case, it is observed that at 1.5 s the jet covers $9.6 \times 10^{-4} \text{ m}^3$ volume ($C/Co > 1\%$) in axial bundle

while $10.8 \times 10^{-4} \text{ m}^3$ volume in the cross bundle. From the result, it can be observed that even though the progression of jet in cross bundle is less than axial bundle, volume of water where $C/Co > 1\%$ is more in cross bundle. From this, it can be concluded that jet spread is more in cross bundle as compared to axial bundle. In axial bundle injection, tubes have a tendency to maintain jet core in injection path whereas, in cross bundle injection, tubes offer flow resistance and dissipate the jet energy faster.

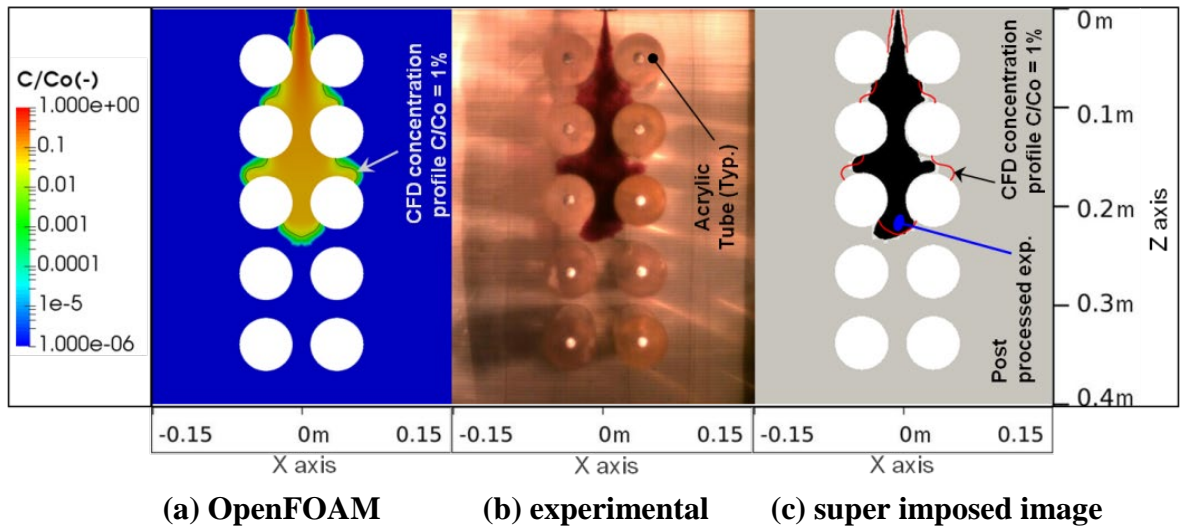


Figure 5.13: Comparison of CFD predicted progression of poison jet with experiment for 2 mm cross jet at $t= 0.7s$

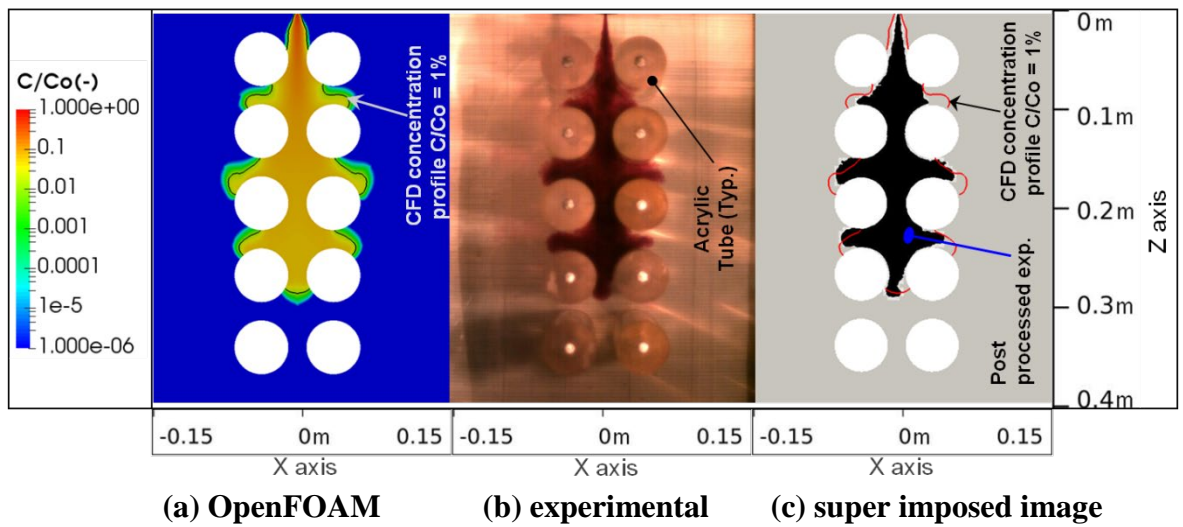


Figure 5.14: Comparison of CFD predicted progression of poison jet with experiment for 2 mm cross jet at $t=1s$

5.3.3.3 Full scale experimental setup

3D CFD analysis for full scale experimental setup is performed for experimental condition and geometry stated in sub-section 4.3.2.2. One quarter of the domain is simulated due to symmetry. When solenoid valves are opened, injection into the calandria is initiated. The grid independence for the case is investigated by considering three different grids (1) 83 thousand, (2) 149 thousand and (3) 215 thousand. Based on the grid independence study, the grid size of 149 thousand is taken for model validation. Figure 5.15 shows the pertinent details of mesh used. During initial injection, only water flow takes place through nozzle followed by flow of dye. The initial water injection acts as an impulsively started jet. By the time, poison reaches the injection nozzle i.e. after dead time (t_d), the flow acts as partially developed jet flow. Due to this, the velocity front of the jet is ahead of the poison front. For interpretation of the results, the velocity front is represented by interface having 1% of initial jet velocity (U_o) and poison front is identified by interface having 1% of initial concentration of the poison.

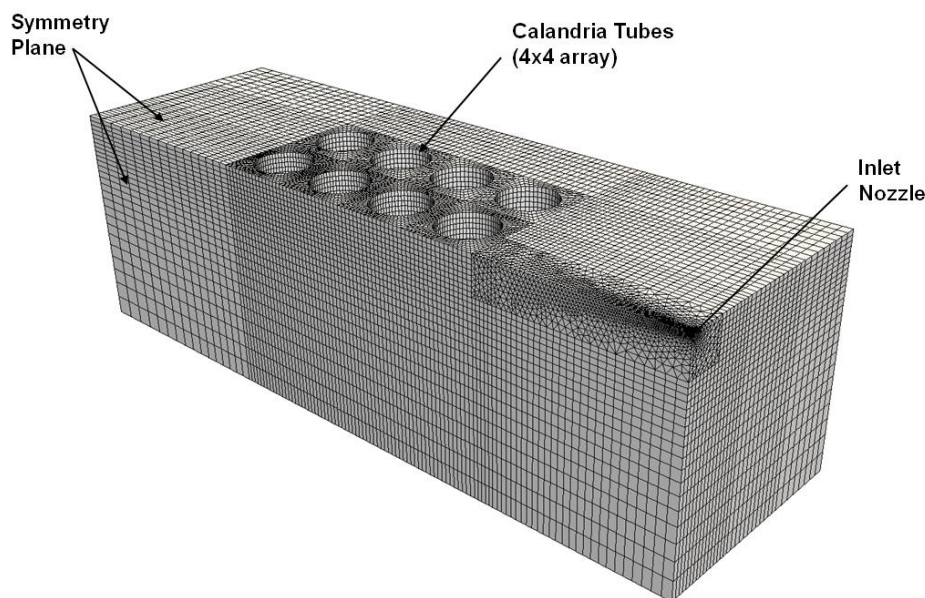


Figure 5.15: Mesh details of quarter symmetry model for poison injection in cross bundle in full scaled facility

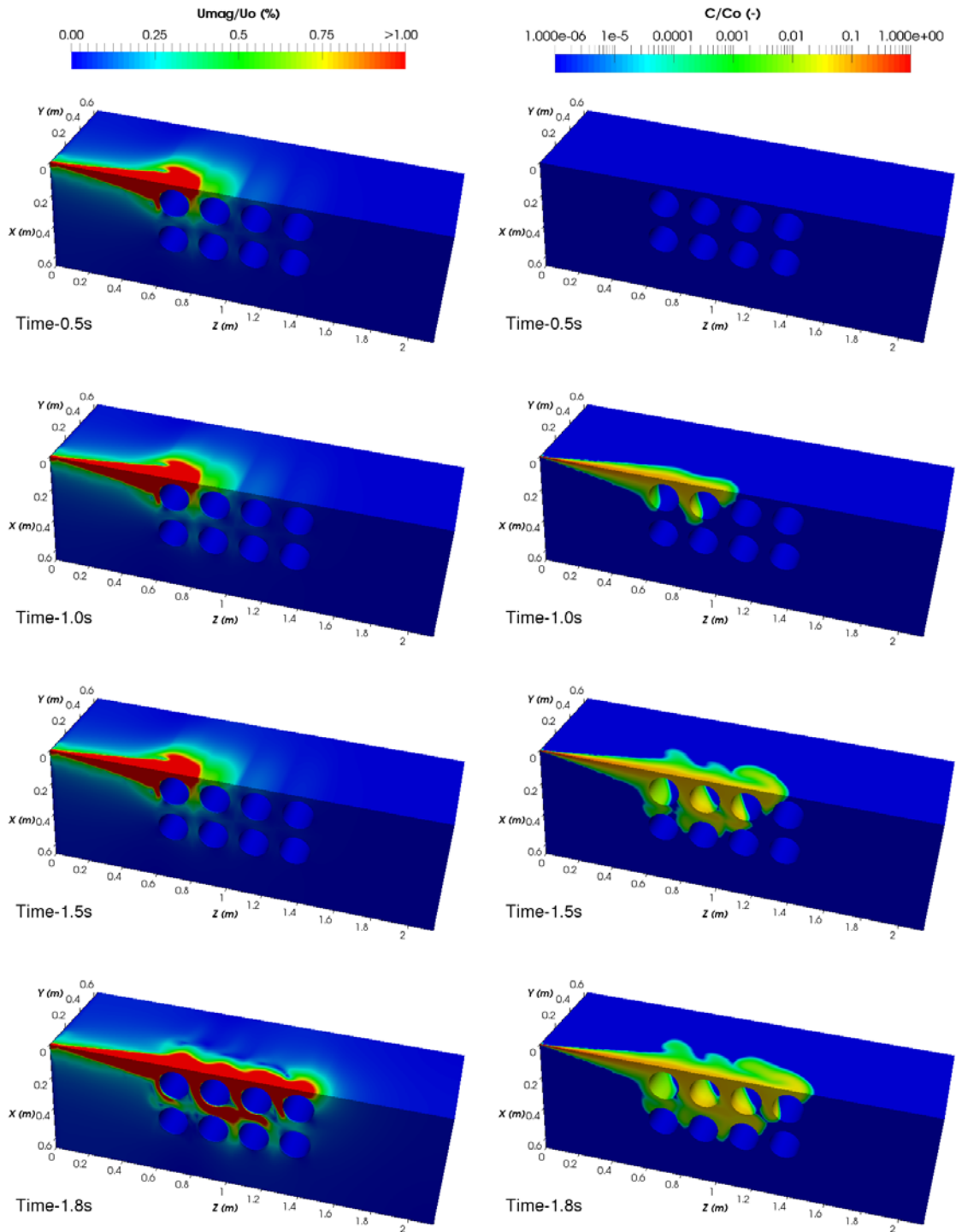


Figure 5.16: CFD predicted velocity and poison concentration contours for full scale facility

The velocity front and poison front are depicted in Figure 5.16. It is observed that at 0.5 s, though the velocity front has crossed the first row of calandria tubes, poison injection is still not initiated. By time 1.8 s, the poison front reaches the fourth row of calandria

tubes. Figure 5.17 gives the comparison between CFD simulations and the experimental data for progression of poison jet. It can be further observed that, though the poison injection is delayed, poison front penetrates at a faster rate due to partially developed nature of the jet before poison injection and apparently catches the velocity front at 1.8 s. Deviation in predicted progression of poison jet is -2.2% at 1.8s as compared with the experimental data.

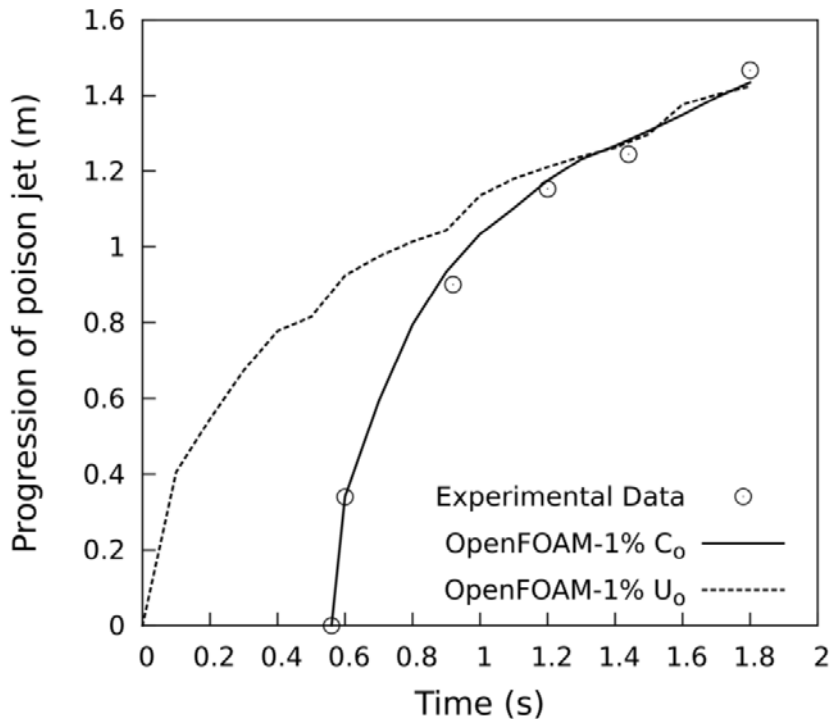


Figure 5.17: Comparison of jet penetration length based on velocity and concentration from CFD simulation and full scale experimental data

5.4 Conclusions

- The capability of developed point source term module for poison jet to simulate the poison jet profile is validated with experimental data and found to be in good agreement.
- Experimental results from the scaled model show that progression of jet issued in axial bundle is more as compared to cross bundle. However, lateral spread of jet is more in cross bundle compared to axial bundle. In axial bundle injection, bundle has a

tendency to maintain jet core in injection path whereas; cross bundle offers flow resistance and dissipate the jet energy faster.

- CFD results from full scale model show that though the poison injection is delayed due to moderator inventory present between poison moderator interface and calandria, poison front penetrates at a faster rate due to partially developed nature of the jet at the time of poison injection and apparently catches the velocity front with time.

Chapter 6

CFD ANALYSIS OF MODERATOR FLOW AND TEMPERATURE DISTRIBUTION

6.1 Introduction

In Shut Down System-2 (SDS-2), poison is injected in calandria that has the moderator in flow condition. Moderator is filled in calandria vessel which is pressurised by cover gas pressure of 0.4 bar (g) and is in sub cooled condition with an average temperature of around 62.5°C. Figure 6.1 shows a typical elevation view of calandria vessel with internals. Figure 6.2 shows the cross sectional view of calandria vessel at inlet nozzle plane. It also shows 513 calandria tubes present in calandria. The purpose of moderator is to maintain criticality in the reactor core by slowing down the high energy neutrons to a lower energy level where their probability of fission capture is greater. A large amount of heat (50 MW) is generated within the moderator mainly due to neutron slowing down and attenuation of gamma radiations. To remove this energy, moderator is kept under continuous circulation through a heat removal system as shown in Figure 6.3. The location and orientation of the moderator inlet and outlet nozzles should be such that the local temperature is below boiling point and the flow velocities across the tubes should

not cause flow induced vibration. Hence, to estimate the liquid poison distribution in AHWR calandria, moderator flow and its temperature field should be known.

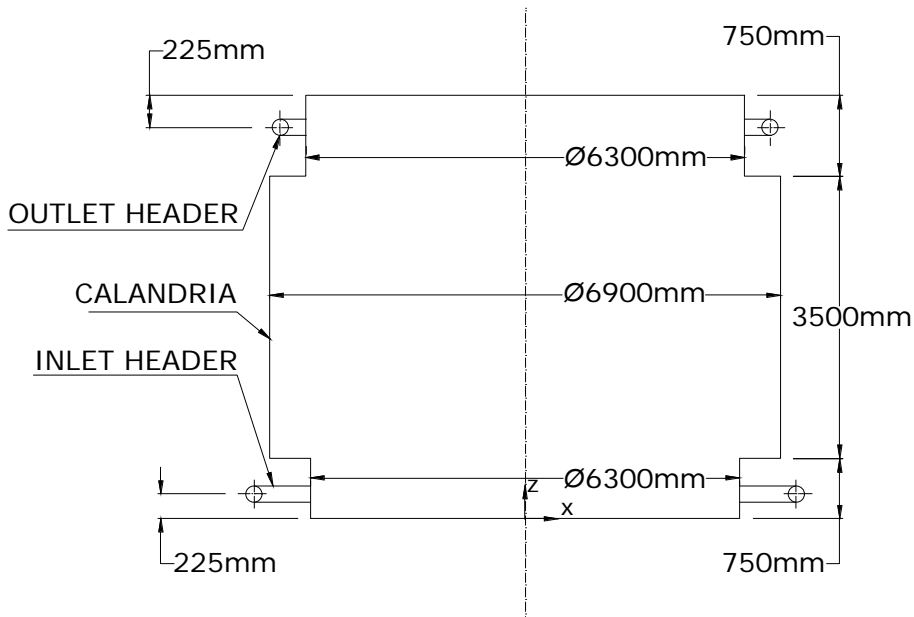


Figure 6.1: Schematic of vertical calandria vessel without internals (elevation)

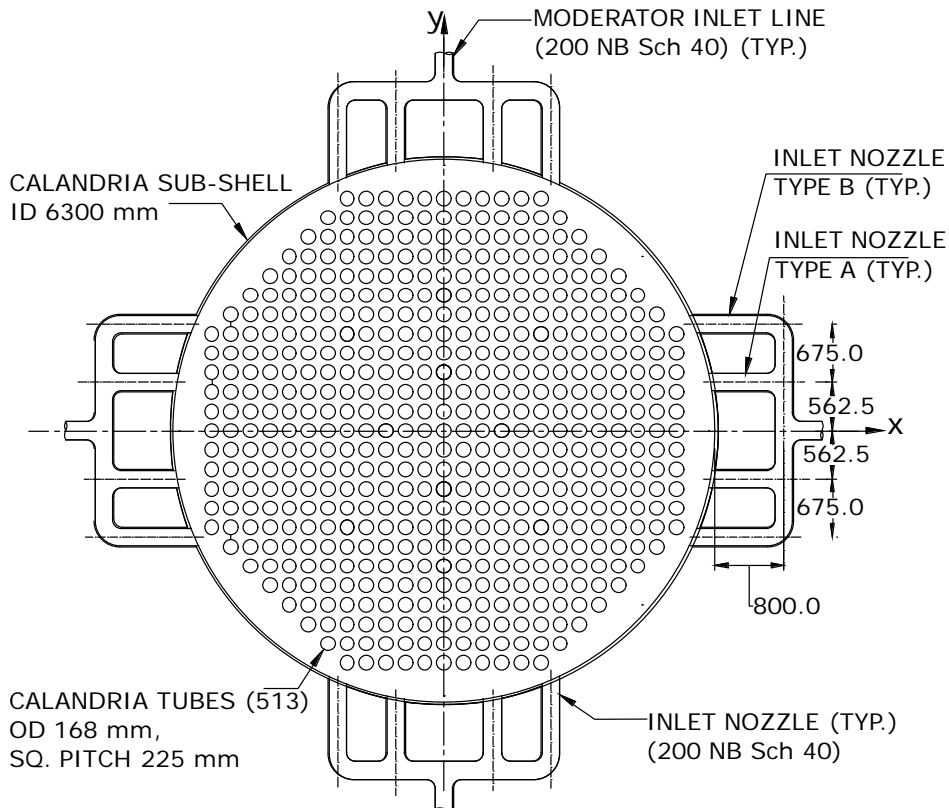


Figure 6.2: Schematic of moderator inlet header in vertical calandria vessel

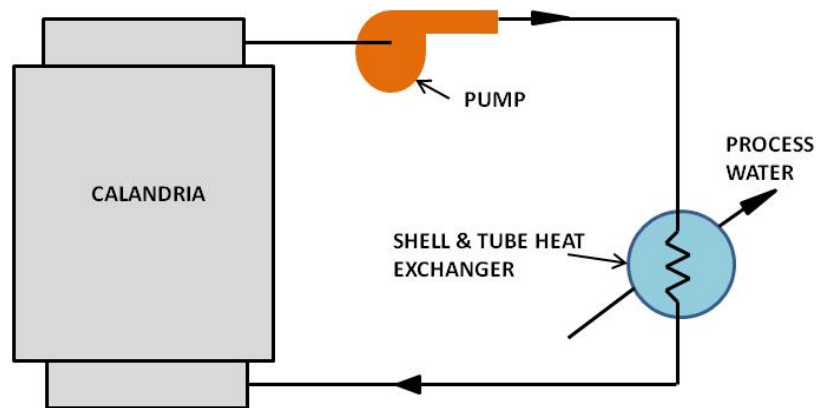


Figure 6.3: Simplified diagram of moderator circuit

Survey of the published literature shows that simulations with calandria tube modelled assume uniform volumetric heat generation. Moreover, the geometry of AHWR is different from CANDU type reactor. In AHWR, calandria vessel is vertical whereas it is horizontal in CANDU type reactor. In addition to this, the ratio of lattice pitch by calandria tube diameter is 1.34, compared to the CANDU 6 where the pitch to diameter ratio is 2.2. Hence, moderator temperature and flow fields should be generated for AHWR for the real case of spatial distribution of volumetric heat generation. In this chapter, moderator flow and temperature distribution in vertical calandria vessel of the nuclear reactor is simulated using OpenFOAM CFD code. Simulations will be performed for three different cases of the normal operating condition. During the simulation uniform heat generation and spatial variation of heat generation are considered. The effect of buoyancy in moderator flow has been studied.

6.2 Computational Fluid Dynamics

6.2.1 Flow geometry

The calandria is a 5 m high vertical cylindrical tank filled with heavy water (Sinha and Kakodkar, 2006). The calandria vessel comprises a main shell with a diameter of 6.9 m and a height 3.5 m. At each end of the main shell there is a smaller diameter sub-shell with

a diameter of 6.3 m and a height of 0.75 m and these regions are known as top and bottom reflectors. Inside the calandria, a total of 513 calandria tubes having diameter of 0.168 m are arranged vertically in a square pitch (p) of 0.225 m to form a lattice array as shown in Figure 6.2. Sixteen inlet nozzles with inner diameter of 0.203 m are installed in the bottom reflector of calandria as shown in Figure 6.2. Sixteen outlet nozzles with inner diameter of 0.203 m are radially installed on the top reflector. These outlet nozzles are connected to the common circular header. Only a quarter of the calandria vessel along with inlet and outlet headers is simulated because of the symmetric arrangement of calandria tubes, inlet and outlet nozzles as shown in Figure 6.4. There are typically two types of inlet nozzles, type A and type B as shown in Figure 6.2. Type A and B inlet nozzles are at 562.5 mm ($2.5 x^*$) and 1237.5 mm ($5.5 x^*$) respectively from symmetry plane, where x^* and y^* are normalized x and y coordinates defined as $x^* = x/p$ and $y^* = y/p$.

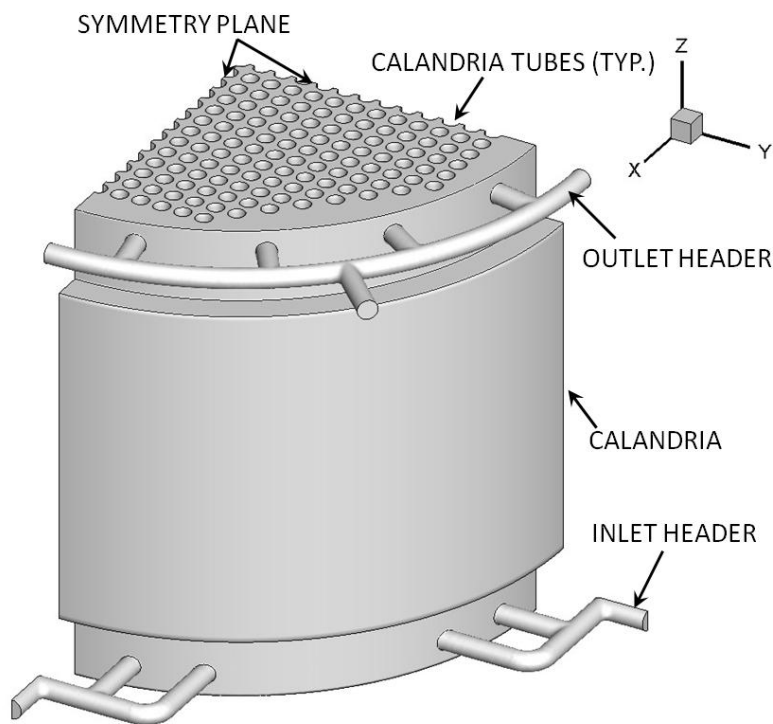


Figure 6.4: Quarter symmetry solid model of calandria

6.2.2 Governing equations

In order to model the incompressible, single phase, variable density, turbulent moderator flow in calandria, the governing equations (continuity, momentum, and energy) with the appropriate Reynolds stress closure need to be solved with boundary conditions. In the present work, the standard k-ε turbulence model is used. Table 6.1 gives the various equations used for simulation. It is considered that the flow to be turbulent based on general criteria of Reynolds number (Re) at inlet. Re at the inlet nozzle is 2.9×10^5 . This value justifies the use of turbulent flow model.

Table 6.1: Governing equations for steady state incompressible buoyant flow

Continuity	$\nabla \cdot (\rho \langle u_k \rangle) = 0$	(6.1)
Momentum	$\nabla \cdot (\rho \langle u_k \rangle \langle u_k \rangle) = -\nabla \langle pr \rangle + \nabla \cdot \bar{\tau}_k + \rho(1 - \beta(T - T_{ref}))\bar{g}$ $\bar{\tau}_k = (\mu + \mu_t)(\nabla \langle u_k \rangle + (\nabla \langle u_k \rangle)^T) - \frac{2}{3} \nabla \langle u_k \rangle I$	(6.2)
Turbulent kinetic energy	$\nabla \cdot (\langle u_k \rangle \rho k) = \nabla \cdot \left[\left(\mu + \frac{\mu_t}{\sigma_k} \right) \nabla k \right] + G_k - \rho \varepsilon$	(6.3)
Turbulent kinetic energy dissipation rate	$\nabla \cdot (\langle u_k \rangle \rho \varepsilon) = \nabla \cdot \left[\left(\mu + \frac{\mu_t}{\sigma_\varepsilon} \right) \nabla \varepsilon \right] + C_{\varepsilon 1} \frac{\varepsilon}{k} G_k - C_{\varepsilon 2} \rho \frac{\varepsilon^2}{k}$	(6.4)
Energy	$\nabla \cdot (\rho \langle u_k \rangle T) = \nabla \cdot \left[\frac{k_{eff}}{c_p} (\nabla \langle u_k T \rangle + (\nabla \langle u_k T \rangle)^T) \right] + \frac{shgvol}{c_p}$ $G_k = \bar{\tau}_{ik} \frac{\partial \langle u_k \rangle}{\partial x_k}, \mu_t = C_\mu \frac{k^2}{\varepsilon}$ $C_\mu = 0.09, \sigma_k = 1, \sigma_\varepsilon = 1.3, C_{\varepsilon 1} = 1.44, C_{\varepsilon 2} = 1.92$ $shgvol = f(x, y, z)$	(6.5)

6.2.3 Model assumptions

The following assumptions have been made:

1. Incompressible single phase fluid.
2. Boussinesq approximation is valid, i.e. density differences are only important in producing buoyancy.
3. Fluid properties are constant, except in the formulation of buoyancy term.
4. An adiabatic boundary condition at the calandria walls is applied.
5. Uniform inlet velocity.

6.2.4 Boundary condition and volumetric heat generation

In the present study, inlet header, outlet headers, calandria tubes and calandria vessel surfaces were considered as adiabatic with no slip boundary condition. Uniform inlet velocity is given as boundary condition at inlet nozzles. Standard wall function is used at all wall surfaces.

Both uniform and non-uniform volumetric heat generations were considered in the simulation. In case of non-uniform volumetric heat generation, spatial distribution is computed separately using Monte-Carlo technique (Suryanarayana et al., 2011) and given as source term in the energy equation. Figure 6.5 shows the distribution of non-uniform volumetric heat generation along the height of calandria at various location of plane $y = 0.5p$. Figure 6.6 shows the distribution of non-uniform volumetric heat generation at various horizontal lines in plane $y = 0.5p$. Fluctuations in horizontal profile are due to lattice locations taken by shut of rods.

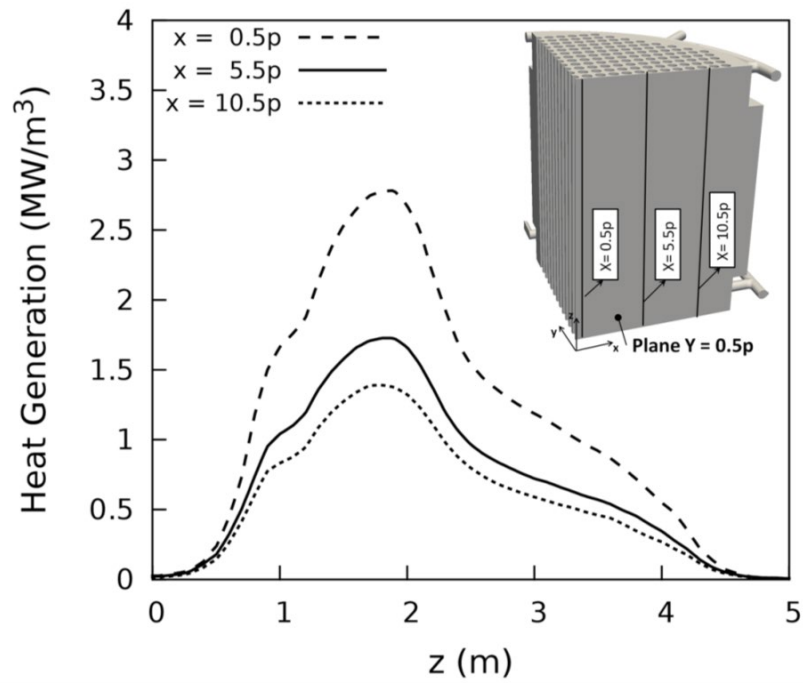


Figure 6.5: Distribution of non-uniform volumetric heat generation at various vertical locations

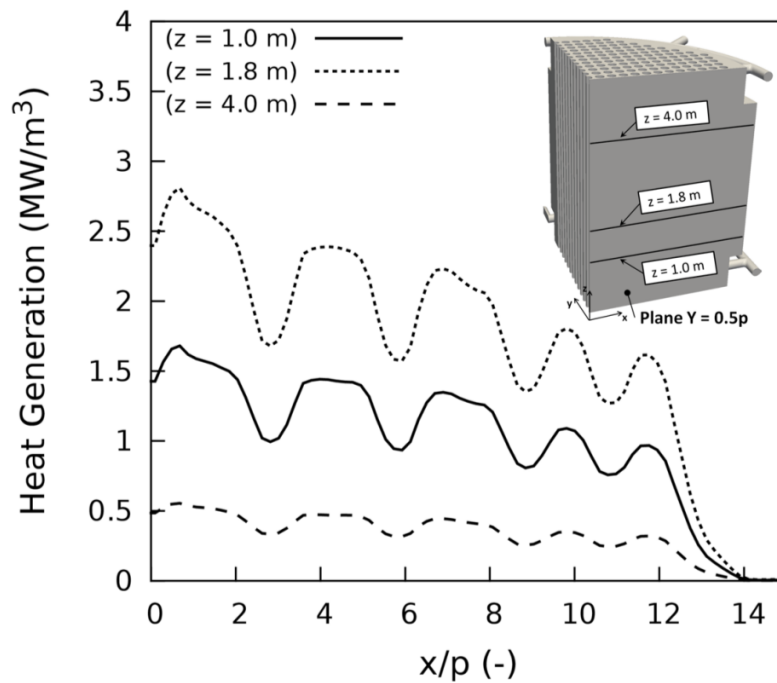


Figure 6.6: Distribution of non-uniform volumetric heat generation at various horizontal locations

6.2.5 Method of solution

CFD simulations have been performed using the open source CFD code OpenFOAM 2.2.2 (2013). The standard steady-state solver for buoyant, turbulent flow of incompressible fluids with heat generation as source term is used for simulation. The governing steady-state equations used for simulation are given in Table 6.1. As this solver cannot take spatial variation of heat generation as input, a new volume field variable for spatial distribution of volumetric heat generation (*shgvol*) is added as a source term in energy equation (6.5).

SIMPLE algorithm (Patankar, 1980) is used to solve equations of pressure, velocity, energy and species. For discretisation of convection term, second order upwind scheme is used and for discretisation of diffusion and gradient term, central differencing scheme is used. Solutions are considered to be fully converged when the sum of scaled residuals is below 10^{-3} .

6.2.6 Grid independence

The grid independence for the steady state case for the geometry described in section 6.2.1 is investigated by considering three different grids: (1) 1.3 million, (2) 3.2 million and (3) 6.0 million. Figure 6.7 shows the computational mesh for calandria vessel for 3.2 million grid size. Out of 3.2 million cells, 74% cells are hexahedral cells.

To check the grid independence, the temperature along the vertical line pass through $(x^*, y^*) = (0.5, 0.5)$ is taken to check buoyancy force. The maximum difference between the results of 3.2 and 6.0 million grid is 0.22°C as shown in Figure 6.8. As the results of 3.2 and 6 million grid are nearly same, hence for the present simulation 3.2 million grid is used.

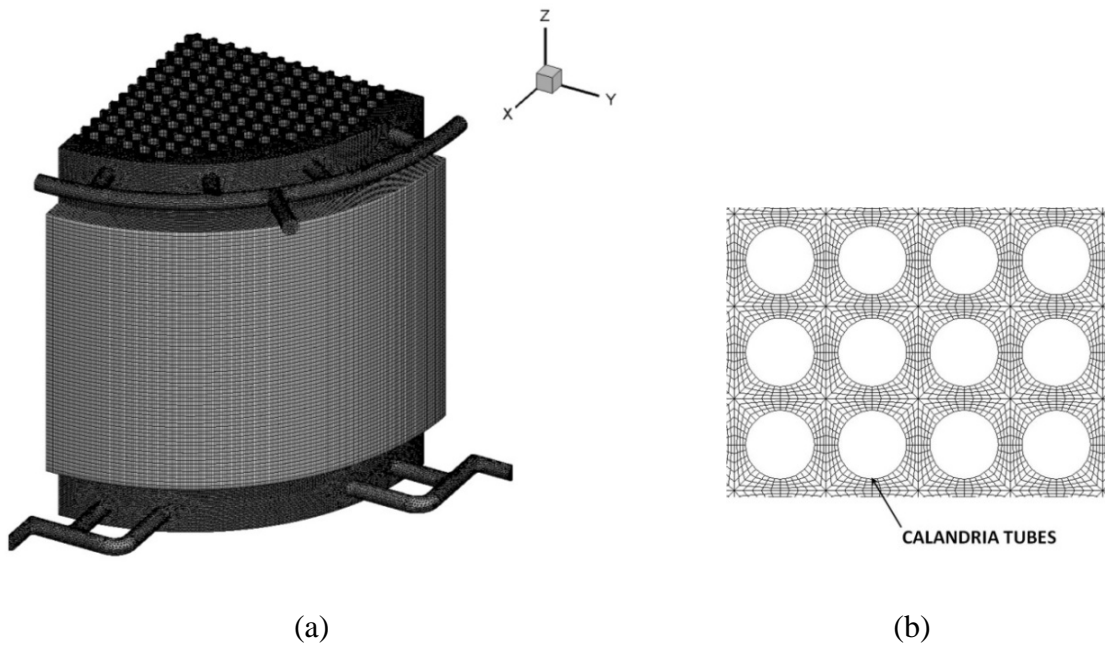


Figure 6.7: Computational mesh of calandria

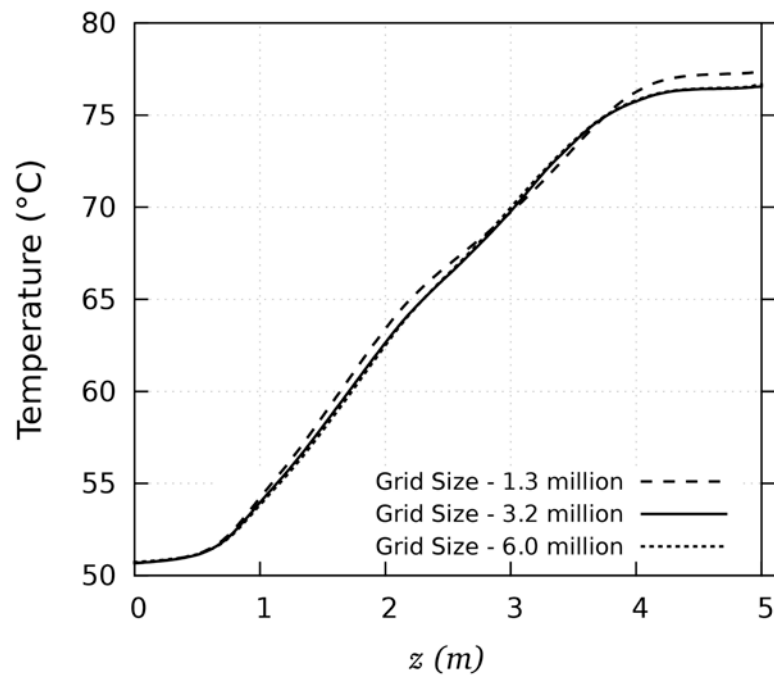


Figure 6.8: Effect of grid size on axial distribution of temperature in calandria vessel

6.3 Results and discussions

As discussed earlier, the model employed in OpenFOAM is first validated with related experimental data available in literature and then the validated model is used for geometry

described in section 6.2.1. The results obtained have been discussed in the following sections.

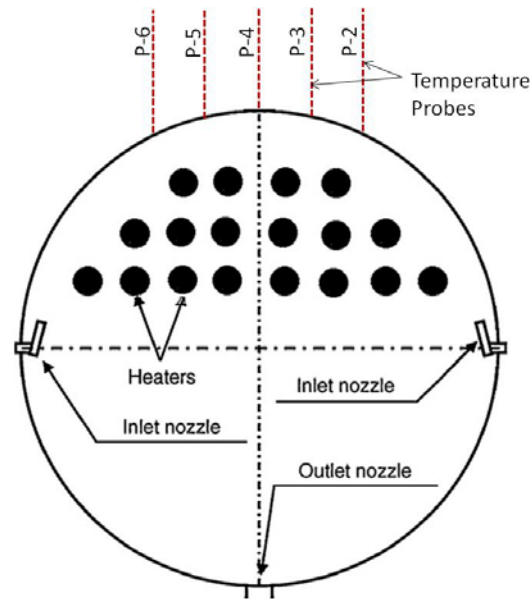


Figure 6.9: Schematic of calandria model in SPEL experimental facility

6.3.1 Validation of CFD model

For validation purpose, SPEL experimental facility (Koroyannakis, 1993) was simulated. The test vessel of SPEL has the features of a typical CANDU reactor, such as jet-induced flow, heating of the water by volumetric heat generation and a matrix of calandria tubes. Figure 6.9 shows the calandria vessel of SPEL facility. It has inner diameter of 740 mm and thickness of 254 mm. The 52 copper tubes having outer diameter of 38 mm forms a tube matrix, which acts as the electrodes with square pitch of 75 mm in the vessel. The two inlet nozzles having 150 mm length and 12.6 mm width were directed upward 14° from the vertical direction. The inlet velocity of 0.13 m/s corresponds to the total volumetric flow rate of $5 \times 10^{-4} \text{ m}^3/\text{s}$. The temperature at the inlet was 30°C and the total heat generation was 10 kW. A single outlet is located at the bottom of the tank. The working fluid was a solution of water and sodium chloride. High amperage, low voltage alternating current was passed via the tubes through the working fluid to generate heat. The

authors provided the local temperature measurements using optical fibre probes installed on ports (P2 to P6) penetrating through the upper circumferential wall.

SPEL experimental facility has been selected for validation because in both the cases of AHWR and SPEL, flow and temperature distribution depends on volumetric heat generation induced buoyancy force, jet induced momentum force and flow around tubes. Flow around tubes is a complex flow, which is neither fully cross flow nor fully in-line flow in both cases. In AHWR, even though calandria tubes are vertical but inlet nozzles are perpendicular to calandria tubes and the phenomenon is nearly cross flow at inlet plane which is similar to SPEL. In addition to this, non-dimensional analysis was done for AHWR and SPEL to check for hydrodynamic similarity between them. Non-dimensional numbers, Reynolds number (Re), Prandtl number (Pr), Archimedes number (Ar) and non-dimensional volumetric heat generation (q^*) are obtained by non-dimensionalising the governing equations given in Table 6.2 where, Ar is the ratio of buoyancy force and inertia force. Non-dimensional numbers Re , Ar and q^* will depend on the combination of temperature difference between inlet and outlet (ΔT), inlet nozzle velocity (u_o) and vertical dimension of vessel (H) only as properties of heavy water in AHWR are of same order as light water in SPEL. In addition, as Prandtl number depends on properties only, it is of same order in both the cases. Therefore by maintaining Re , Ar and q^* same for both AHWR and SPEL, the hydrodynamic similarity inside the calandria vessel can be maintained. It can be seen from Table 6.3 that although Ar and q^* are nearly same, Reynolds numbers is different for AHWR and SPEL. The impact of abandoning the Reynolds number equivalence is that the relative contributions of the momentum diffusion ($(\nabla^*)^2 U^*/Re$) and energy diffusion ($(\nabla^*)^2 T^*/(Re.Pr)$) by molecular motion are not the same between AHWR and SPEL. However, by ensuring a turbulent flow, the relative

contributions of these diffusion processes to the overall balances in momentum and energy equations can be neglected (Rhee and Kim, 2014) as shown in Table 6.3. From these arguments, using SPEL data for validation is justified.

Table 6.2: Non dimensional governing equations of SPEL and AHWR

Governing equations

$$\text{Continuity,} \quad \nabla \cdot \mathbf{u} = 0 \quad (6.8)$$

$$\text{Momentum,} \quad \frac{\partial \mathbf{u}}{\partial t} + (\mathbf{u} \cdot \nabla) \mathbf{u} = -\frac{1}{\rho_{ref}} \nabla pr + \frac{\mu}{\rho_{ref}} \nabla^2 \mathbf{u} + \mathbf{g} \left(\frac{\rho - \rho_{ref}}{\rho_{ref}} \right) \quad (6.9)$$

$$\text{Energy,} \quad \frac{\partial T}{\partial t} + (\mathbf{u} \cdot \nabla) T = \frac{kc}{\rho_{ref} c_p} + \frac{\dot{q}}{\rho_{ref} c_p} \quad (6.10)$$

Dimensionless variables can be defined as below

$$\begin{aligned} u^* &= \frac{u}{u_o} & T^* &= \frac{T - T_{ref}}{T_{outlet} - T_{inlet}} & pr^* &= \frac{pr}{\rho_{ref} u_o^2} \\ t^* &= \frac{t}{(H/u_o)} & \nabla^* &= H \nabla & Re &= \frac{\rho_{ref} u_o H}{\mu} \\ Pr &= \frac{\mu c_p}{k} & Ar &= \frac{g \beta (T_{outlet} - T_{inlet}) H}{u_o^2} & q^* &= \frac{\dot{q}(x,y,z) \cdot H}{\rho_{ref} c_p u_o (T_{outlet} - T_{inlet})} \end{aligned}$$

Where,

u_o = inlet nozzle velocity

H = vertical dimension of vessel

Re = Reynolds number

Ar = Archimedes number

Pr = Prandtl number

q^* = Non-dimensional volumetric heat generation

H for AHWR and SPEL is calandria vessel height and vessel diameter respectively

Non dimensional equations

$$\text{Continuity,} \quad \nabla^* \cdot \mathbf{u}^* = 0 \quad (6.11)$$

$$\text{Momentum,} \quad \frac{\partial \mathbf{u}^*}{\partial t^*} + (\mathbf{u}^* \cdot \nabla^*) \mathbf{u}^* = -\nabla^* pr^* + \frac{1}{Re} (\nabla^*)^2 \mathbf{u}^* + Ar \cdot T^* \quad (6.12)$$

$$\text{Energy,} \quad \frac{\partial T^*}{\partial t^*} + (\mathbf{u}^* \cdot \nabla^*) T^* = \frac{1}{Re \cdot Pr} (\nabla^*)^2 T^* + q^* \quad (6.13)$$

Table 6.3: Order of magnitude of non dimensional equations

Order of magnitude of non dimensional equations for SPEL	Order of magnitude of non dimensional equations for AHWR
<p><u>Input Data</u></p> <p>$H = 0.740\text{m}$, $p = 0.075\text{m}$, $u_o = 0.13 \text{ m/s}$, $\mu = 812 \times 10^{-6} \text{ kg/m s}$, $\rho_{\text{ref}} = 996 \text{ kg/m}^3$, $\text{Pr} = 5.5$, $\beta = 298 \times 10^{-6} \text{ K}^{-1}$, $T_{\text{outlet}} = 34.76^\circ\text{C}$, $T_{\text{inlet}} = 30^\circ\text{C}$</p> <p><u>Momentum equation</u></p> <p>$u \approx u_o$ (conservatively maximum value is assumed), $u^* = 1$</p> <p>$\nabla^* = \frac{H}{p} = \frac{0.740}{0.075} = 9.87$ (approx.)</p> <p>$(\nabla^*)^2 u^* = 97.4$</p> <p>$Re = \frac{\rho_{\text{ref}} u_o H}{\mu} = \frac{996 \times 0.13 \times 0.74}{812 \times 10^{-6}} = 1.18 \times 10^5$</p> <p>$\frac{1}{Re} (\nabla^*)^2 u^* = \frac{97.4}{118000} = 8.26 \times 10^{-4}$</p> <p>$Ar = \frac{g\beta(T_{\text{outlet}} - T_{\text{inlet}})H}{u_o^2} = 0.61$</p> <p>$T^* = 0.5$ (average value is taken)</p> <p>$Ar.T^* = 0.61 \times 0.5 = 0.31$</p> <div style="border: 1px solid black; padding: 2px; width: fit-content; margin: 5px auto;"> $\frac{1}{Re} (\nabla^*)^2 u^* \ll Ar.T^*$ </div> <p>O(Momentum equation) ≈ 0.31</p> <p><u>Energy equation</u></p> <p>$\frac{1}{Re.Pr} (\nabla^*)^2 T^* = \frac{97.4 \times 0.5}{118000 \times 5.5} = 7.5 \times 10^{-6}$</p> <p>Average volumetric heat generation, $\dot{q} = 0.106 \text{ MW/m}^3$</p> <p>$q^* = \frac{\dot{q}(x,y,z).H}{\rho_{\text{ref}} c_p u_o (T_{\text{outlet}} - T_{\text{inlet}})} = 0.030$</p> <div style="border: 1px solid black; padding: 2px; width: fit-content; margin: 5px auto;"> $\frac{1}{Re.Pr} (\nabla^*)^2 T^* \ll q^*$ </div> <p>O(Energy equation) ≈ 0.030</p>	<p><u>Input Data</u></p> <p>$H = 5\text{m}$, $p = 0.225\text{m}$, $u_o = 0.842 \text{ m/s}$, $\mu = 650 \times 10^{-6} \text{ kg/m.s}$, $\rho_{\text{ref}} = 1095 \text{ kg/m}^3$, $\text{Pr} = 4.5$, $\beta = 430 \times 10^{-6} \text{ K}^{-1}$, $T_{\text{outlet}} = 75^\circ\text{C}$, $T_{\text{inlet}} = 50^\circ\text{C}$</p> <p><u>Momentum equation</u></p> <p>$u \approx u_o$ (conservatively maximum value is assumed), $u^* = 1$</p> <p>$\nabla^* = \frac{H}{p} = \frac{5}{0.225} = 22.22$ (approx.)</p> <p>$(\nabla^*)^2 u^* = 493.83$</p> <p>$Re = \frac{\rho_{\text{ref}} u_o H}{\mu} = \frac{1093 \times 0.842 \times 5}{650 \times 10^{-6}} = 7 \times 10^6$</p> <p>$\frac{1}{Re} (\nabla^*)^2 u^* = \frac{493.83}{7 \times 10^6} = 7.05 \times 10^{-5}$</p> <p>$Ar = \frac{g\beta(T_{\text{outlet}} - T_{\text{inlet}})H}{u_o^2} = 0.74$</p> <p>$T^* = 0.5$ (average value is taken)</p> <p>$Ar.T^* = 0.74 \times 0.5 = 0.37$</p> <div style="border: 1px solid black; padding: 2px; width: fit-content; margin: 5px auto;"> $\frac{1}{Re} (\nabla^*)^2 u^* \ll Ar.T^*$ </div> <p>O(Momentum equation) ≈ 0.37</p> <p><u>Energy equation</u></p> <p>$\frac{1}{Re.Pr} (\nabla^*)^2 T^* = \frac{493.83 \times 0.5}{7 \times 10^6 \times 4.5} = 7.8 \times 10^{-6}$</p> <p>Average volumetric heat generation, $\dot{q} = \frac{50\text{MW}}{120.78 \text{ m}^3} = 0.414 \text{ MW/m}^3$</p> <p>$q^* = \frac{\dot{q}(x,y,z).H}{\rho_{\text{ref}} c_p u_o (T_{\text{outlet}} - T_{\text{inlet}})} = 0.022$</p> <div style="border: 1px solid black; padding: 2px; width: fit-content; margin: 5px auto;"> $\frac{1}{Re.Pr} (\nabla^*)^2 T^* \ll q^*$ </div> <p>O(Energy equation) ≈ 0.022</p>

To validate OpenFOAM capability to predict flow distribution in buoyancy dominated flow, full geometry of SPEL has been simulated. The grid independence for the steady state case was investigated by considering three different grids (1) 0.20 million, (2) 0.40 million and (3) 0.80 million. For all the grids, 99.9% cells are hexahedral. To check the grid independence, temperature along the port 4 is taken. The maximum difference between 0.40 million and 0.80 million grid is 0.1°C. The comparison of the temperature field has been depicted in the form of non-dimensional temperature as defined in equation 6.6:

$$T^* = \frac{T - T_{inlet}}{T_{outlet} - T_{inlet}} \quad (6.6)$$

Figure 6.10 shows the effect of grid size on predicted temperature (non-dimensional) along probe 4 (shown in Figure 6.9). Based on grid independence study, grid of size 0.80 million is taken for validation of model.

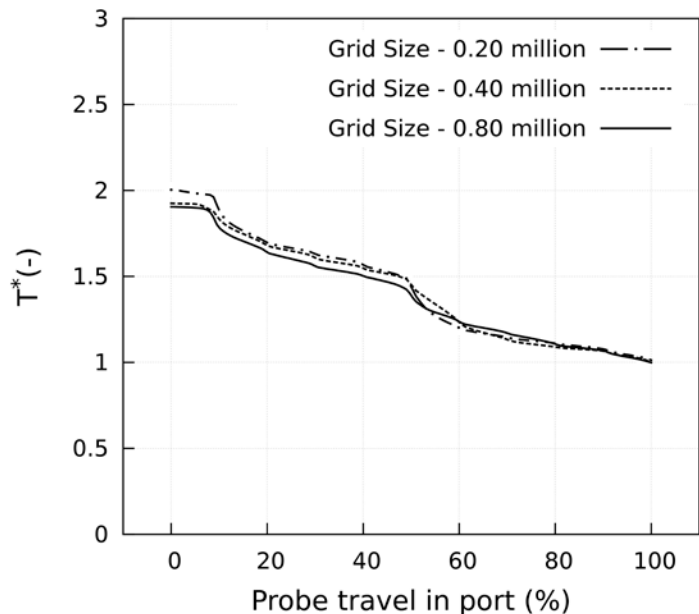
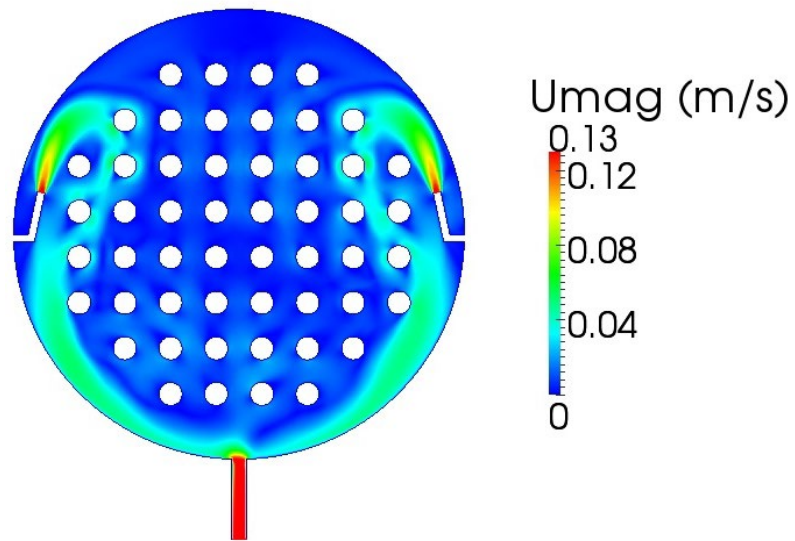
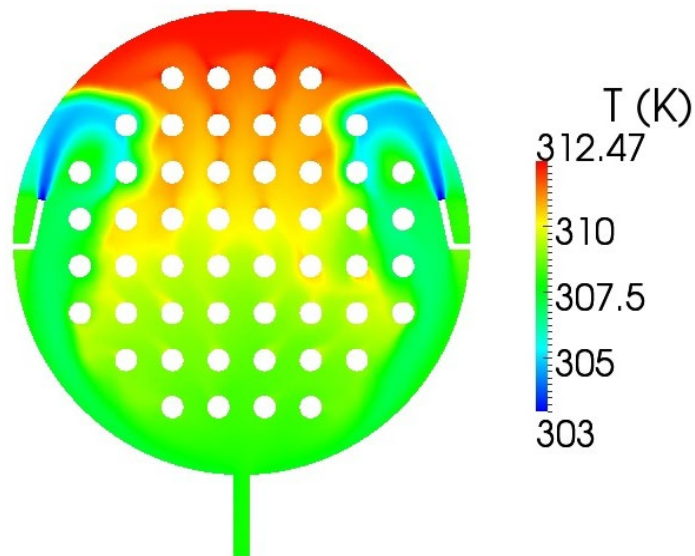


Figure 6.10: Effect of grid size on CFD predicted temperature along prob 4 of SPEL experiment



(a) Velocity distribution



(b) Temperature distribution

Figure 6.11: Velocity and temperature distribution in axial mid-plane of SPEL experimental setup

Figures 6.11 (a) and (b) show the velocity and temperature distribution in axial mid plane of SPEL experimental facility. From Figure 6.11(a) it can be observed that the jet coming out of the inlet nozzle takes a downward turn after some distance and does not reach to the top portion of the calandria vessel. This is because of buoyancy force, which opposes the inertia force of the jet. It can be seen from Figure 6.11(b) that a high

temperature stagnation zone is formed due to buoyancy dominated flow. Figure 6.12 shows that the vertical component of velocity is positive i.e. flow is in upward direction along ports 4 and 5 (shown in Figure 6.9) up to 90% distance from the top. Velocity turns downward just before the outlet. This upward velocity again shows that the buoyancy force dominates over momentum force.

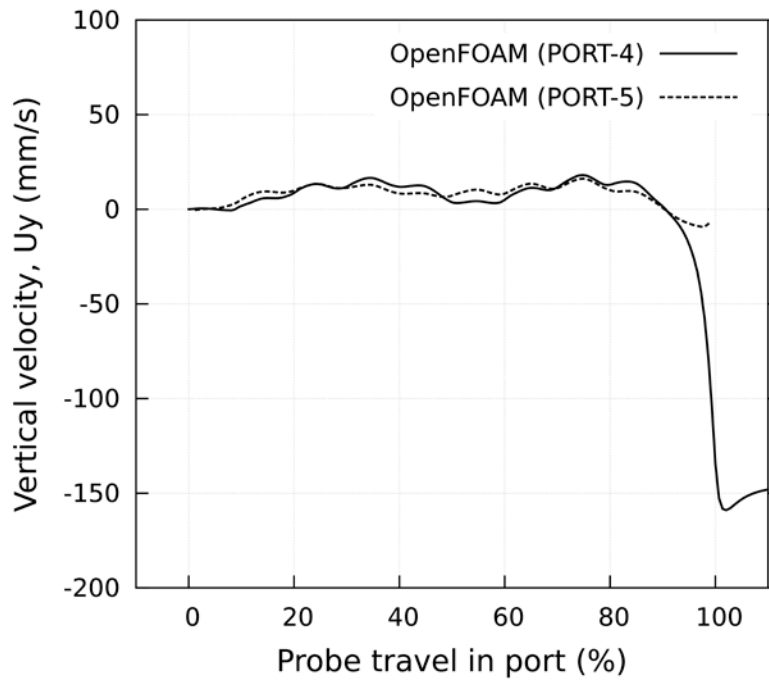
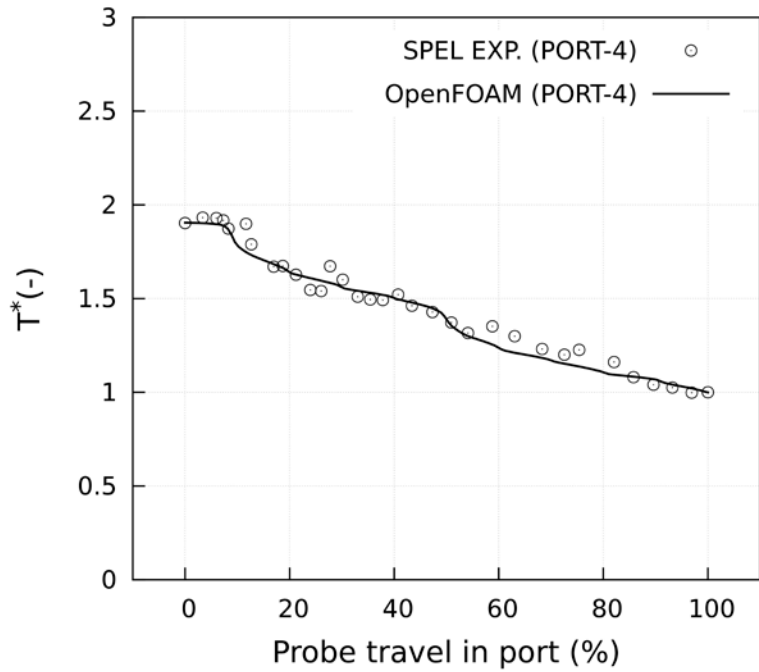


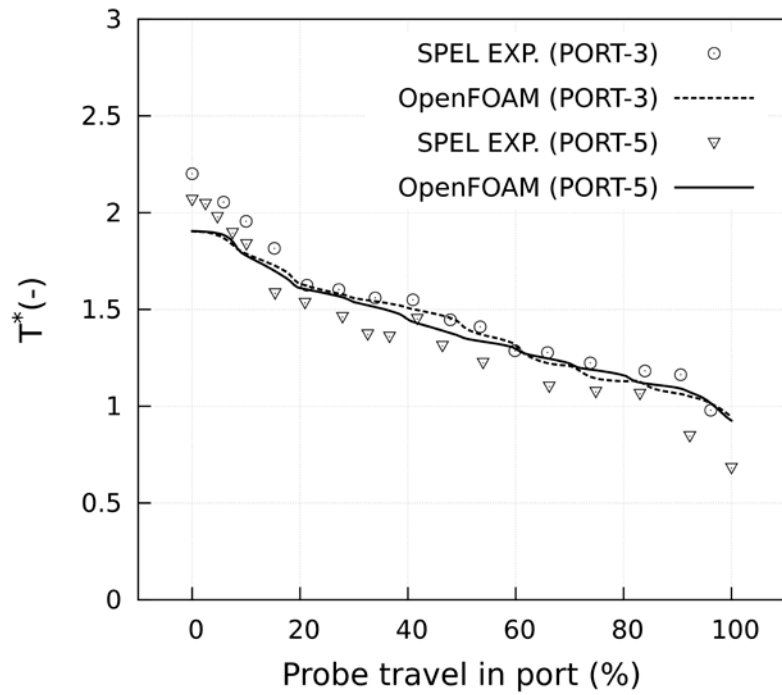
Figure 6.12: Predicted vertical component of velocity along ports 4 and 5 of SPEL experimental setup

Figure 6.13(a) shows the comparison of CFD predictions and experimental data at the vertical centre line (port 4). It can be seen from Figure 6.13(a) that the temperature in CFD analysis at the top most point matches well with experimental data. It can also be observed from SPEL experimental results that the temperature is nearly constant for initial travel of probe in port 4, which is rightfully captured by OpenFOAM. Figures 6.13 (b) and (c) show comparison of CFD predictions and experimental data for ports 3, 5 and ports 2, 6 respectively. Temperature difference between CFD predictions and experimental data at the top of port 2, 3, 4, 5 and 6 is -2°C , -0.85°C , 0°C , -0.20°C and -0.28°C respectively,

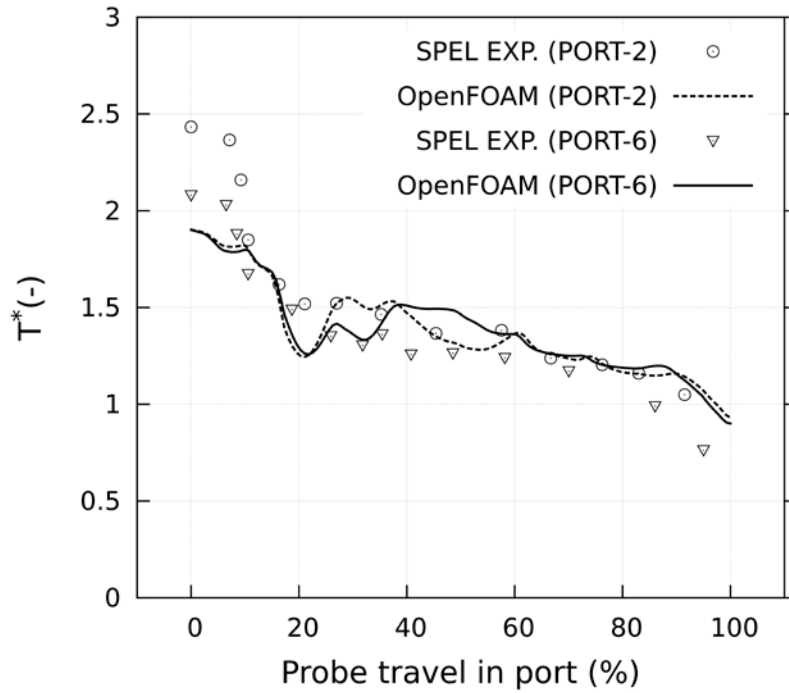
which is consistent with CFD prediction of Kim et al. (2006) and Yoon et al. (2002) for the same experimental facility.



(a) Along port 4



(b) Along port 5



(c) Along port 6

Figure 6.13: Comparison of predicted results with experimental data of SPEL experimental facility

Volumetric average temperature is defined by equation (6.2), where Vol, T and i are volume, temperature and grid cell number respectively. Non-dimensional volumetric average temperature (T_{avg}^*) (equations 6.6 and 6.7) of SPEL vessel is 1.28 T_{avg}^* is more than outlet temperature which is evident from the value of T^* along prob 4, 5 and 6 which is mostly above 1. From the above comparison, it can be stated that OpenFOAM has the capability to simulate the flow and temperature fields when the buoyancy and momentum forces are simultaneously present.

$$T_{avg} = \frac{\sum_{i=1}^n (Vol_i \cdot T_i)}{\sum_{i=1}^n Vol_i} \quad (6.7)$$

6.3.2 Moderator flow and temperature fields inside calandria vessel

3D CFD analysis of moderator flow and temperature distribution inside calandria vessel is performed for the geometry described in section 6.2.1. Analysis has been performed for normal operating condition using actual heat distribution (spatial variation) in moderator. Effect of uniform and non-uniform distribution of heat generation has also been studied. Further, the effect of Archimedes number on temperature distribution has been studied.

6.3.2.1 Normal operating condition having spatial variation of heat generation

In a typical boiling water reactor with bulk boiling, the axial power profile is bottom-peaked and this increases the thermal margin in the top region of the fuel where the void fraction is high. In AHWR, in order to achieve a desirable axial power distribution for obtaining adequate thermal margin, graded enrichment is used along the length of the fuel assembly (Sinha and Kakodkar, 2006). This is achieved by using higher enrichment in the lower half of the fuel assembly as compared to the upper half of the fuel assembly. As the flux distribution is bottom peaking in AHWR, the volumetric heat generation in moderator is also bottom peaking. The non-uniform heat generation in moderator was computed separately using Monte-Carlo technique (Suryanarayana, 2011). Figure 6.14 gives the distribution of volumetric heat generation in moderator. Under the normal operating condition, total volumetric heat load to the moderator is taken to be 50 MW. The total flow rate through the sixteen inlet nozzles is 476 kg/s with 50°C of inlet temperature.

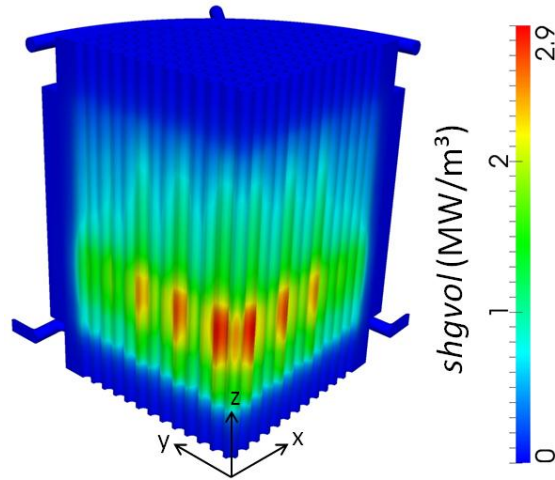


Figure 6.14: Distribution of volumetric heat generation in calandria vessel

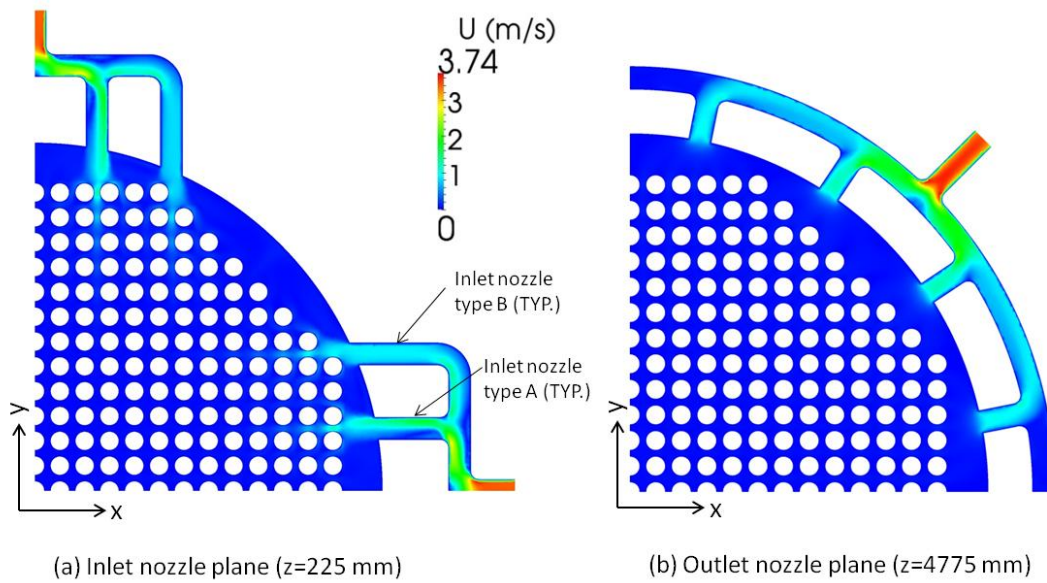


Figure 6.15: Velocity distribution at inlet and outlet nozzle plane of calandria vessel

Figure 6.15 shows flow distribution at inlet and outlet nozzle plane of calandria vessel. Even though flow through nozzle of type B is more uniform than nozzle of type A as shown in Figure 6.15 (a), mass flow rate is nearly same ($\pm 0.1\%$ of mean flow).

Figure 6.16 shows velocity distribution along the axis of inlet nozzle type A and type B (as shown in Figure 6.15 (a)). A local peaking in the velocities is observed and it is because of flow area necking between two calandria tubes. As jets approaches symmetry plane that is $x^* = 0$, type A nozzle velocity decays faster as its distance from calandria tube bundle is more as shown in Figure 6.15 (a). At $x^* = 8$, both type A and B nozzle velocities are less than 0.2 m/s.

Figure 6.17 shows the velocity and temperature distribution inside calandria vessel in normal operating condition induced by the combination of the buoyancy and inlet momentum forces and by the geometric effects such as the presence of calandria tubes at plane $x^* = 0.5$. It shows fluid heated in the core region flows upward by the buoyancy force. As discussed earlier, steady state equations are used for the simulation, however, the transient analysis was also performed to check the unsteadiness of the flow field and it is found that there is no temperature fluctuation in analysis after achieving the steady state.

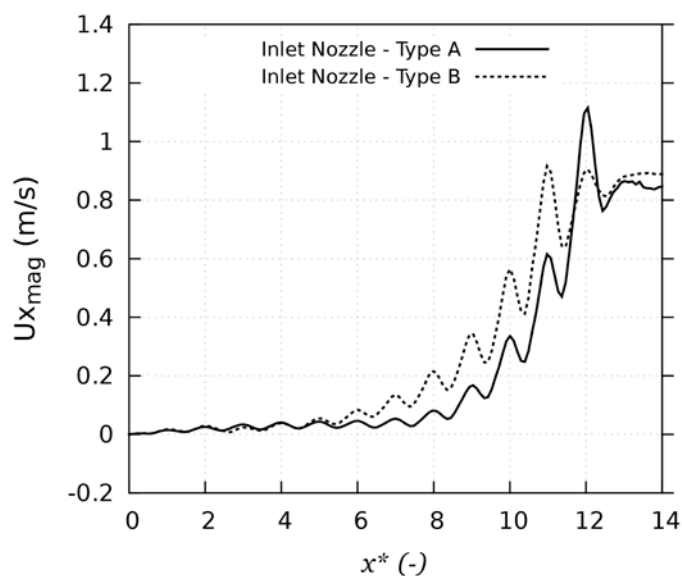
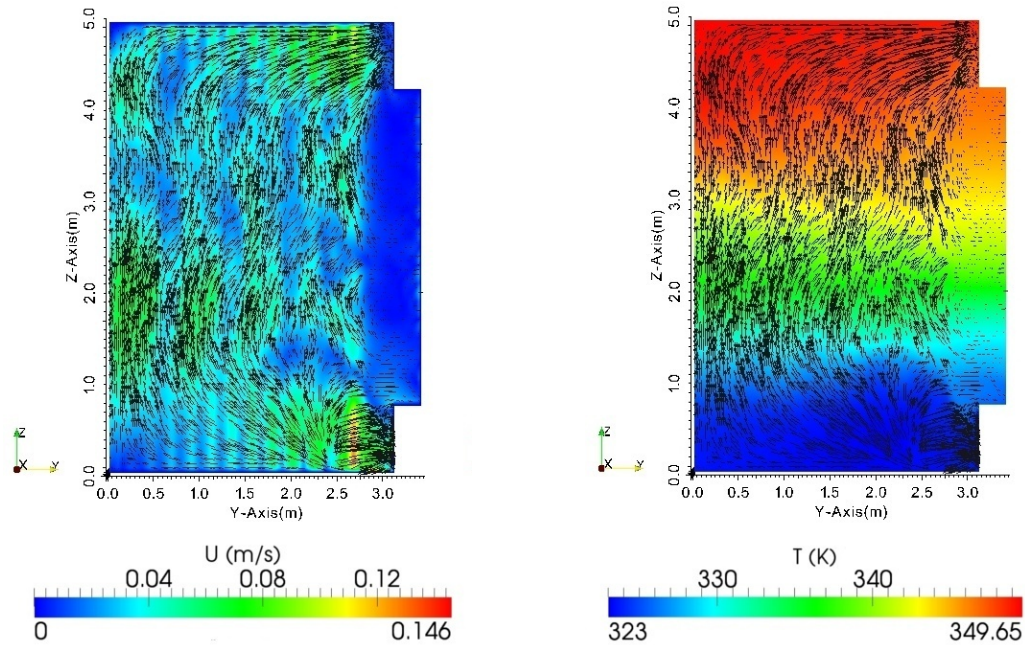


Figure 6.16: Velocity distribution in calandria vessel along the axis of inlet nozzles



(a) Velocity distribution

(b) Temperature distribution

Figure 6.17: Velocity and temperature distribution in calandria vessel under normal operating condition at plane $x^*=0.5$

6.3.2.2 Effect of volumetric heat distribution

To study the effect of volumetric heat generation on flow and temperature fields, three cases have been considered. These three cases are (a) no heat generation (b) uniform heat generation and (c) spatial variation of heat distribution in the moderator. In both the cases (b) and (c), total volumetric heat generation is considered to be 50 MW.

Figure 6.18 shows the effect of volumetric heat generation distribution in calandria on the vertical component of velocity along the axis of calandria. It shows velocity is always positive between two ends due to upward flow generated due to buoyancy force when compared with no heat generation case. It can be seen further that the maximum velocity came down from 95 mm/s to 66 mm/s when spatial distribution of heat generation is modelled. Figure 6.19 shows the distribution of vertical component of velocity at $z = 2.5$ m for three cases (a) spatial Distribution of volumetric heat generation (b) uniform

distribution of volumetric heat generation and (c) without heat generation. Figure 6.19 (a) shows flow is upward in core and very small downward flow in radial reflector region. This is due to very small volumetric heat generation in this region for the case with spatial distribution of volumetric heat generation. Figure 6.19 (b) shows flow is uniformly going upward throughout the section. This is due to uniform volumetric heat generation throughout the section. Figure 6.19 (c) shows that in case of no heat generation, flow is bypassing the core and creating recirculation zone in radial reflector. From these results it can be concluded that flow through core is established due to heat generation in moderator.

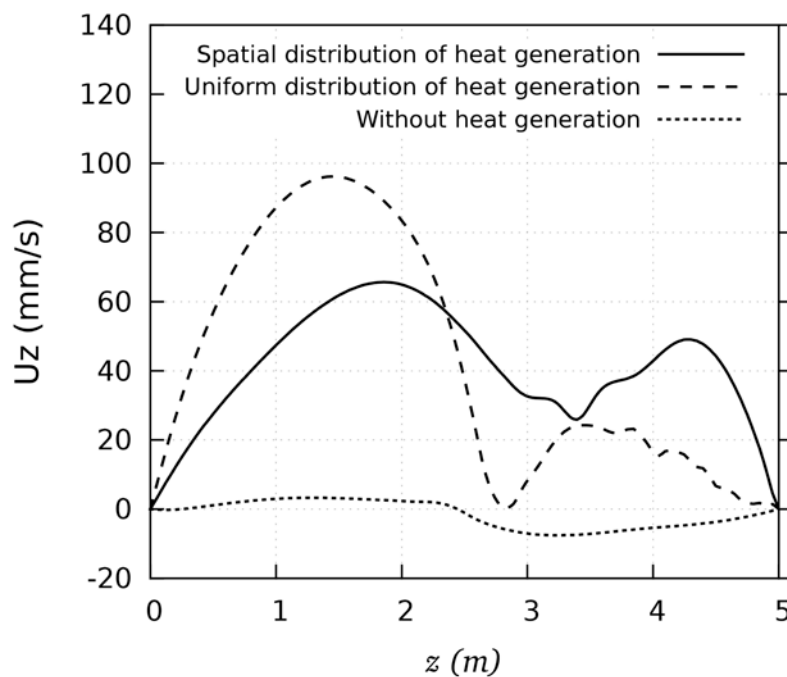


Figure 6.18: Effect of volumetric heat generation distribution on vertical component of velocity along axis of calandria vessel

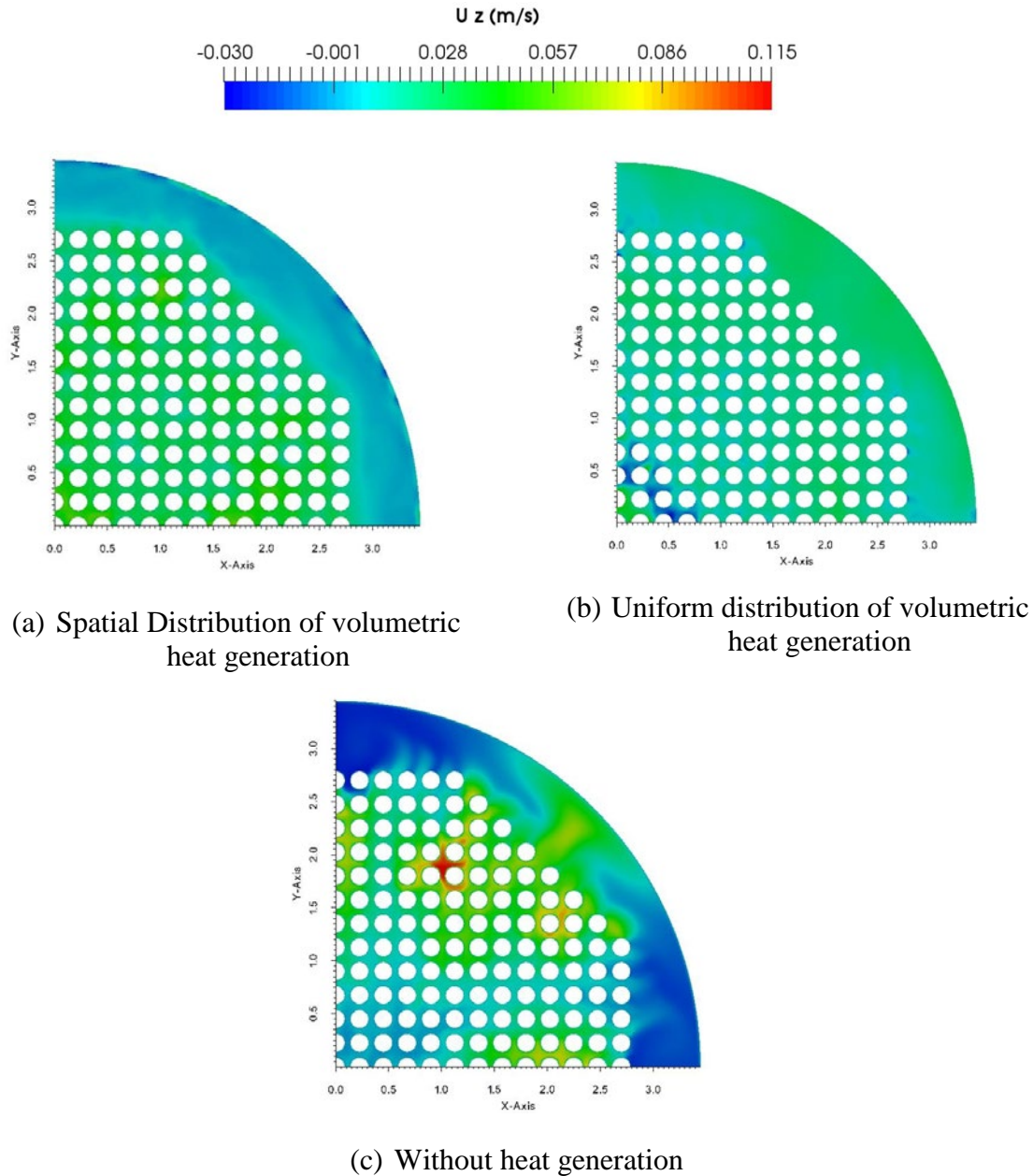


Figure 6.19: Distribution of vertical component of velocity at plane $z = 2.5$ m

Figure 6.20 shows the effect of volumetric heat generation distribution on temperature distribution in calandria vessel. When results for the case with spatial variation of heat generation are compared with uniformly distributed volumetric heat generation, it is observed that the maximum moderator temperature come down by 6.4°C from 83.7°C . Figure 6.21 shows comparison of centre line temperature for both the cases. In case of uniform heat generation, temperature at bottom reflector ($z=0$) of calandria vessel is 56°C

which is 6°C more than inlet temperature whereas, in case of non-uniform heat generation, it is equal to inlet temperature. Similar behaviour can be observed in top reflector at $z = 5\text{m}$. This is because of very small amount of heat generation in top and bottom reflector when non-uniform heat generation in the moderator is considered.

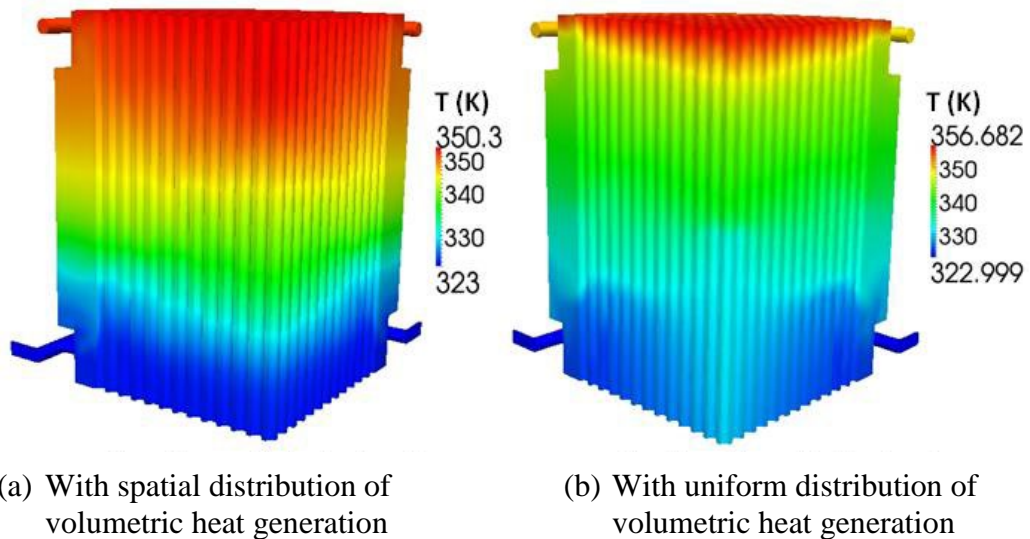


Figure 6.20: Effect of volumetric heat generation distribution on temperature distribution

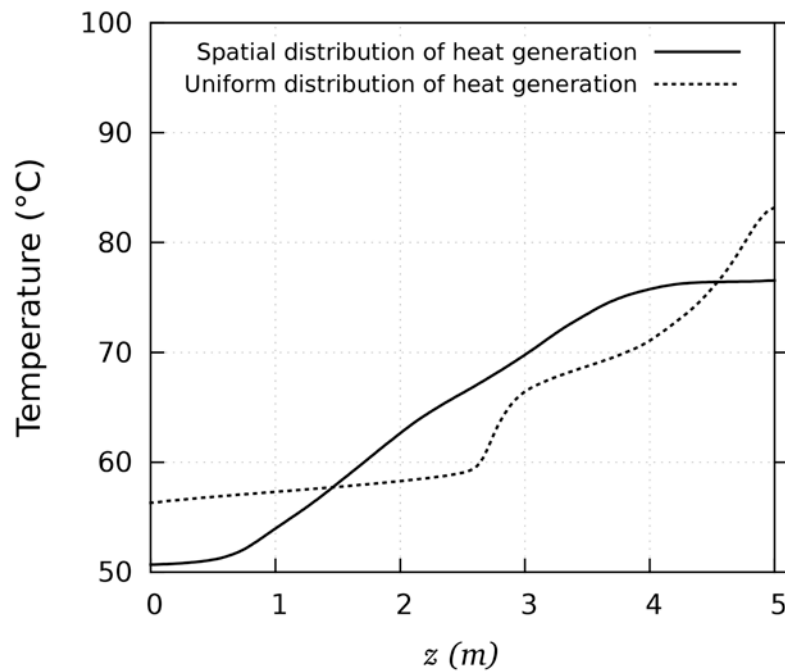


Figure 6.21: Effect of volumetric heat generation distribution on temperature distribution in calandria vessel

6.3.2.3 Effect of Archimedes number

To study the effect of Ar number on maximum and volumetric average temperature of moderator, total heat input to calandria is varied keeping flow rate and temperature at inlet nozzle same. This means only buoyancy force is changed keeping the inertia force constant. Figure 6.22 shows that with increase in Ar number, non-dimensional maximum temperature (T_{max}^*) decreases. It shows that as buoyancy force increases, maximum moderator temperature is approaching moderator outlet temperature. Here $Ar = 0.74$ shows the normal operating condition as described in section 6.3.2.1. Figure 6.22 also gives the variation of non dimensional volumetric average temperature (T_{avg}^*) with Ar number. It shows (T_{avg}^*) decreases with increase in Ar number. Results of Archimedes number effect on moderator temperature are summarised in Table 6.4. From results, it can be observed that T_{avg}^* is more than 0.5 for all the cases, where value of 0.5 shows arithmetic mean of inlet and outlet temperature. Hence, for the all the cases analysed volumetric average temperature of moderator is more than arithmetic mean of inlet and outlet temperature.

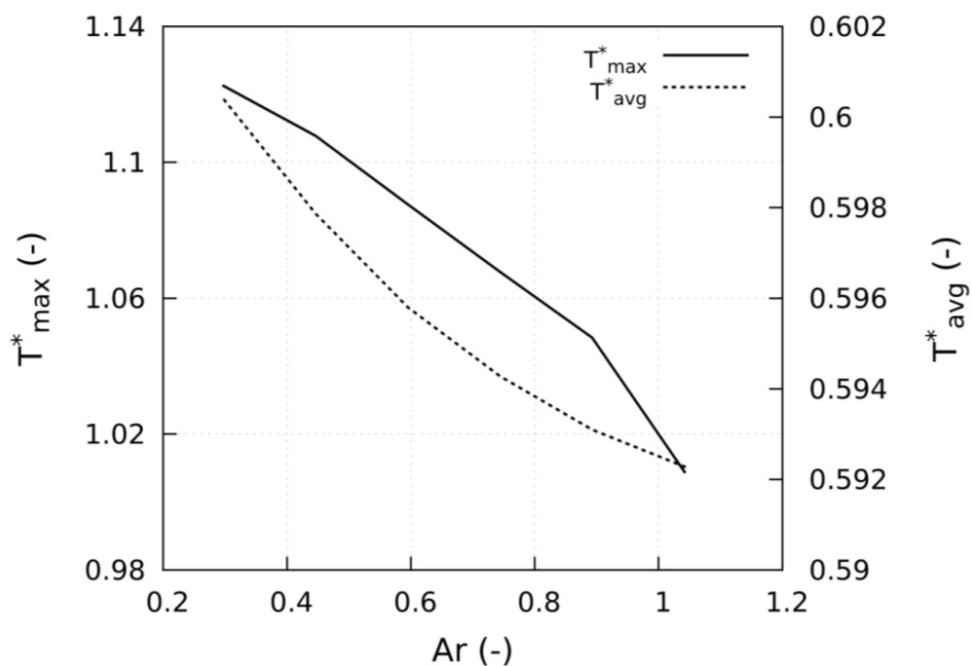


Figure 6.22: Effect of Archimedes number on maximum and volumetric average moderator temperature in calandria vessel

Table 6.4: Effect of Archimedes number on maximum and average moderator temperature

Heat load (MW)	T_{inlet} (°C)	ΔT (°C)	Ar (-)	T_{avg} (°C)	T_{max} (°C)
70	50	35	1.04	70.7	85.3
60	50	30	0.89	67.8	81.5
50	50	25	0.74	64.9	76.7
40	50	20	0.59	61.9	71.8
30	50	15	0.44	59.0	66.6
20	50	10	0.30	56.0	61.2

6.3.2.4 CFD Analysis of full calandria

As there is no symmetry plane for poison injection, hence full calandria has to be modelled for simulating the poison injection. Thus, for generating moderator flow and temperature field condition for transient study of poison injection, full calandria was analysed for spatial distribution of volumetric heat generation. Governing equations, model assumptions and solution, in this case, is same as discussed for the one-fourth model. Regarding boundary condition, as full calandria is modelled hence no symmetry condition is applied. Grid taken in full calandria model is four times the grid used in the one-fourth. Figure 6.23 shows solid model of full calandria that is considered in the analysis. Figure 6.24 and Figure 6.25 shows the temperature and velocity field distribution in the section view of full calandria. Figure 6.26 shows comparison of calandria centre line temperature of full calandria model and one-fourth model. The result shows both the temperature profiles are nearly overlapping. Thus it can be concluded that one-fourth model of calandria can be used to study moderator flow in the present case.

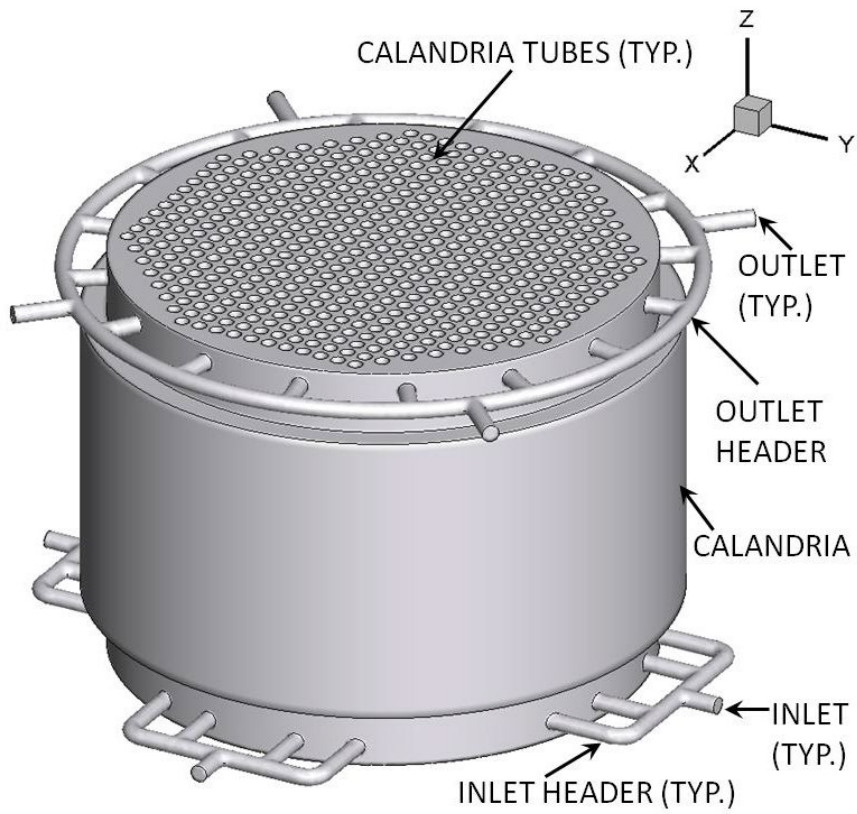


Figure 6.23: Solid model of full calandria

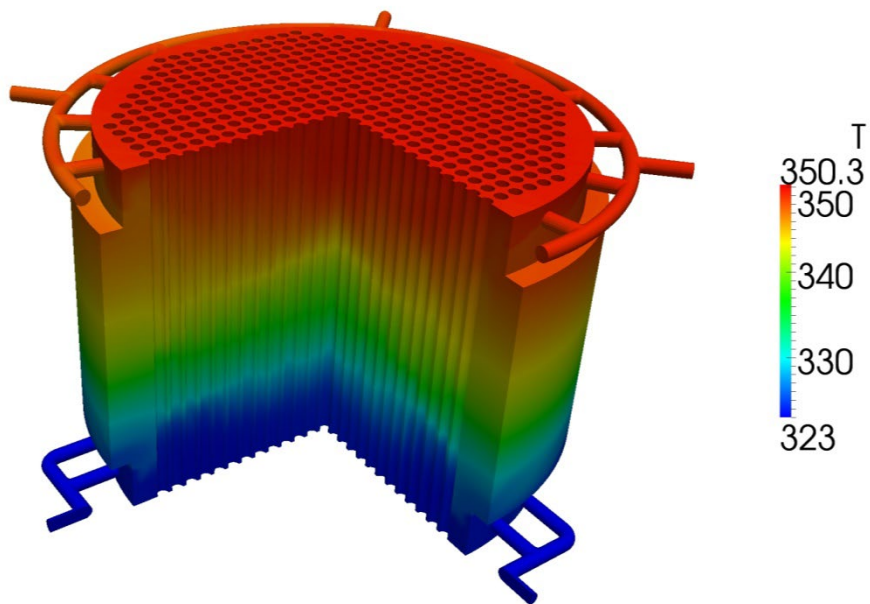


Figure 6.24: Temperature distribution in three-fourth section view of calandria

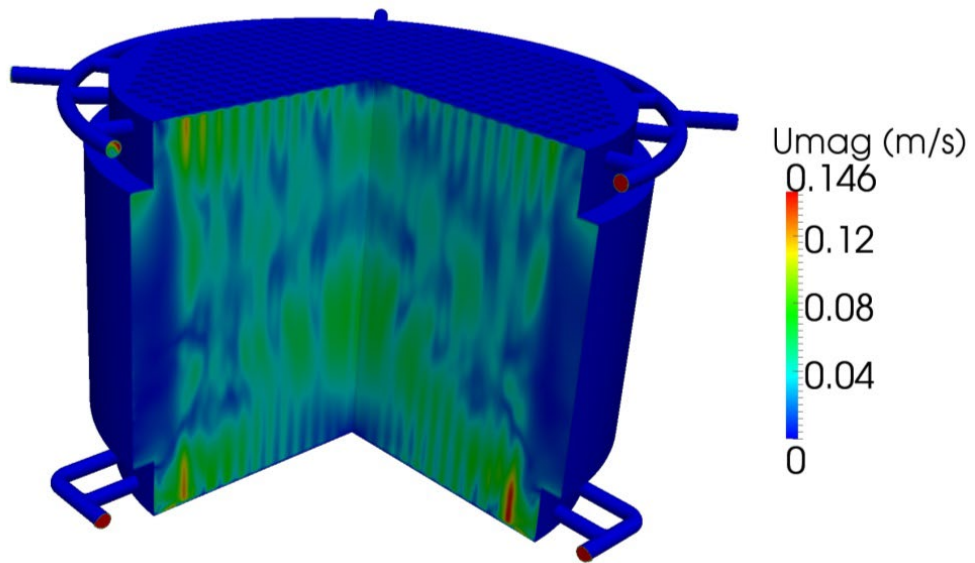


Figure 6.25: Velocity distribution in three-fourth section view of calandria

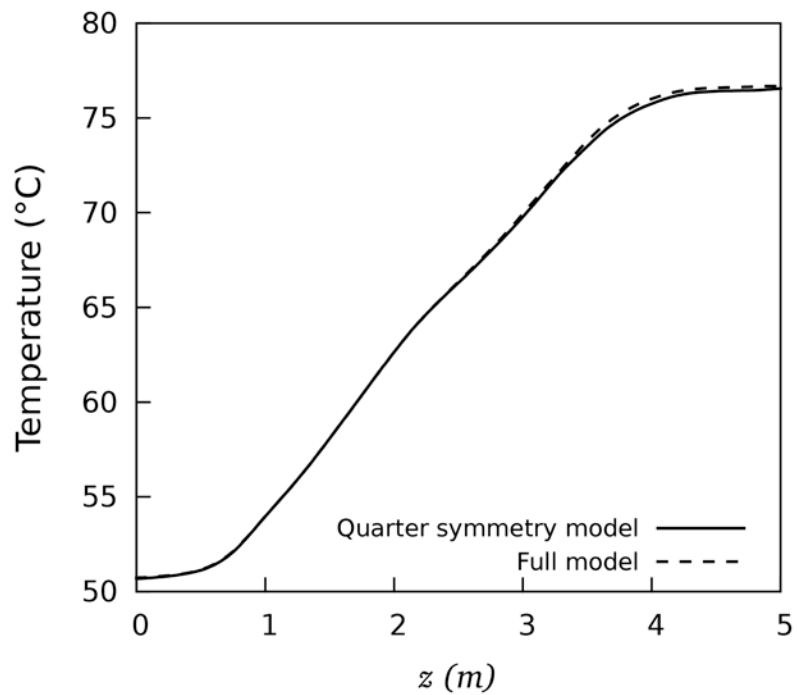


Figure 6.26: Comparison of centre line temperature of full calandria model with one-fourth model

6.4 Conclusions

Moderator flow and temperature distribution in vertical calandria vessel of the nuclear reactor were simulated using OpenFOAM. Simulations were performed for three different cases of normal operating condition, effect of volumetric heat distribution and the effect of Archimedes number. The main conclusions are as follows:

- The comparison with the SPEL experimental data shows that OpenFOAM can simulate simultaneous buoyancy and momentum dominated flows in complex geometry.
- There is no significant mal-distribution in mass rate through two types of inlet nozzles.
- By taking spatial distribution of volumetric heat generation in CFD simulation, the maximum moderator temperature reduces by 6.4°C when compared with the case of uniform distribution of heat generation.
- With increase in Archimedes number, the maximum moderator temperature approaches moderator outlet temperature.
- Volumetric average temperature of moderator is more than arithmetic mean of inlet and outlet temperature and it approaches arithmetic mean with the increase in Archimedes number.

Chapter 7

POISON INJECTION IN AHWR CALANDRIA: FLOW PATTERN AND MIXING CHARACTERISTICS

7.1 Introduction

The effectiveness of poison injection depends on the dispersion of poison in the moderator throughout the calandria in a short time. Based on the dispersion of poison, the absorption of neutrons takes place and the reactor shuts down. Detailed knowledge of poison distribution in calandria is a prerequisite for reactor physics calculation for reactivity worth of SDS-2. Experimental techniques can give poison concentration at only limited number of locations in calandria. Thus, the scope of work in the present chapter is to perform CFD analysis of liquid poison injection and its dispersion into the moderator in calandria.

CFD studies conducted for CANDU-6 reactor (Rhee et al., 2007) related to liquid poison injection assumes negligible effect of calandria tubes and modelled only a sector of full geometry. Published literature shows in the case of Advanced Candu Reactor (ACR) (Song et al., 2008) where ratio of calandria tube pitch to diameter is in same order as

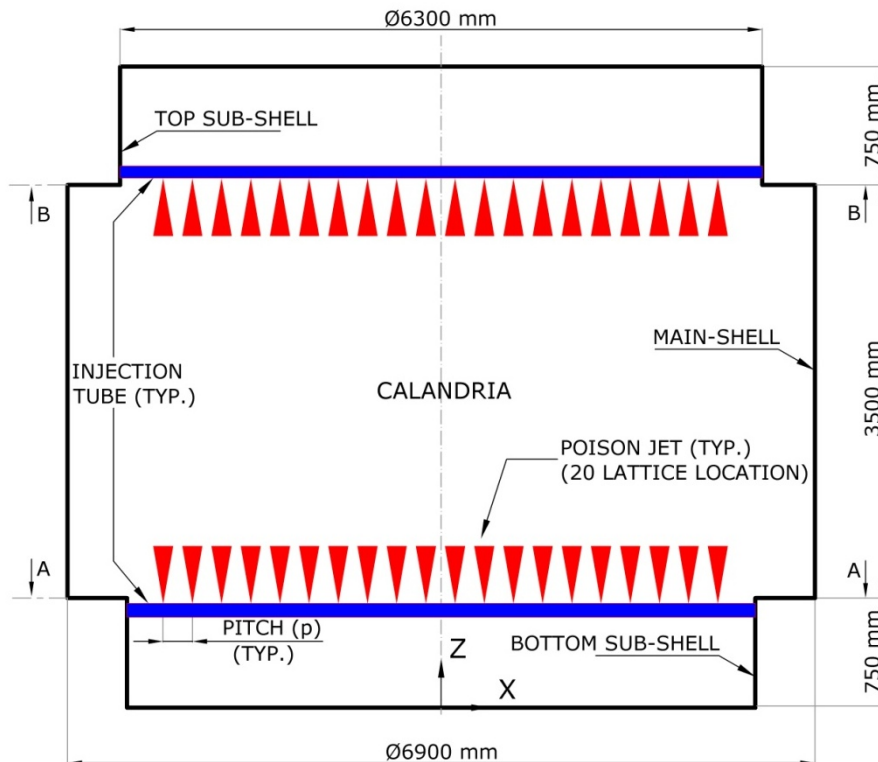
AHWR, a limited number of calandria tubes were included in the CFD simulations. In ACR, jet axis is perpendicular to calandria tube axis, compared to near parallel axis of jets and calandria tubes in AHWR. Moreover, the effect of moderator flow and temperature distribution is not considered in published literature. In chapter five and six, experimental studies and CFD model validation were done for a poison jet emanating from the circular nozzle in the presence of inline and cross bundle. In this chapter, CFD analysis performed for distribution of poison in the moderator present in calandria is described. In addition to this, the effect of calandria tubes and effect of neighbouring group of injection nozzles on poison jet progression will be studied. Results of CFD simulations will also be compared to computer code COPJET. These results are very useful in analysing the performance of SDS-2.

7.2 Computational Fluid Dynamics

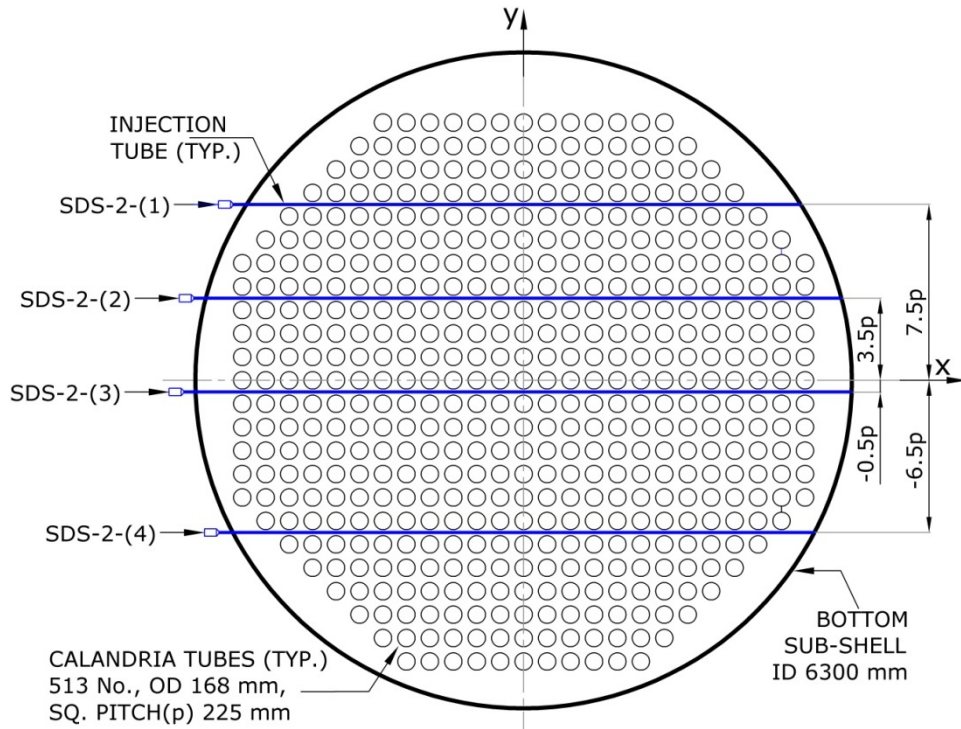
7.2.1 Flow geometry

Calandria of AHWR is a vertical cylindrical tank filled with heavy water (Sinha and Kakodkar, 2006). The calandria vessel comprises a main cylindrical shell of 6.9 m diameter and net height of 5 m as shown in Figure 7.1 (a). At either end of the main shell, sub-shell of 6.3 m diameter and 0.75 m height is provided. These sub-shells form the top and bottom reflector regions of the reactor core. Inside the calandria, 513 calandria tubes having of 0.168 m diameter are arranged vertically in a square pitch (p) of 0.225 m to form an array of the lattice. There are eight liquid poison tanks in SDS-2. Each tank is connected to a piping circuit penetrating the calandria horizontally as shown in Figure 1.2. Four injection tubes are located at 0.75 m and other four injection tubes are located at 4.25 m elevation from calandria bottom as shown in Figure 7.1 (a). Figures 7.1 (b) and (c) show the location of injection tubes at these elevations. The injection tube inner diameter is 38.1 mm. These injection tubes contain circular openings called injection nozzles. There are

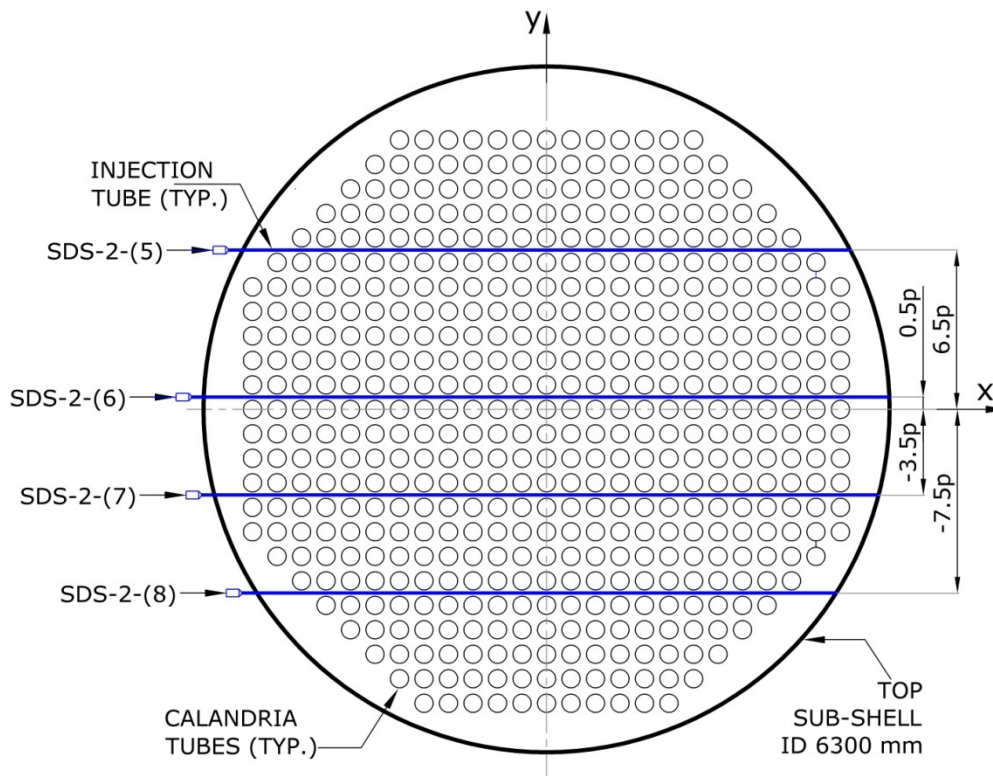
four injection nozzles located centrally between calandria tubes forming a group of injection nozzles as shown in Figure 7.2. Each injection tube has 20 such groups of injection nozzles. Hence, there are total 640 injection nozzles of diameter 6 mm in eight injection tubes for poison injection in calandria. Direction of injection is towards the centre of calandria. Out of four injection nozzles, the axis of two central nozzles is parallel to calandria and the other two are inclined at $\pm 20^\circ$ angle to the axis of calandria. Axial nozzles provide penetration and inclined nozzles provide lateral spread of poison.



(a) Elevation view without internals



(b) Plan view-Section AA



(c) Plan view-Section BB

Figure 7.1: Schematic of SDS-2 injection tubes

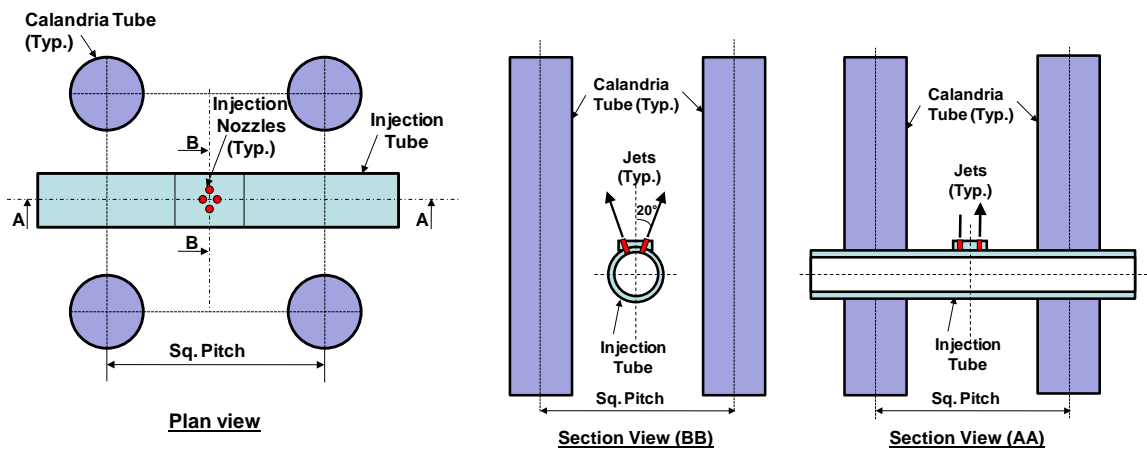


Figure 7.2: Schematic arrangement of jet nozzles in typical lattice location

7.2.2 Governing equations

Table 5.1 lists the governing equations used in the CFD code OpenFOAM to model the transient, incompressible, single phase and multi species flow in calandria. In the model, standard k- ϵ turbulence model was used.

7.2.3 Model assumptions

The following assumptions have been made:

1. Incompressible single phase fluid.
2. Average density in control volume is estimated by species fraction weighted density.
3. Fluid properties are constant except density in the formulation.
4. An adiabatic boundary condition at the calandria wall was employed.

7.2.4 Method of solution

CFD simulations have been performed using the open source CFD code OpenFOAM 2.2.2 (2013). Mass, momentum, energy and species equations as given in Table 5.1 are modelled. The incompressible Unsteady Reynolds Average Navier Stokes (URANS) modelling based on the finite-volume method (FVM) and the predictor–corrector algorithm (Issa, 1986) is used for solution of equations. The dynamic adjustable time stepping

technique is used to guarantee the local Courant number less than 1. Validated model described in chapter five for using source terms as inlet boundary condition is used in the present simulation. For discretisation of convection term, second order upwind scheme is employed and for discretisation of diffusion and gradient term, the central differencing scheme is followed. Solutions are considered to be fully converged when the sum of scaled residuals is below 10^{-3} .

7.2.5 Boundary conditions

In the model, the calandria tubes and calandria vessel surfaces were considered as adiabatic with no slip boundary condition. Standard wall function was used on all the wall surfaces. Boundary conditions for inlets from the nozzles in injection tubes are generated using computer code COPJET as explained in chapter three. Time varying uniform inlet jet velocities as shown typically in Figure 3.12 for injection nozzle group number 11 were taken as source term and starting time of poison injection adopted in species equation is shown in Figure 3.9.

7.2.6 Grid independence studies

From Figure 7.1 it can be seen that there is no symmetry plane for poison injection hence full calandria has been modelled for simulating the poison injection. Thus, full calandria with 640 injection nozzles was modelled. The grid independence for the transient case for the geometry described in section 7.2.1 was investigated by considering three different grids: (1) 15 million, (2) 19 million and (3) 24 million. The computational mesh for calandria vessel for 19 million grid size has 96% hexahedral cells and rest prism cells.

To check the grid independence, the progression of poison jet along the vertical line passing through $(x, y) = (-0.5p, -3.5p)$ is taken, where p is the lattice pitch. Intersection of calandria axis with calandria bottom is taken as the centre of coordinate as shown in Figure

7.1. Location along the jet axis having concentration of 1% of initial concentration (C_0) is taken as progression of poison jet. The difference between jet progressions for 19 and 24 million grids is 30 mm at 2 s as shown in Figure 7.3. As the results of 19 and 24 million grids are found to be within 1.2%, all the present simulations are done using 19 million grids.

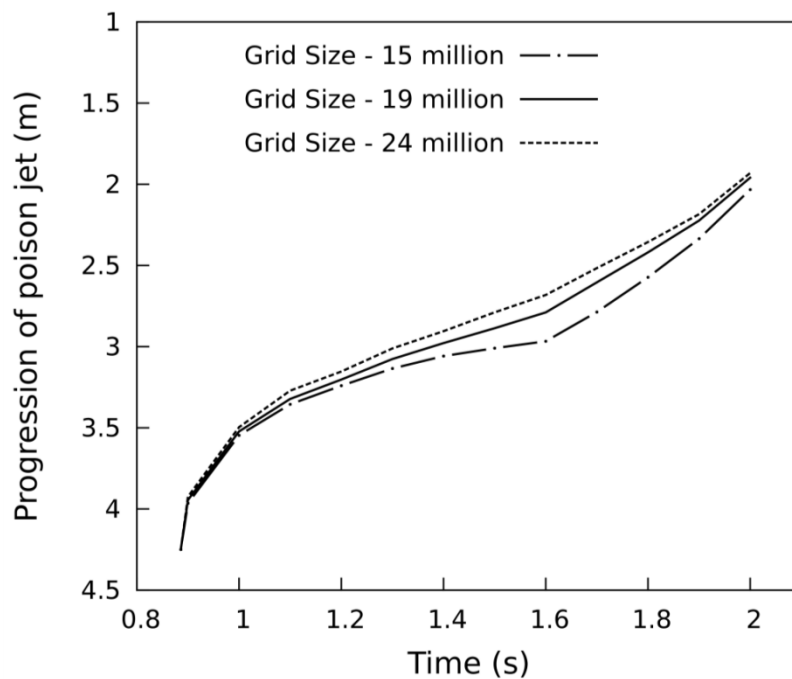


Figure 7.3: Effect of grid size on CFD predicted progression of poison jet from $(x, y, z) = (-0.1125 \text{ m}, -0.7875 \text{ m}, 4.25 \text{ m})$

7.3 Results and Discussions

As discussed earlier in chapter 5, the model employed in OpenFOAM was first validated with experimental results and with the data available in the literature. This validated model was used for AHWR geometry described in section 7.2.1. The results obtained are discussed in the following sections.

7.3.1 Effect of calandria tubes on poison jet progression

CFD simulations were done to understand poison jet progression from a group of injection nozzles as shown in Figure 7.2. To understand the effect of calandria tubes on poison jet progression two cases are considered: the first case is without calandria tubes and the other case is with calandria tubes. A section of the grids as discussed in section 7.3.6 is taken for the simulations as shown in Figure 7.4 having height of 5 m. The location of group of injection nozzles is ($x = 2.5 p$, $y = 3.5 p$, $z = 0.750m$).

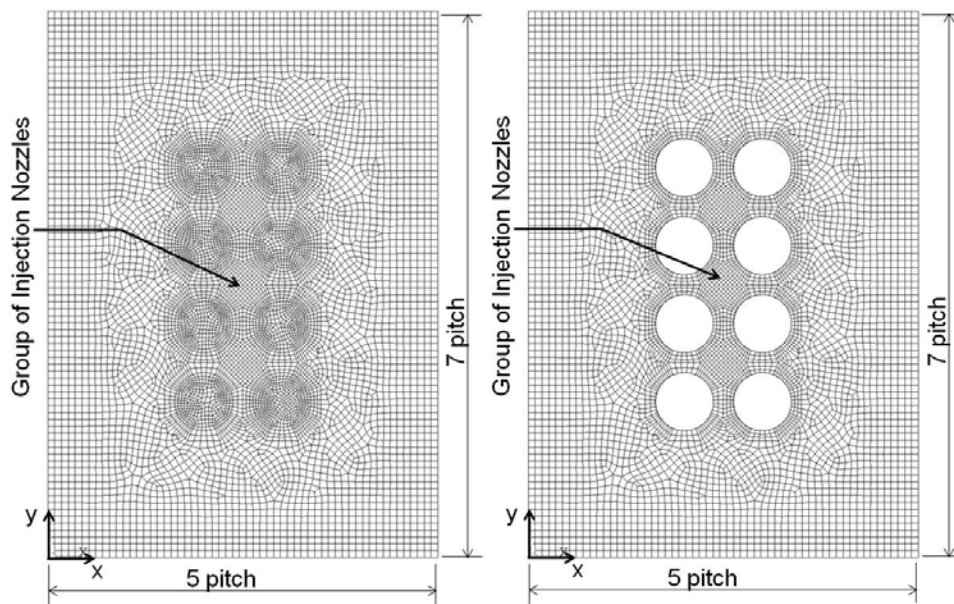


Figure 7.4: Model grid details for a lattice location

Figure 7.5 and Figure 7.6 shows poison jet progression at plane $x = 2.5 p$ and plane $y = 3.5 p$ respectively with time for 11th group number of injection nozzles. Dead time for this group is 0.891 s as shown in Figure 3.11. It shows that poison spread in y direction is more compared to x direction spread because of two 20° inclined poison jets. It also shows, poison jet spread more in all directions when it passes through calandria tubes. Figure 7.7 shows the distribution of poison at $z = 2 m$ from the bottom. It shows poison spreading effect due to calandria tubes.

Figure 7.8 shows the comparison of poison jet progression for the above cases with computer code COPJET. Results show that the COPJET predicted progression of jet at 2 s is deviated by 1.4 % and -3.9 % compared to OpenFOAM poison jet simulation without and with calandria tube respectively.

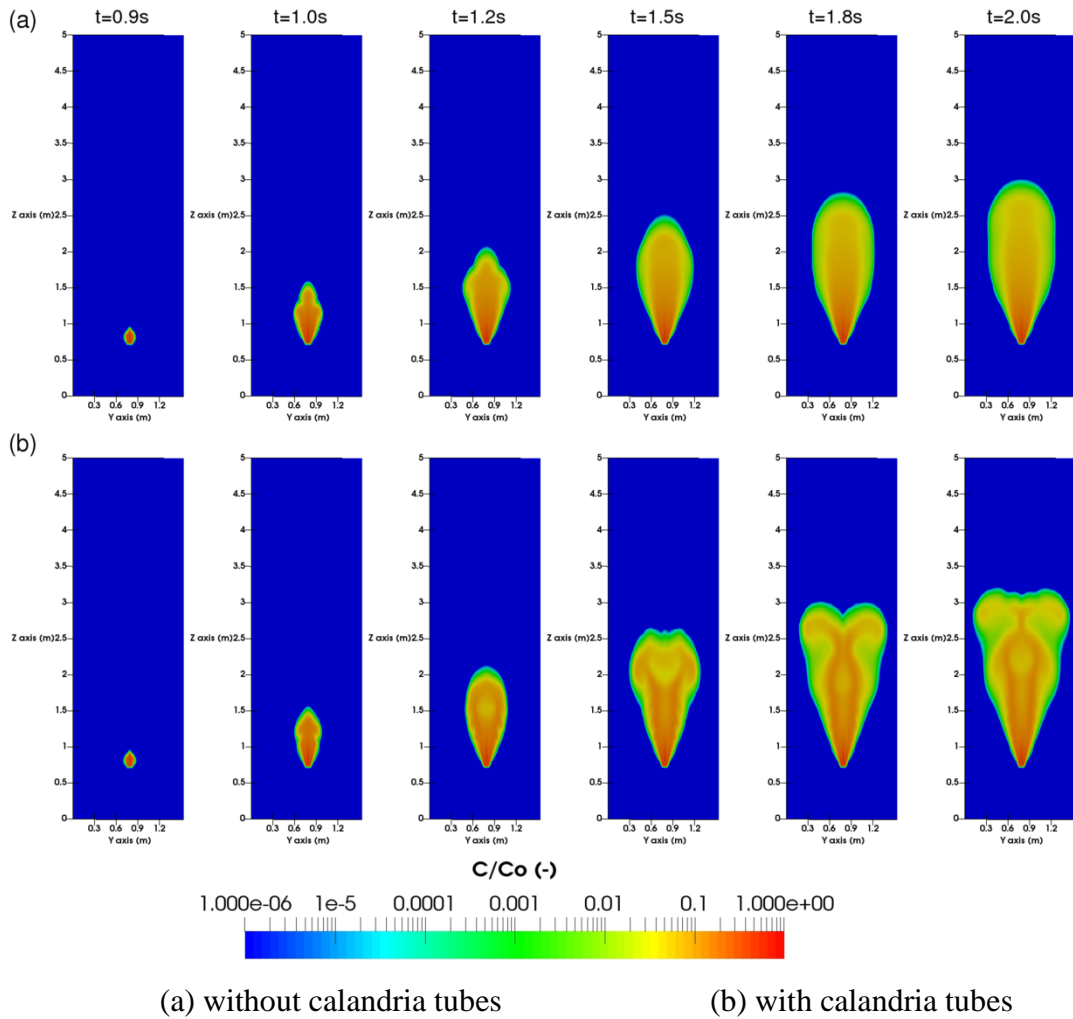


Figure 7.5: Poison jet progression with time at plane $x = 2.5$ p

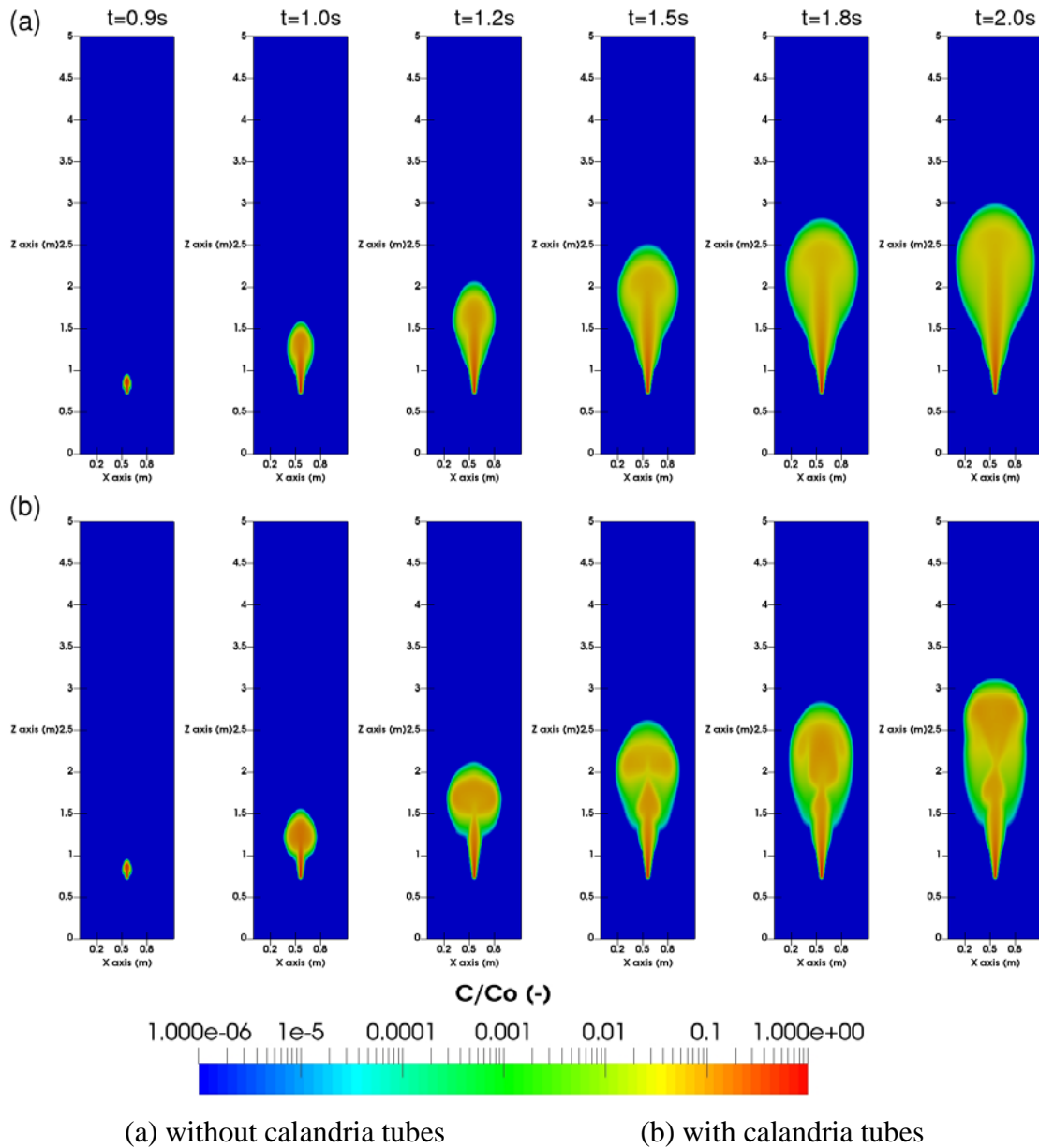


Figure 7.6: Poison jet progression with time at plane $y = 3.5 p$

Similarly all other groups of injection nozzles are individually simulated in CFD and compared with COPJET. Figure 7.9 shows the comparison of poison jet progression between CFD and COPJET prediction. Results show that the COPJET predicted progression of jet at 2 s is deviated by 2.0 % and 3.8 % compared to OpenFOAM simulation of injection tube at first and last group of injection nozzle respectively.

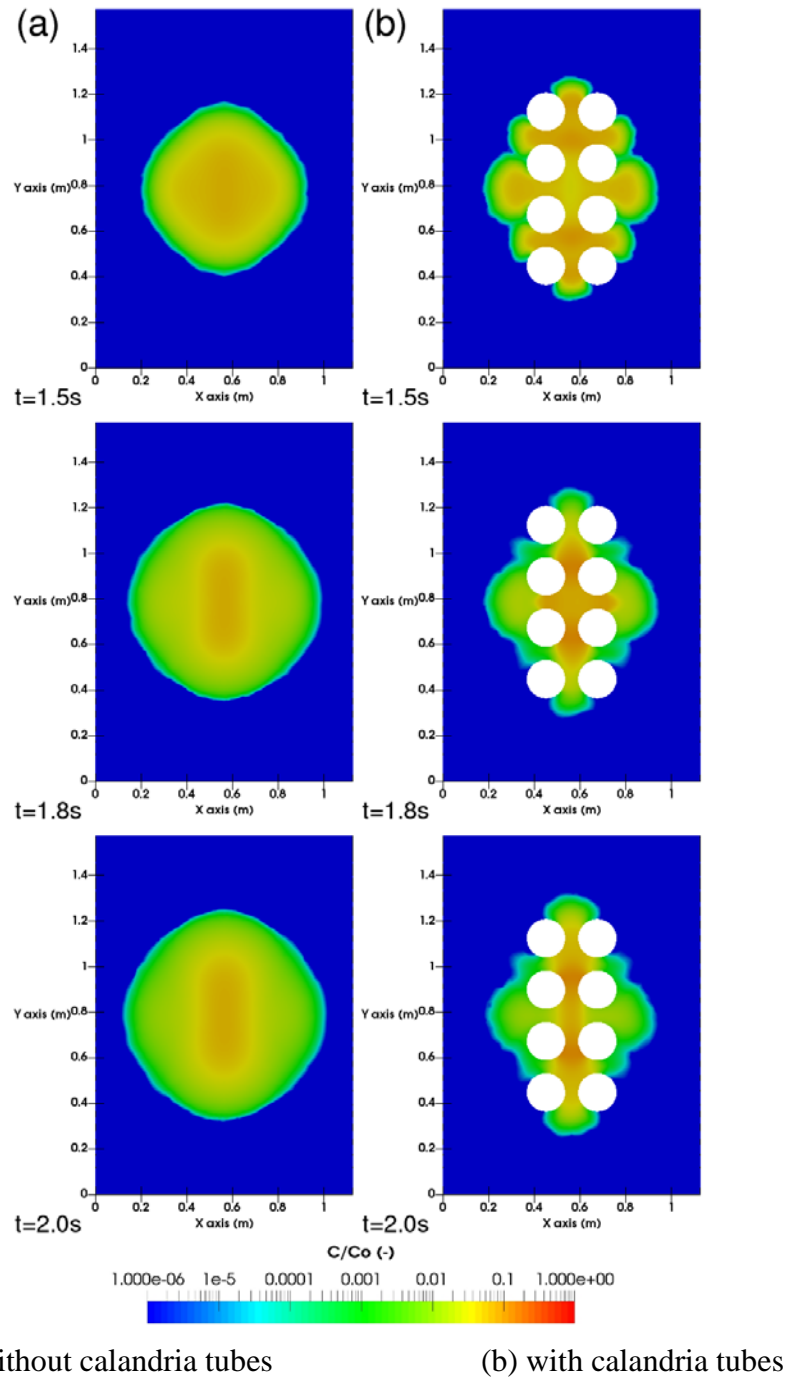


Figure 7.7: Poison jet progression at plane $z = 2$ m

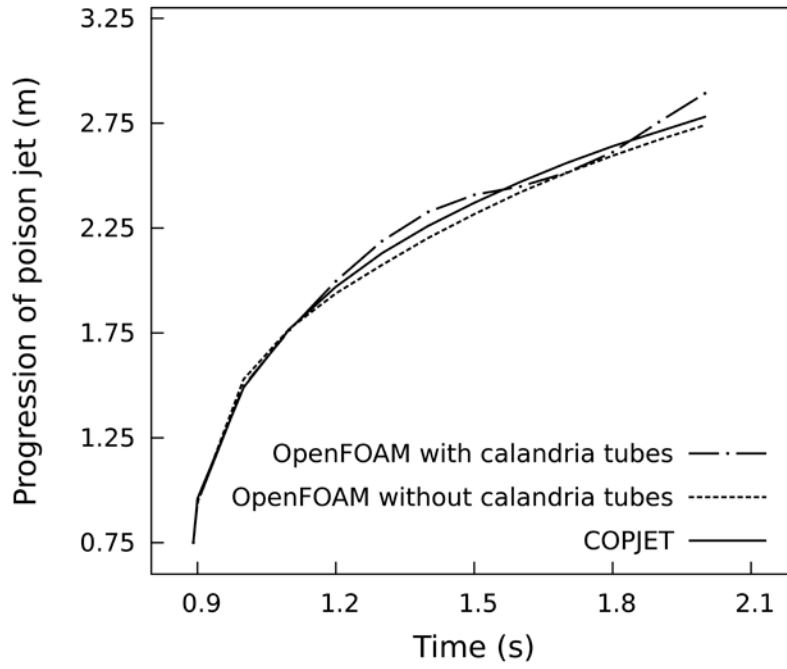


Figure 7.8: Comparison of OpenFOAM and COPJET prediction for 11th group of injection nozzle

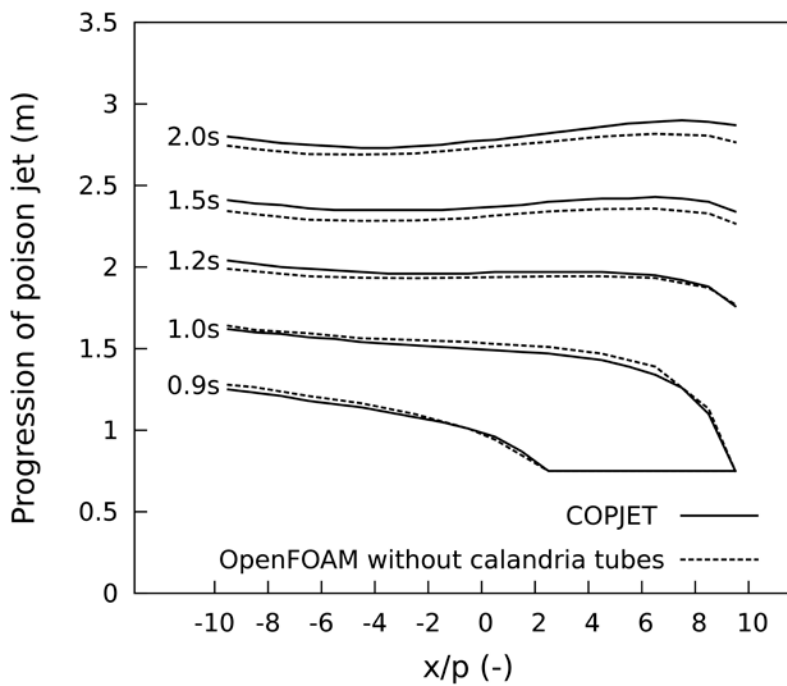


Figure 7.9: Comparison of OpenFOAM and COPJET predicted progression of poison jet along the injection tube

7.3.2 Effect of neighbouring group of injection nozzles on poison jet progression

In each injection tube, there are 20 groups of injection nozzles. In AHWR, where p/d ratio of lattice is small, neighbouring group of injection nozzles will affect the poison jet progression. Hence, one injection tube is simulated to understand the effect of neighbouring group of injection nozzles without calandria tubes. Figure 7.10 shows the domain details in xy plane along with injection tube axis. Injection tube is at height of 0.75 m in domain having total height of 5 m. Figure 7.11 shows the poison progression at contour plane $y = 0$ with time. Contour plot at 0.9 s and 1.0 s, effect of different starting time on poison injection can be seen. At 1.2 s, the progression of poison jet is same along the length, after that the progression of poison from the injection tube's last group of injection nozzles exceeds the progression of poison from the first group. Figure 7.12 shows comparison of OpenFOAM predicted progression of poison jet with and without neighbouring group. The comparison shows at 0.9 s and 1.0 s, when the interaction between neighbouring groups of injection nozzles are not dominating, the progression of poison is identical in both the cases. With time, the effect of neighbouring groups of injection nozzles start dominating and the poison progression from both ends of injections tube accelerates as compared to without the neighbouring group effect case. Progression of poison from last group of injection nozzles is 9% more at 2 s due to the effect of neighbouring groups of nozzles.

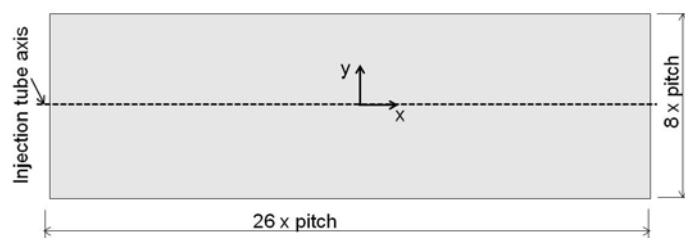


Figure 7.10: Domain details for full injection tube without calandria tubes

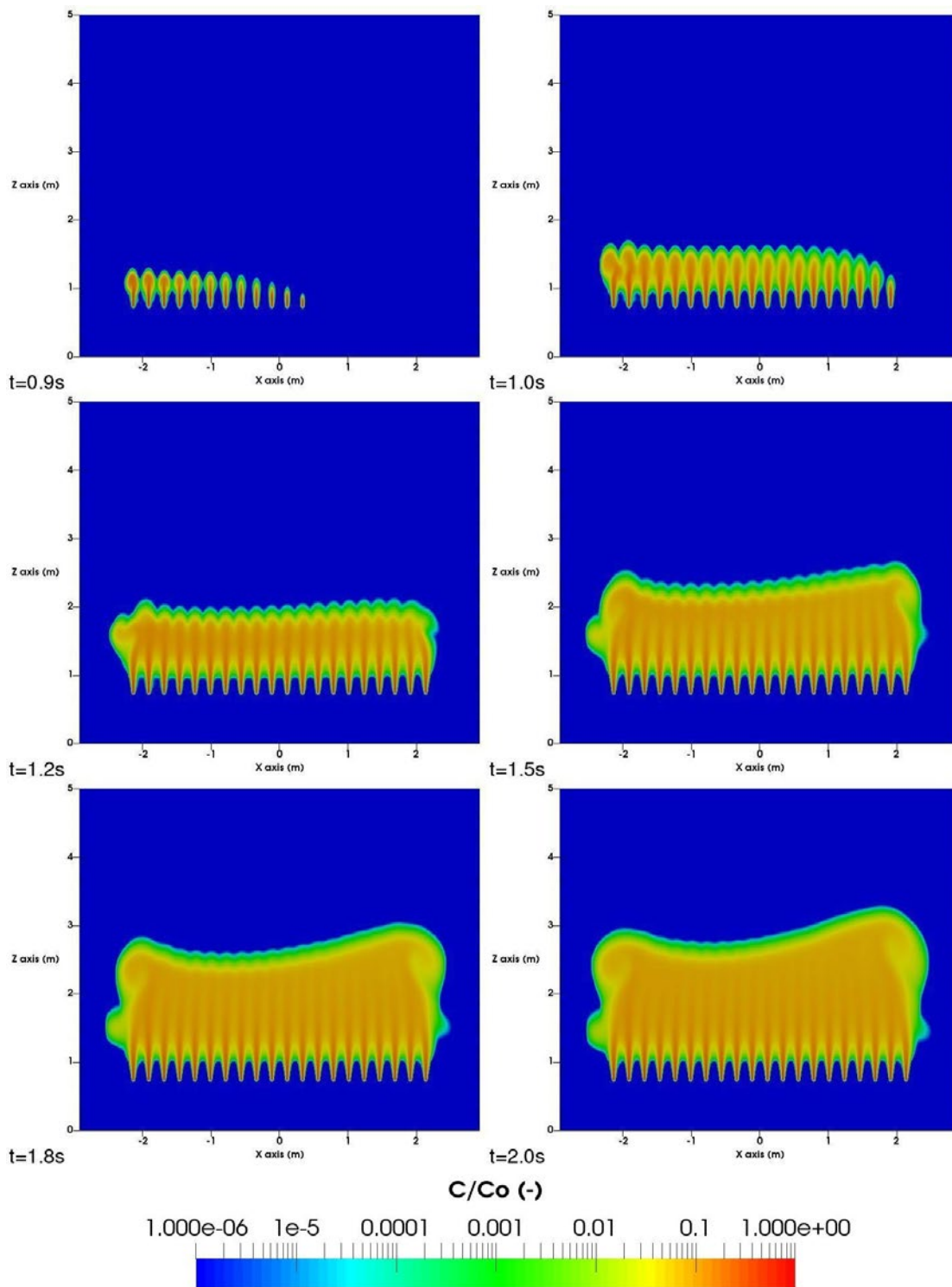


Figure 7.11: Poison jet progression with time at plane $y = 0$

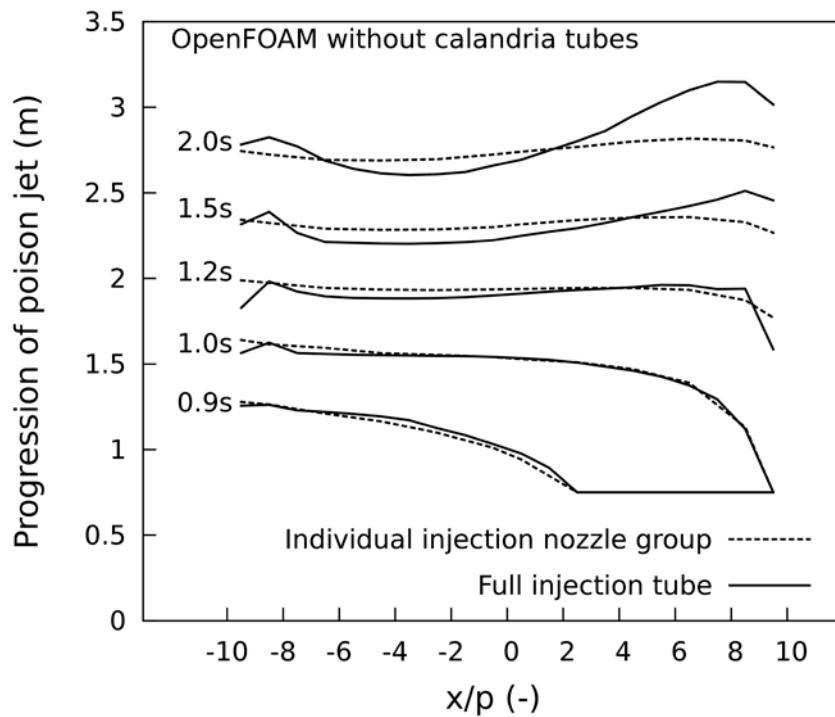


Figure 7.12: Comparison of OpenFOAM predicted progression of poison jet with and without neighbouring group

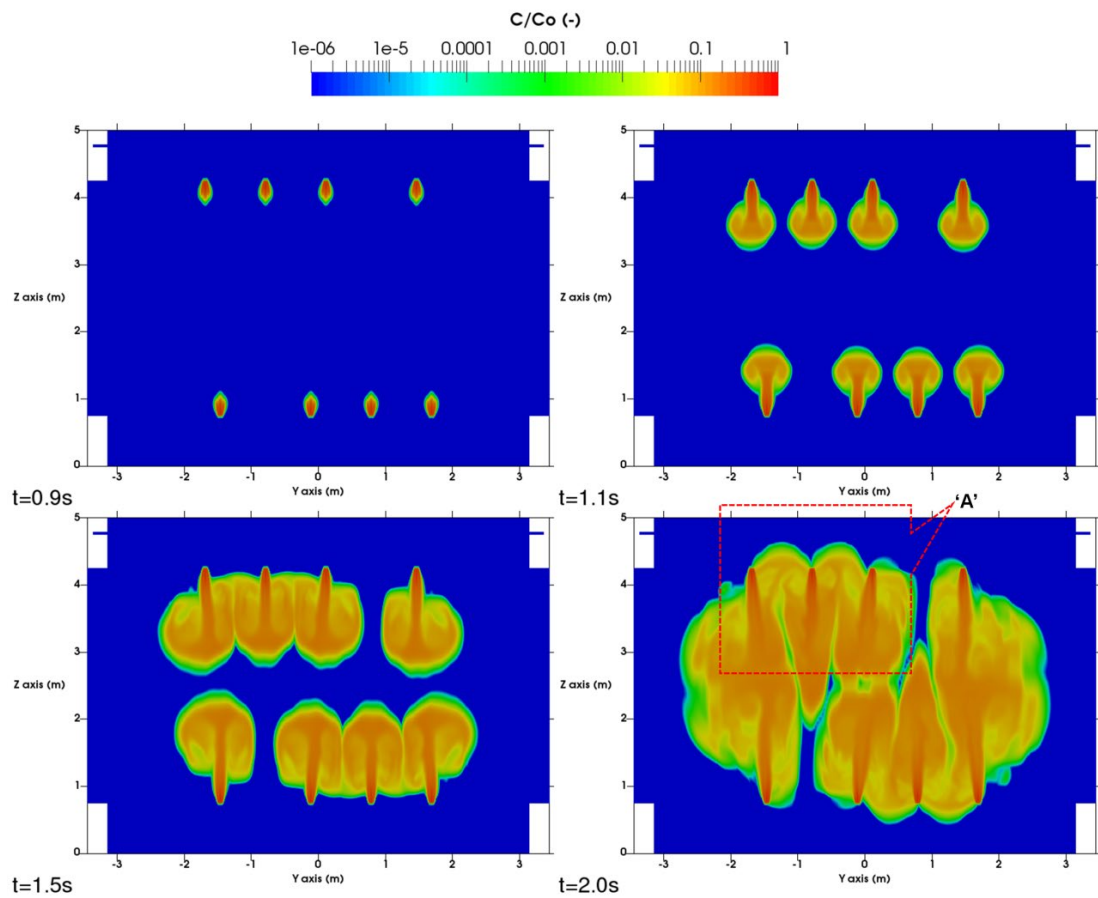
7.3.3 Poison distribution in calandria

Based on the validated CFD model, poison distribution analysis was carried out for AHWR to evaluate various design options for poison injection in moderator to achieve faster negative reactivity insertion rate for reactor shutdown. The general scheme for poison injection is indicated in Figure 7.1. For each injection nozzle, injection velocity with time was estimated from the 1-D thermal hydraulic code COPJET based on actual layout of the system. Dead time for injection was also estimated from COPJET and found to be 0.85 s.

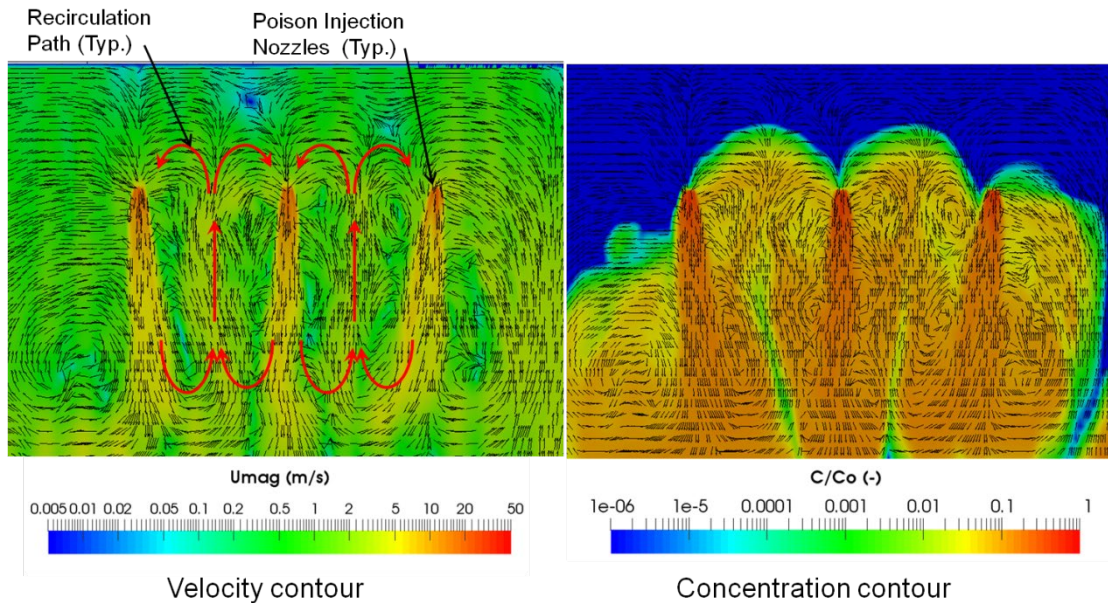
Velocity as a function of time was used as a boundary condition for inlet in CFD. Dead time and poison concentration were used as boundary condition for concentration. To understand the flow pattern and mixing characteristics of poison injection in AHWR calandria, the following three cases have been considered.

7.3.3.1 In stagnant moderator condition

To understand the flow pattern and mixing characteristics of poison injection, CFD analysis is performed without moderator flow distribution that is moderator in calandria is in a stagnant condition. Figure 7.13 (a) shows the time progression of poison at plane $x = 0.5 p$ where p is lattice pitch. It shows poison injection from eight injection tubes at $x = 0.5 p$. From the figure, it can be observed at $t = 1.5$ s and $t = 2.0$ s, poison is flowing in the direction opposite to the jet flow as shown in highlighted box 'A' at $t = 2.0$ s. To understand this, flow pattern at a box 'A' is highlighted and explained in Figure 7.13 (b). Figure 7.13 (b) shows the velocity and concentration contour along with velocity vector in highlighted box 'A'. It shows that jets emanating, interact with each other and creates the recirculation flow between them. These flow patterns govern the mixing of the poison in the calandria. Figure 7.14 shows flow pattern and concentration distribution at various vertical planes at 2 s. It can be seen from Figure 7.14 that poison jets reach the centre of calandria after 2 s of injection. Figure 7.15 shows the concentration distribution at various horizontal planes (cross sectional views) at 2 s. It can be seen from Figure 7.15 that almost full cross section at different plane is covered by poison. It can be further be seen from Figure 7.15 (c) that the poison is spreading outside the calandria tubes array at four corners. This is due to the position of first and last groups of injection nozzles on injection tube towards the ends of calandria tube array.



(a) Time progression of poison at plane $x = 0.5p$



(b) Detail 'A'-Velocity and concentration contour along with velocity vector

Figure 7.13: Time progression of poison at plane $x = 0.5p$

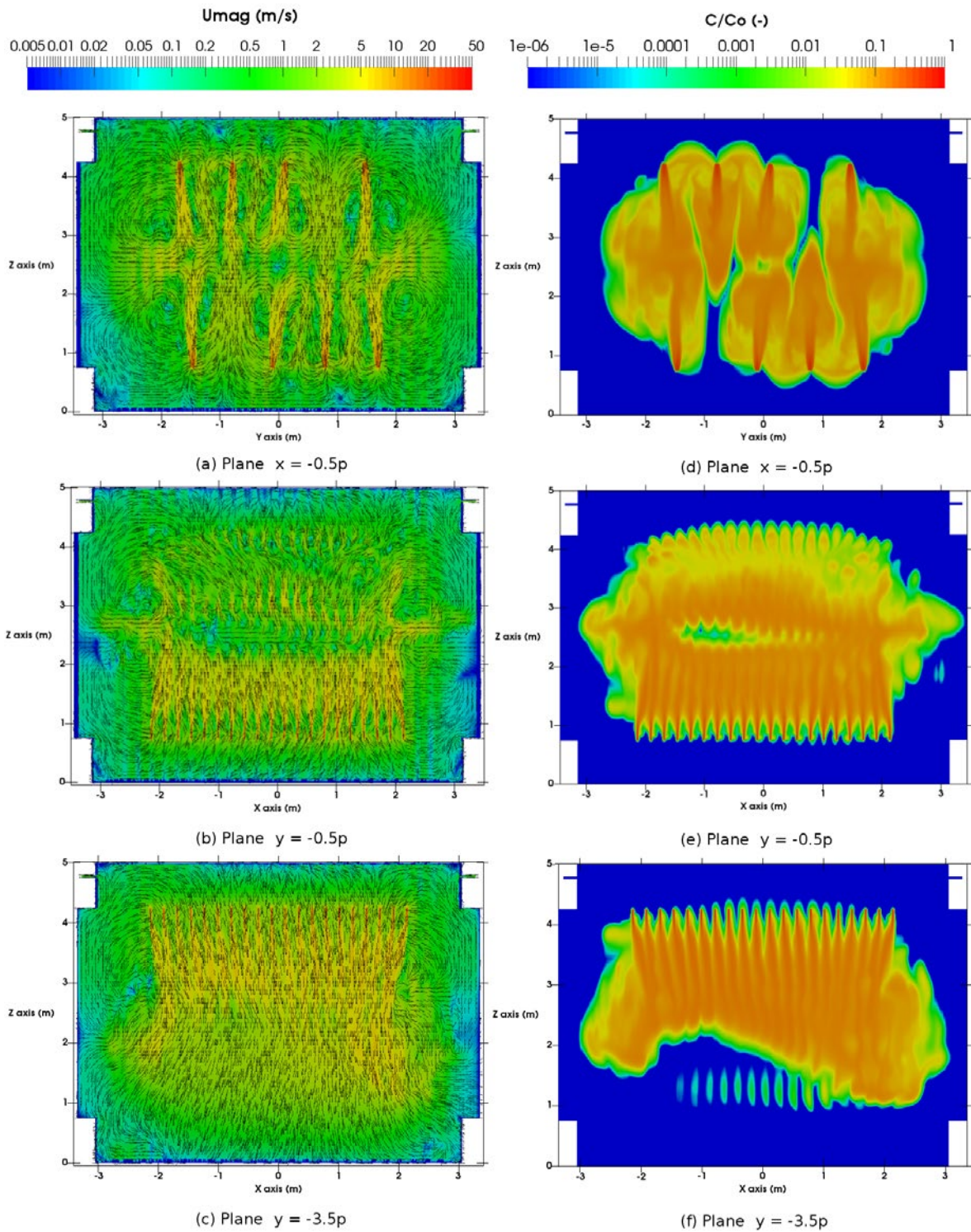


Figure 7.14: Flow pattern and concentration distribution at various vertical planes at 2 s

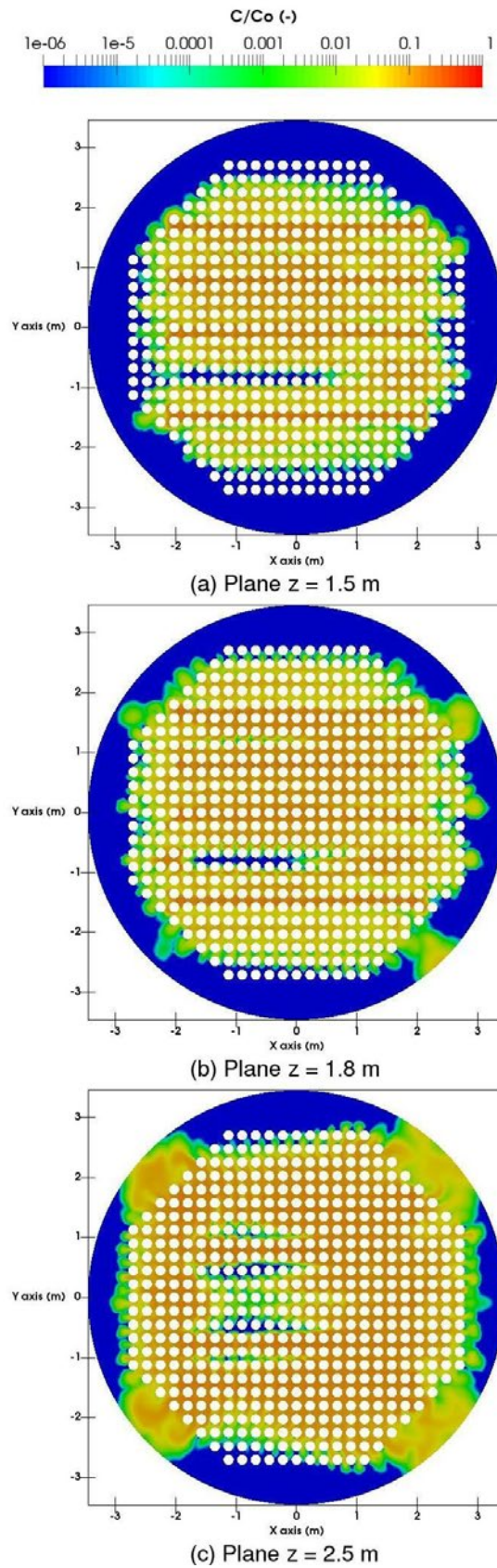


Figure 7.15: Concentration distribution at various horizontal planes at 2 s

Figure 7.16 shows the progression of poison jet front for the injection tube located at $y = -3.5p$ with time. Jet progression from injection tube starts from vertical location 4.25 m as shown in Figure 7.1. To quantify the poison mixing in calandria, two non-dimensional numbers are used. The first number is calandria poison fraction and second is mixing number. They are defined as follows:

$$\text{Calandria poison fraction} = \frac{\text{Moderator volume where } C/C_0 > 1\% \text{ in calandria}}{\text{Moderator volume of active core}}$$

$$\text{Mixing Number} = \frac{\text{Moderator volume where } C/C_0 > 1\% \text{ in calandria}}{\text{Poison volume injected in calandria}}$$

In the definition of “calandria poison fraction”, active core volume is the moderator volume in calandria excluding the volume of the reflector regions. Figure 7.17 shows the variation of calandria poison fraction and mixing number with time. Results show that calandria poison fraction increases linearly with time and at 2 s reaches a value of 0.65. It means moderator having poison concentration more than 1% of initial poison concentration covers 65% volume of active core in 2 s. Further, it can be seen from Figure 7.17 that initially mixing number changes sharply with time but as time progresses the slope of the curve gets saturated. At 2 s, mixing number is 385 which signify that moderator volume having poison concentration more than 1% of initial poison concentration is 385 times the poison volume injected in calandria.

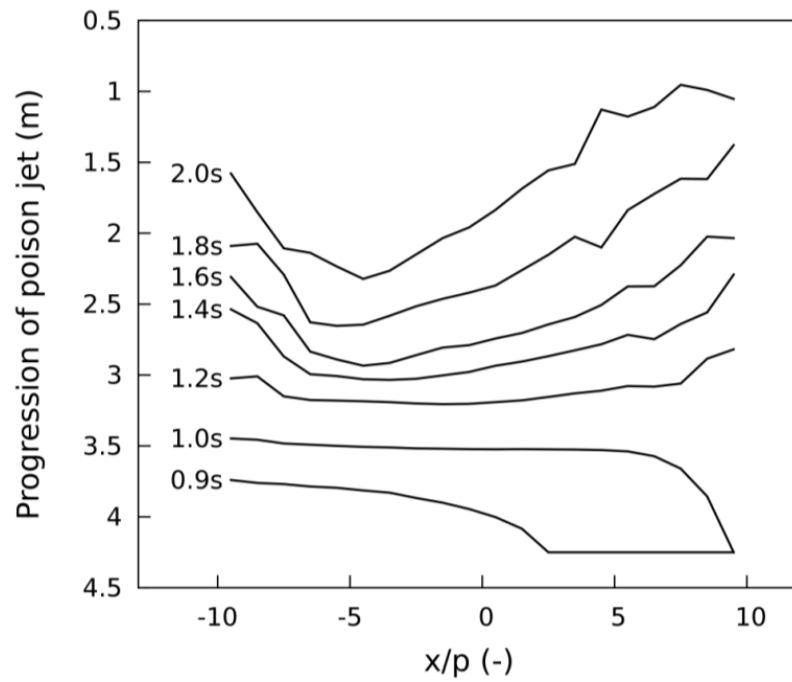


Figure 7.16: Progression of poison jet for injection tube at $y = -3.5p$ with time

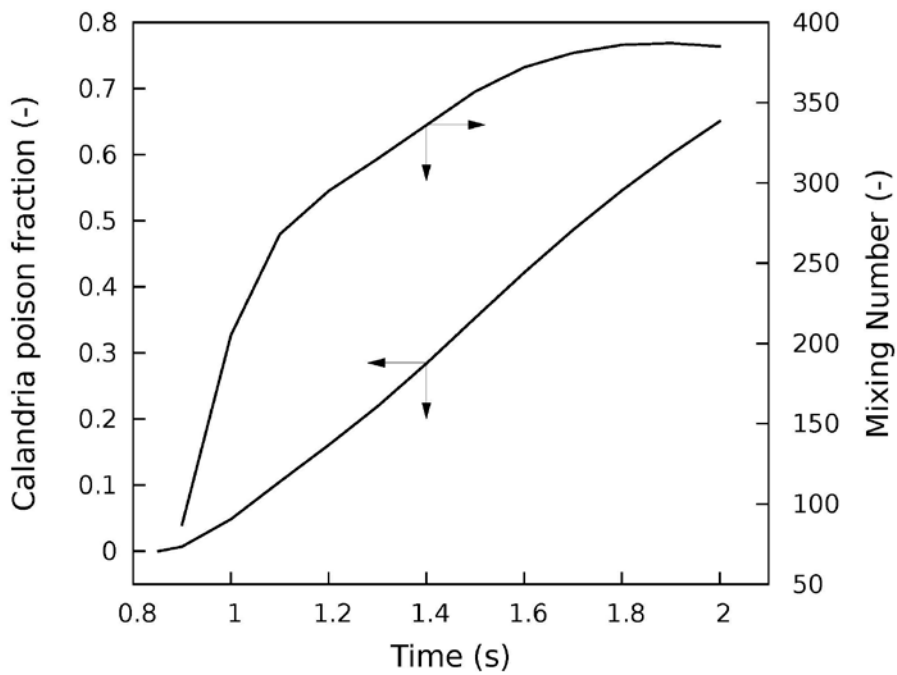


Figure 7.17: Poison mixing characteristics with time

7.3.3.2 Effect of moderator flow distribution without heat generation

To understand the effect of moderator flow distribution in calandria on flow pattern and mixing characteristics of poison injection, a CFD analysis was carried out. First, moderator flow field is obtained in calandria as discussed in chapter 6. After obtaining the moderator flow field, transient studies on poison injection are carried out. All the 640 poison jets are simulated in the modelling. Results show that the effect of moderator flow on liquid poison injection is negligible. Contour plots of poison concentration with and without moderator flow are nearly same. Moreover, results show that poison, having concentration more than 1% of initial concentration covers 64.7% volume of active core in 2 s which is same as in the last case.

7.3.3.3 Effect of moderator flow distribution with heat generation

A large amount of heat (50MW) is generated within the moderator due to neutron slowing down and attenuation of gamma radiations. Due to this, moderator flow distribution in calandria is buoyancy dominated as discussed in chapter 6. Moreover, the temperature of injected poison is 35°C compared to moderator inlet and outlet temperature of 50°C and 75°C respectively. This temperature difference may lead to some effect, which may alter poison distribution. Hence, to understand the effect of moderator flow distribution with spatial distribution of heat generation on flow pattern and mixing characteristics of poison injection, a CFD analysis was carried out. First, a steady state solution is obtained for moderator flow and temperature distribution inside calandria. Results obtained show that the effect of moderator flow with temperature distribution on liquid poison injection is negligible. Contour plots of poison concentration with and without moderator flow are nearly same. Moreover, results show that poison, having concentration more than 1% of initial concentration covers 64.6% volume of active core in 2 s which is same as in two cases described earlier. Figure 7.18 shows temperature profile

of moderator due to low temperature poison injection. Results show that effect of moderator flow, with and without heat generation is negligible on liquid poison distribution. This is due to low velocity of moderator flow as compared to injection velocity of poison. The effect may also be small due to short period of poison injection.

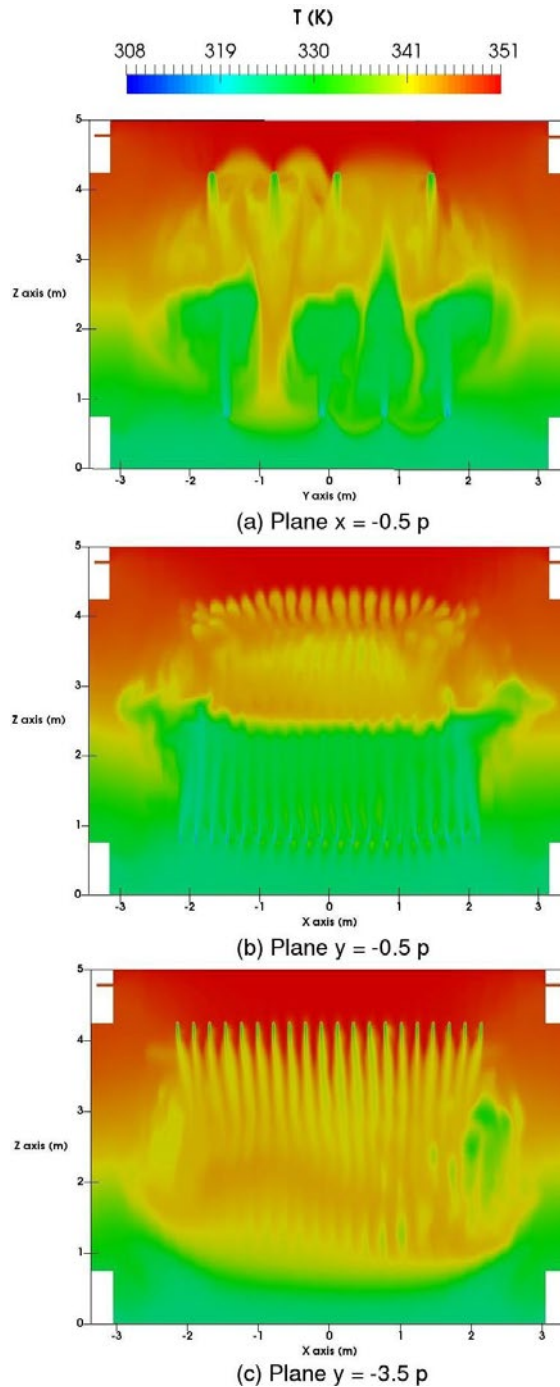


Figure 7.18: Temperature distribution at various vertical planes at 2 s

7.4 Conclusions

Validated model is used for simulation of flow pattern and mixing characteristics of high pressure poison injection of shut down system - 2 of AHWR. Effect of calandria tubes on poison jet progression were studied and compared with prediction capability of COPJET. The comparison shows that COPJET predictions are in very close agreement with CFD prediction for the case without calandria tubes. Simulations were performed for three cases; without moderator flow, moderator flow without heat generation and moderator flow with heat generation. The main conclusions are as follows:

- Effect of moderator flow and temperature on liquid poison injection is found to be insignificant and hence moderator can be assumed stagnant in liquid poison injection analysis.
- CFD simulation performed in calandria with 640 numbers of injection nozzles revealed that poison reaches significant portion inside the calandria in a given time to shut down the reactor. The result shows that poison, having concentration more than 1% of initial concentration covers 65% volume of active core in 2 s.

Chapter 8

CONCLUSIONS AND RECOMMENDATIONS FOR FUTURE WORK

In Advanced Heavy Water Reactor (AHWR) two active, independent, functionally diverse, fast acting shut down systems are provided. Shut Down System-1 (SDS-1) consists of mechanical shut off rods and Shut Down System-2 (SDS-2) is based on liquid poison injection into the moderator. Gadolinium nitrate solution acts as a neutronic poison, which is injected in heavy water moderator through a set of nozzles located inside calandria vessel. Each shut down system is fully capable of independently shutting down the reactor and keeping it under safe shut down condition for a prolonged period. In this research, liquid poison injecting by shut down system-2 has been taken for the investigation of various associated thermal hydraulic and fluid dynamics phenomena.

Based on the literature survey, the investigation on SDS-2 is divided into (i) transient flow distribution from lateral holes in a sparger tube, (ii) transient submerged jet injection in water, (iii) Moderator flow and temperature distribution in calandria and (iv) Liquid poison injection and its dispersion in calandria. There are few reported studies carried out for the cases of poison distribution in partial calandria model with calandria tubes and without calandria tubes. In AHWR calandria, 513 calandria tubes are arranged vertically in

a square pitch having p/d ratio of 1.34. In addition to this, calandria has a total eight poison injection tubes having total 640 injection nozzles of diameter 6 mm without any symmetry plane. To model such complex problem, a computer code called 'COPJET' is developed which provides the time varying input condition for all the nozzles for distributing the poison into the calandria. COPJET is validated against the experimental data available in the literature. Inlet condition of poison was modelled as the source term in the conservation equations used in the CFD code. Effect of heat generation in the moderator on the flow pattern and mixing characteristic of the poison into the moderator is investigated. The important findings in the present research work are listed below

- Computer code COPJET is developed which predict travelling of poison from poison tank to calandria vessel along with the distribution of poison from nozzles along the injection tube.
- A non-dimensional semi-empirical equation for modelling progression of poison jet in moderator with time is developed. Developed equation takes into account delay time caused due to poison moderator interface which is outside the calandria. This equation is used to check the adequacy of design parameters before detailed design.
- Experiments are carried out in two orientation of tube bundle with respect to poison jet direction. Results show that progression of jet injected in the axial direction of the bundle is more compared to that injected in the cross bundle. However, the lateral spread of jet is more in cross bundle compared to axial bundle. In axial bundle injection, the bundle has a tendency to maintain jet core in injection path whereas; cross bundle offers flow resistance and dissipate the jet energy faster.
- By considering the spatial distribution of volumetric heat generation in the moderator, CFD simulation shows that the maximum moderator temperature

reduces as compared to the case of uniform distribution of heat generation in the moderator.

- In the configuration with bottom inlet and top outlet moderator nozzles in AHWR, moderator volumetric average temperature is close to average of inlet and outlet temperature.
- CFD simulation of the experiment with poison moderator interface shows that though the poison injection is delayed due to moderator inventory present between poison moderator interface and calandria, poison front penetrates at a faster rate due to partially developed nature of the jet before the poison injection and apparently catches the velocity front with time.
- The effect of moderator flow and temperature on liquid poison injection is found to be insignificant and hence moderator can be assumed in stagnant condition in liquid poison injection analysis.
- CFD simulation of full calandria with 640 injection nozzles revealed that poison reaches the significant volume of calandria in given time to shut down the reactor. Results show that poison having concentration more than 1% of initial concentration covers 65% volume of active core in 2 seconds.

Based on the above studies it is found that shut down system-2 of AHWR works effectively for the configuration considered in the study.

In the future scope of this work, Large Eddy Simulations (LES) can be taken up as it can model physics of turbulent jets more closely. To reduce computational time due to large mesh size, dynamic mesh generation can be incorporated in CFD model. In computer code COPJET, diffusion of poison moderator interface is neglected, which can modelled and included in the code.

REFERENCES

- [1] Abramovich, G.N., 1963. *The Theory of Turbulent Jets*. MIT Press, Cambridge, Massachusetts.
- [2] Acrivos, A., Babcock, B.D., Pigford, R.L., 1959. *Chem. Eng. Sci.*, 10, 112–124.
- [3] Bajura, R.A., Jones, E.H., 1976. *J. Fluid Eng., Trans. ASME*, 654–666.
- [4] Balakrishnan, K., Kannan, U., Kakodkar, A., 1993. Reactivity worth of liquid poison jets in the moderator, *Annals of Nuclear Energy*, Volume 20 (6), Issue 6, 391-405.
- [5] Ball, C.G., Fellouah, H., Pollard, A., 2012. The flow field in turbulent round free jets, *Progress in Aerospace Sciences*, 50, 1-26.
- [6] Benedict, R.P., 1980. *Fundamentals of the Pipe Flow*, A Wiley-Interscience Publication, USA.
- [7] Binnie, A.N., 1942. The turbulent spreading of a water jet, *The turbulent spreading of a water jet*, *Engineering*, 153, 503-504.
- [8] Carlucci, L.N., 1982. Numerical Simulation of Moderator and Temperature Distribution in a CANDU Reactor Vessel, *Atomic Energy of Canada Ltd., AECL-7911*.
- [9] Central electricity authority–India, 2017. Power Sector July-2017, http://www.cea.nic.in/reports/monthly/executivesummary/2017/exe_summary-07.pdf (accessed on 11 sep. 2017).
- [10] Chae, K.M., Choi, H., Rhee, B.W., 2001b. Jet flow analysis of liquid poison injection in a CANDU reactor using source term, KAERI/TR-1739/2001, Korea Atomic Energy Research Institute.
- [11] Chae, K.M., Yoo, S.Y., Rhee, B.W. and Choi, H. B., 2001a. A Numerical Study on Transient High Speed Free Jet into a Confined Enclosure, *Proc. 9th Int. Conf. Nuclear Engineering*, Lyon, France.
- [12] Churchill, S.W., 1977. Friction factor equation spans all fluid flow ranges, *Chemical engg*, 84, 91-92.
- [13] Dharne, S.P. and Gaitonde, U.N., 1997. Analysis of the moderator flow and temperature distribution inside the calandria of Indian PHWRs, 3rd ISHMT - ASME Heat and Mass Transfer Conference, IIT Kanpur, 1083-1088.
- [14] Glasstone, S. and Sesonske, A., 2004. *Nuclear Reactor Engineering: Reactor Design Basics*, 4th Edition, Vol. 2.
- [15] Greskovich, E.J. and O’Bara, J.T., 1968. Perforated-pipe distributors, *Ind. Eng. Chem. Proc. Des. Dev.* 7, 593–595.

-
- [16] Hassan, Y.A., Barsamian, H.R., 2004. Tube bundle flows with the large eddy simulation technique in curvilinear coordinates, *Int. J. Heat Mass Transfer* 47, 3057–3071.
- [17] Horn, G. and Thrino, M.W., 1956. Angle of Spread of Free Jets, *Nature*, 178, 205-206.
- [18] Huget, R.G., Szymanski, J.K. and Midvidy, W.I., 1990. Experimental and numerical modelling of combined forced and free convection in a complex geometry with internal heat generation, *Proceeding of 9th international heat transfer conference*, Vol 3, 327.
- [19] Huget, R.G., Szymanski, J.K. and Midvidy, W.I., 1989. Status of physical and numerical modelling of CANDU moderator circulation, *Proceedings of 10th Annual Conference of the Canadian Nuclear Society*, Ottawa.
- [20] IAEA Safety Standards Series No. NS-SSR-2/1 (Rev. 1), 2016. *Safety of Nuclear Power Plants: Design*, Vienna.
- [21] Issa, R., 1986. Solution of the implicitly discretized fluid flow equations by operator splitting, *J Comput Phys*, 62, 40–65.
- [22] Johari, H. and Paduano, R., 1997. Dilution and mixing of unsteady jet, *Experiments in Fluids*, 23, 272- 280.
- [23] Johari, H., Zhang, Q., Rose, M.J. and Bourque, S.M., 1997. Impulsively Started Turbulent Jets, *AIAA Journal*, Vol. 35, No. 4, 657-662.
- [24] Kim, M., Yu, S.O. and Kim, H.J., 2006. Analyses on fluid flow and heat transfer inside calandria vessel of CANDU-6 using CFD, *Nuclear Engineering and Design*, Volume, 236 (11), 1155-1164.
- [25] Koroyannakis, D., Hepworth, R.D. and Hendrie, G., 1983. An Experimental Study of Combined Natural and Forced Convection Flow in a Cylindrical Tank. AECL Report, TDVI-382.
- [26] Kulkarni, A.V., Roy, S.S. and Joshi, J.B., 2007. Pressure and flow distribution in pipe and ring spargers, *Chem. Eng. Jour.*, 133, 173-186.
- [27] Nawathe, S., Umashankari, P., Balakrishnan, K., Mahajan, S.C. and Kakodkar, A., 1991. Development of Liquid Injection System SDS-2 for 500 MWe PHWRs, BARC019910E0001, Bhabha Atomic Research Centre.
- [28] OpenFoam 2.2.2, 2013. User guide to OpenFoam 2.2.2, www.openfoam.org.
- [29] Patankar, S.V., 1980. *Numerical Heat Transfer and Fluid Flow*, Hemisphere Publishing Corporation/Taylor & Francis Group, New York.
- [30] Paul, S.S., Ormiston, S.J. and Tachie M.F., 2008. Experimental and numerical investigation of turbulent cross-flow in a staggered tube bundle, *International Journal of Heat and Fluid Flow*, 29, 387-414.
- [31] Paul, S.S., Tachie, M.F., and Ormiston, S.J., 2007. Experimental study of turbulent cross-flow in a staggered tube bundle using particle image velocimetry, *Int. J. Heat Fluid Flow*, 28, 441–453.
-

REFERENCES

- [32] Prabhakarana, K.M., Goyala, P., Duttaa, A., Bhasina, V., Vazea, K.K., Ghosha, A.K., Pillai, A.V. and Mathew, J., 2012. Studies on flow induced vibration of reactivity devices of 700 MWe Indian PHWR, *Nuclear Engineering and Design*, 244, 1-16.
- [33] Rajaratnam, N., 1976. *Turbulent Jets*, Elsevier Publishing Co., Amsterdam and New York.
- [34] Rhee, B.W., Choi, J.H., Park, J.H., Chae, K.M., and Yun, H J., 2007. A Three-Dimensional CFD Model for a Performance Verification of the Liquid Poison Injection System of a CANDU-6 Reactor, *Nuclear Technology*, 159, 158-166.
- [35] Rhee, B.W., and Kim, H.T., 2014. A Review of the Scaling Study of the CANDU-6 Moderator Circulation Test Facility, *Journal of Power and Energy Engineering*, 2, 64-73.
- [36] Rollet-Miet, P., Laurence, D. and Ferziger, J., 1999. LES and RANS of turbulent flow in tube bundles, *Int. J. Heat Fluid Flow*, 20, 241–254.
- [37] Simonin, O. and Barcouda, M., 1988. Measurement and prediction of turbulent flow entering a staggered tube bundle, *Proceedings of the 4th forth International Symposium on Applications of Laser Anemometry to Fluid Mechanics*, Lisbon, Portugal.
- [38] Singh, R.K. and Rao, A.R., 2009. Simplified theory for flow pattern prediction in perforated in perforated tubes, *Nucl. Eng.Des.*, 239, 1725-1732.
- [39] Sinha, R.K. and Kakodkar, A., 2006. Design and development of the AHWR-the Indian thorium fuelled innovative nuclear reactor, *Nucl. Eng. Des.*, 236, 683–700.
- [40] Song, F., Noghrehkar, R. and Hau, K.F., 2008. CFD modelling of liquid poison injection in ACR-1000 shutdown system, *Proceedings of the 16th International Conference on Nuclear Engineering (ICONE-16)*, Florida.
- [41] Suryanarayana, P., Gathibandhe, M.V. and Agrawal, R.A., 2011. Nuclear Heat Distribution in AHWR Moderator, *BARC Report No. RPD/AHWR/63 /2011/REV-0*.
- [42] Watterson, J.K., Dawes, W.N., Savill, A.M. and White, A.J., 1999. Predicting turbulent flow in a staggered tube bundle, *Int. J. Heat Fluid Flow*, 20, 581–591.
- [43] Witre, P.O., 1980. The impulsivity started incompressible turbulent jet, *Sandia Laboratories, SAND80-8617*.
- [44] Yoon, C., Rhee, B.W. and Min, B.J., 2002. Validation of a CFD analysis model for predicting CANDU-6 moderator temperature against SPEL experiments, *Proceedings of ICONE 10, Virginia, USA*.
- [45] Yoon, C., Rhee, B.W. and Min, B.J., 2004. 3-D CFD analysis of the CANDU-6 moderator circulation under normal operating conditions, *Journal of the Korean Nuclear Society*, 36 (6), 559-570.